MODELING AND SIMULATION OF CONGESTION CONTROL STRATEGIES ON FREEWAYS: PRICING, RAMP METERING, AND VARIABLE SPEED LIMIT

A Dissertation
Presented to
The Academic Faculty

by

Hyun Woong Cho

In Partial Fulfillment
of the Requirements for the Degree
Doctor of Philosophy in the
School of Civil and Environmental Engineering

Georgia Institute of Technology
AUGUST 2017

MODELING AND SIMULATION OF CONGESTION CONTROL STRATEGIES ON FREEWAYS: PRICING, RAMP METERING, AND VARIABLE SPEED LIMIT

Approved by:

Dr. Jorge A. Laval, Advisor
School of Civil and Environmental Engineering
Georgia Institute of Technology

Dr. Bhargava R. Chilukuri
Department of Civil Engineering
Indian Institute of Technology, Madras

Dr. Michael P. Hunter
School of Civil and Environmental Engineering
Georgia Institute of Technology

Dr. David Goldsman
School of Industrial and Systems Engineering
Georgia Institute of Technology

Dr. Angshuman Guin
School of Civil and Environmental Engineering
Georgia Institute of Technology

Date Approved: July, 6th, 2017

ACKNOWLEDGEMENTS

First and foremost, I would like to give thanks to God for grace. Every accomplishment in my life would not be possible without his love and guidance.
I am eternally blessed for the love, support, and encouragement of my wife, Jiyoung Lee. She has been my rock and my support since we first met in 2007. She always inspires me to be a better person and a scholar. Also, above getting my Ph.D. degree, she accomplished our biggest achievements, Jaelyn and Haelyn. My dear daughters, remember that your mother is a very strong, beautiful, wise, and wonderful woman, so please listen to her.

I would like to express my deep gratitude to my advisor Dr. Jorge A. Laval for his support and guidance. I feel very fortunate and privileged to have been his student ever since I arrived at Georgia Tech, and I am humbled by his passion, insight, and inspiration. I regret that because of my extraordinary respect, I feared him during the doctoral journey even though he always greeted me with a big smile and the words "Dear Hyun." I will never forget his kind consideration, generosity, humor, and friendship, which impressed me even more than his superb research.

My thanks also go to my dissertation committee members, Drs. Michael Hunter, Angshuman Guin, and David Goldsman, and especially to Dr. Bhargava Rama Chilukuri for being my mentor and friend. I would also like to thank Drs. Wonho Suh, Sihyun Kim, and Chunhee Cho for their counsel whenever I needed it.

I thank Pastor Sungjin Ryu, Dr.Woo-Baeg Choi, and Shin-Ae Choi, and members of the Crystal Korean Church for their warm hearts and prayers. I am thankful for my SEB 207 office mates, Yi Zhou (Joy), Rafael Delpiano, Xiaodan Xu, Daejin Kim, Ali Etezady, Kai Yuan, Rafegh Aghamohammadi, and Xu Tu for their inspiration. I also thank the many Korean students in CEE and Young Hoon Choi for their friendship.

I would like to express appreciation to my professors at my alma mater, Seoul National University: the late Dr. Chang-Ho Park and Drs. Kyung-Soo Chon, Sung-Mo Rhee, Seung-Young Kho, Chungwon Lee, Kiyun Yu, and Dong-Kyu Kim for their encouragement. I must also extend my gratitude to Drs. Keechoo Choi and Koohong Chung, who motivated me to study transportation engineering in the United States. Their words changed my life.

I wish to thank all of my family, my only brother Hyun Joon, my mother- and father-in-law, sisters-in-law Jisun and Jimin, and other family members for their love and support throughout this endeavor.

I would like to emphasize my deep gratitude to my beloved mother and father. Their unconditional love, prayers, encouragement, compliments, and expectations made me who I am. I dedicate this work to them. Finally, I wish for this work to be "a beacon of light" to my two daughters, similar to the quote in the epilogue in my father's doctoral dissertation 23 years ago, which has come true.

TABLE OF CONTENTS

LIST OF TABLES

LIST OF FIGURES

LIST OF SYMBOLS AND ABBREVIATIONS

HOT Lane	High-Occupancy Toll Lane
GP Lane	General Purpose Lane
UE	User Equilibrium
SO	System Optimum
MTL	Managed Toll Lane
VSL	Variable Speed Limit
RM	Ramp Metering

SUMMARY

When demand exceeds supply (capacity), freeways become congested. However, in a congested state, compared to the uncongested state, the capacity of a freeway decreases. The purpose of freeway operations and traffic management systems is to maximize capacity and utility of the freeway system. For decades, researchers have introduced traffic congestion control strategies such as managed toll lanes, on-ramp metering, and variable speed limits. This dissertation examines the modeling and simulations of demand- and supply-side management strategies that reduce freeway congestion.

The first part of this dissertation analyzes real-time pricing strategies for controlling the demand for a managed lane facility, such as the HOT lane. We devise a system-optimal real-time congestion pricing strategy capable of handling variable capacity because of the weaving activity and find that the proposed model outperforms existing methods in minimizing total delay savings, particularly when bottleneck capacities vary significantly. The method is simple to implement with current technology.

The second part of this dissertation investigates supply-side strategies. It proposes a variable speed limit and ramp metering (VSL-RM) control strategy for preventing and recovering from losses in freeway capacity at freeway merge bottlenecks. Using kinematic wave theory, this study derives analytical models that are implemented in the microsimulation model GTsim and finds that the combined VSL-RM system outperforms both systems in preventing traffic breakdown; if only one system has to be used, the choice depends on the distribution of traffic demand.

The third part of this dissertation presents a case study that implements the VSL-RM strategy in a real-life freeway corridor in Atlanta. Using a stochastic simulation-based optimization framework that combines GTsim and a genetic algorithm-based optimization module, we determine the optimal parameter values of a combined VSL-RM system that minimizes total vehicle travel time.

CHAPTER I INTRODUCTION

1.1. Background

The Federal Highway Administration (FHWA) reported that the number of hours of congestion on freeways in 2016 was four hours and forty-three minutes (FHWA, 2015). The causes of congestion were bottlenecks (40%), traffic incidents (25%), bad weather (15%), work zones (10%), poor signal timing (5%), and special events/other (5%). The most common cause, bottlenecks, occur when traffic demand exceeds the freeway capacity (supply). As bottlenecks are the major causes of congestion and a tractable phenomenon, managing bottlenecks would be the most efficient way of relieving congestion.

Transportation planners and engineers have proposed and developed a number of methods for controlling supply and demand. One of the methods of reducing demand on the freeway is high-occupancy vehicle (HOV) lanes, which guarantee the free-flow speed of HOVs by restricting access to single-occupancy vehicles (SOVs). The main purpose of HOV lanes is to carry more people to their destinations faster and to encourage car-pooling, thereby reducing the number of single-occupancy vehicles. The first HOV lanes in the United States opened in 1969 in the Washington D.C. area, and they have expanded to other metropolitan areas in the country. However, HOV lanes have been underutilized, and the necessity of the right-of-way of HOV lanes to SOVs have risen. In this context, high-occupancy toll (HOT) lanes were implemented in 1995 on State Route 91 in Orange County, California. After successful revenue collection from the SR-91 toll lanes, the concept has become quite popular and widely accepted by many transportation

authorities. Currently, more than twenty managed toll lanes are in operation in the United States, with more being constructed or planned.

From the perspective of controlling supply (bottleneck capacity), one method that has proven effective at controlling freeway bottlenecks is on-ramp metering (RM) (Gomes, Horowitz, Kurzhanskiy, Varaiya, & Kwon, 2008; Papageorgiou, Hadj-Salem, & Blosseville, 1990; Papageorgiou, Hadj-Salem, & Middelham, 1997; Smaragdis & Papageorgiou, 2003; L. Zhang & Levinson, 2010). When a ramp is metered, it controls the demand of input flow to the freeway and results in a decrease in total delay if applied properly, that is, with the objective of preventing or recovery from a capacity drop (Papageorgiou & Kotsialos, 2002). It is well known that capacity drops are recurring phenomena of merge bottlenecks, in which the discharge rate drops by about 15% after queues have formed (Cassidy & Bertini, 1999; Cassidy & Rudjanakanoknad, 2005). One study showed that a likely explanation for this phenomenon traces back to lane changes by vehicles slowing down both in the on-ramp and/or freeway queues (Laval & Daganzo, 2006).

Another method that is becoming popular at controlling freeway bottlenecks is the variable speed limit (VSL) strategy, which entails setting speed limits dynamically as a function of traffic and/or weather conditions. Smulders (1990) proposed an early VSL system that aimed to homogenize and stabilize traffic to improve traffic flow and safety. Subsequent studies presented the effectiveness of the VSL regarding the enhancement of safety and reduction in the risk of accidents (Abdel-Aty, Cunningham, Gayah, & Hsia, 2009; Abdel-Aty, Dilmore, & Dhindsa, 2006; Lee, Hellinga, & Saccomanno, 2006), the efficiency of traffic flow (Bertini, Boice, & Bogenberger, 2006; Papageorgiou,

Kosmatopoulos, & Papamichail, 2008), and solutions to shock waves (Hegyi, De Schutter, & Hellendoorn, 2005b; Hegyi, Hoogendoorn, Schreuder, Stoelhorst, & Viti, 2008).

Recent studies have suggested that combining the VSL and the RM or near-future technology such as connected vehicles (CVs) could reinforce the benefits of the VSL system (Chen & Ahn, 2015; Khondaker & Kattan, 2015a). Carlson, Papamichail, Papageorgiou, & Messmer (2010b) developed a new approach to the VSL, an RM control strategy referred to as ALINEA. In their work, the VSL decreases mainstream flow to the potential bottleneck segment, impeding the activation of bottlenecks at under-critical occupancies. Although their study proposed a theoretically sound method and results, their approach has not provided any insights into the practical implementation of traffic control.

1.2. Research Objectives

To further our understanding of freeway congestion control, this dissertation studies the above methods (i.e., managed toll lanes, variable speed limits, and on-ramp metering) and develops advanced traffic operation techniques for handling freeway bottlenecks. In particular, specific objectives are presented as follows:

- To understand a system-optimal real-time pricing strategies to control the demand for a managed-lane facility.
- To establish a combined variable speed limit and ramp metering control strategy that prevent and recover from losses in freeway capacity at freeway merge bottlenecks.
- To implement the VSL-RM strategy to a real-life freeway corridor in Atlanta.

1.3. Research Contributions

The contributions of this study are as follows:

(i) It strengthens the system-optimum linear toll pricing strategy and suggest that an operator of the manage lanes can implement practical toll systems that incorporate the real-time discharge rates of bottlenecks.

(ii) It develops the combined VSL-RM model to deal with capacity drop, which has not been studied yet.

(iii) It provides the queue warning and queue flush system to VSL-RM system.

(iv) It provides modeling and simulation of shoulder lane only VSL.

1.4. Dissertation Outlines

Toward this end, this dissertation is organized as follows. Chapter 2 presents background and literature review on managed toll lanes, capacity drop, the VSL, and the RM. Chapter 3 presents analytical and simulation models of the real-time congestion pricing strategy which relaxes the constant capacity assumption in (Laval, Cho, Muñoz, & Yin, 2015). Chapter 4 explains the combined VSL-RM system for capacity drop control at merge bottleneck. Chapter 5 discusses a simulation based parameter optimization of the combined VSL-RM system models that incorporate the real-world data. Conclusions and future research work are introduced in Chapter 6.

CHAPTER II LITERATURE REVIEW

2.1. Managed Toll Lane

A number of studies have examined the performance of HOT lanes (see, for example, Burris & Stockton (2004); Supernak et al. (2002), Supernak, Steffey, & Kaschade (2003); Zhang, Yan, & Wang (2009)), and travelers' willingness to pay (Burris & Appiah, 2004; Finkleman, Casello, & Fu, 2011; Podgorski & Kockelman, 2006; Zmud, Bradley, Douma, & Simek, 2007); only a few studies, however, have been devoted to the pricing strategies of managed lanes. Existing studies focus on ad-hoc objectives that the tolling agencies may seek to achieve, such as ensuring free-flow conditions on HOT lanes. For example, Li and Govind (2002) developed a toll evaluation model that assesses the optimal pricing strategies of HOT lanes to accomplish myriad objectives such as ensuring a minimum speed, traveling in the general-purpose lanes (GPL), or maximizing toll revenue. Zhang, Wang, Wei, and Yi (2008), by keeping the HOT lane speed higher than 45mph, applied a feedback-based algorithm to calculate the optimal flow ratios and then used logit models to estimate dynamic toll rates. Yin & Lou (2009) explored two approaches, including feedback and self-learning methods, to determine dynamic pricing strategies for HOT lanes, and the results of their comparative study showed that the self-learning controller is superior to the feedback controller given that a free-flow traffic condition for managed lanes is maintained. Lou, Yin, and Laval (2011) further developed the self-learning approach in Yin and Lou (2009), incorporating the effects of lane-changing using the hybrid traffic flow model in Laval and Daganzo (2006). Burris, Ungemah, Mahlawat, and Pannu (2009) examined the potential impacts of various tolling strategies on carpools, including removing or reducing their preferential treatment in HOV lanes.

A recent study on managed toll lane operation system in (Yin et al. (2012) compared the pricing algorithm implemented on the 95 express lane in South Florida with static and time-of-day tolls. The study suggested that when the demand pattern is predictable, time-of-day or even static tolling performs as well as dynamic tolling provided that the toll profiles are optimized for the demand pattern. Nonetheless, dynamic tolling performs in a more robust and stable manner because of its adaptive nature to demand fluctuations. Recognizing that dynamic tolling is beneficial but costly to implement, the authors further conducted a cost-benefit analysis to examine whether the benefits from dynamic tolling justified the additional costs of its implementation or not.

2.2. Capacity Drop

Since Edie (1961) presented the phenomenon of discontinuity between the flow rates of non-congested and congested states and a reduction in the flow rate when the density of the Lincoln Tunnel, New York, was greater than 90 *veh./mile*, the phenomenon, called "capacity drop," was not extensively studied until Cassidy (1998) and Cassidy and Bertini (1999) empirically and graphically (with cumulative count curves of vehicles, see Figure 1) showed a capacity drop in which the discharge rate from a queue is close to 10% lower in congested flow than in uncongested flow. During this time gap, Banks (1991a, 1991b), Hall and Agyemang-Duah (1991), and Hall and Hall (1990) discovered the capacity drop phenomenon, that is, the discharge is 3 ~ 6% less when a queue forms at a bottleneck.

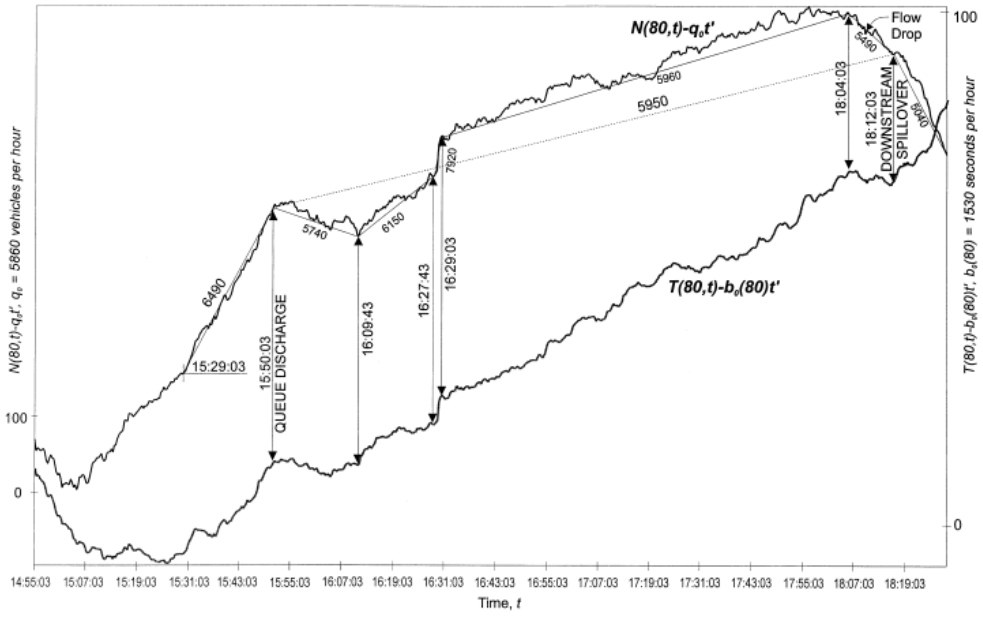

Figure 1 Oblique count curve representation of the capacity drop(Cassidy & Bertini, 1999)

The mechanism of the capacity drop has been extensively investigated. A number of studies have presented the relationship between the capacity drop and a lane-changing

of a vehicle and its bounded acceleration capability (Cassidy & Rudjanakanoknad, 2005; Coifman & Kim, 2011; Laval & Daganzo, 2006; Leclercq, Knoop, Marczak, & Hoogendoorn, 2016; Leclercq, Laval, & Chiabaut, 2011; Oh & Yeo, 2015). Several other studies examined the capacity drop from the perspective of driver behavior or car-following characteristics (Chen, Ahn, Laval, & Zheng, 2014; Chen, Laval, Ahn, & Zheng, 2012; Oh & Yeo, 2015; Treiber, Kesting, & Helbing, 2006; Yeo, 2008; Yuan, Knoop, & Hoogendoorn, 2017; H. M. Zhang & Kim, 2005).

In addition to research that furthers our understanding of the mechanism of the capacity drop, many studies also have also explored prevention of capacity drops and/or the increase in the discharge rates of bottlenecks. One approach is ramp metering, which was proposed and empirically tested by Papageorgiou et al. (1990, 1997). Ramp metering controls the inflow of on-ramps to prevent freeway congestion, reducing total travel time by increasing the discharge rate of the freeway.

Cassidy (2003), Cassidy and Rudjanakanoknad (2005), and Chung, Rudjanakanoknad, and Cassidy (2007) later adopted the ramp metering strategy to increase the discharge rate of merge bottlenecks, that is, reducing the capacity drop (see Figure 2). Chung et al. (2007) verified the relationship between density (per lane) and capacity drops and proposed an adjusted metering rate that incorporates the density of a lane. Inspired by ramp metering, a new view of a variable speed limit (VSL) that controls the inflow of a mainline of a freeway emerged.

(a) Oblique count curves on the freeway

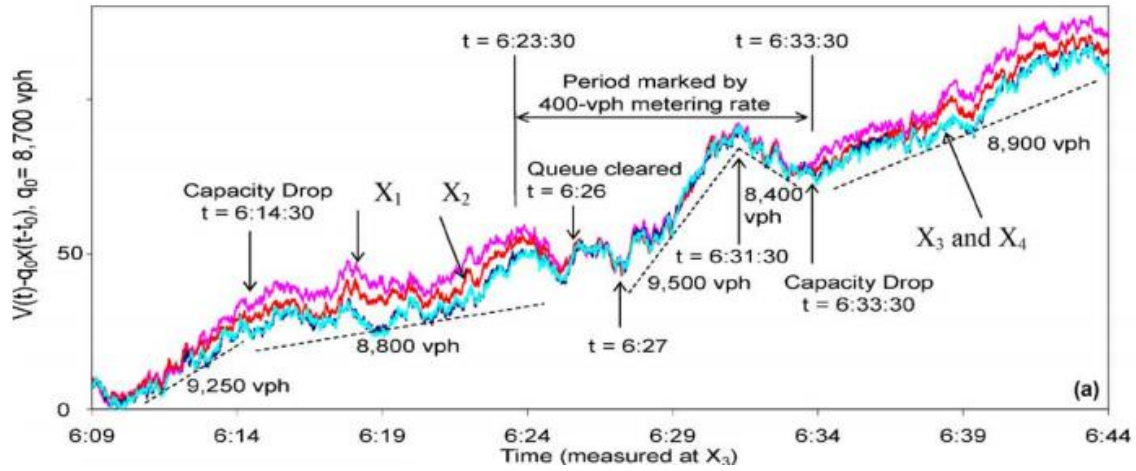

(b) Oblique curve of the median-lane **(c) Oblique curve of the on-ramp**

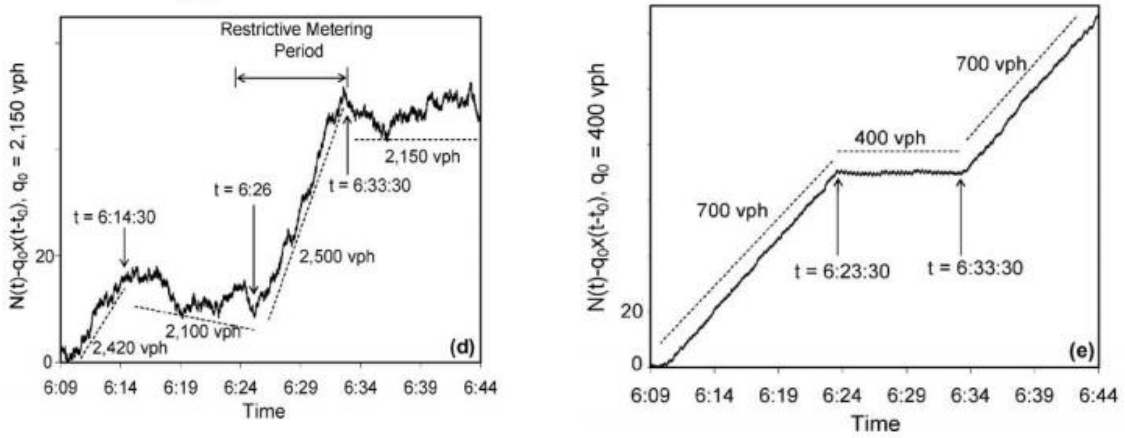

Figure 2 Increasing the discharge rate of a bottleneck using ramp metering and the oblique count curves of (a) a freeway, (b) a median lane, and (c) an on-ramp
(Cassidy & Rudjanakanoknad, 2005)

2.3. Variable Speed Limit

Early VSL systems were proposed by Smulders (1990), who aimed to homogenize and stabilize traffic to improve flow and safety. Subsequent studies presented the effectiveness of the VSL in terms of the enhancement of safety and the reduction of accidents (Abdel-Aty et al., 2009, 2006; Lee et al., 2006), the efficient of traffic flow (Bertini et al., 2006; Papageorgiou et al., 2008), and solutions to shock waves (Hegyi et al., 2005b, 2008). Recent studies have suggested that combining VSL and ramp metering or near future technology such as the connected vehicle (CV) would reinforce the benefits of the VSL system (Chen & Ahn, 2015; Han, Chen, & Ahn, 2017; Khondaker & Kattan, 2015a).

This chapter presents a literature review of the effects of the VSL on traffic flow, research methodologies on the VSL such as the kinematic wave model, capacity drops, simulation modeling, and traffic control.

2.3.1. Theoretical background

Effects of VSL on traffic flow

Papageorgiou et al. (2008) studied the impact of VSL on traffic flow characteristics and presented a fundamental diagram, shown in Figure 3. As in the Figure, they found changes in both the slope and the critical occupancy. Considering that the VSL algorithm that they used was an imperfect rule-based algorithm, their findings shed light on future research on the effectiveness of VSL on traffic flow.

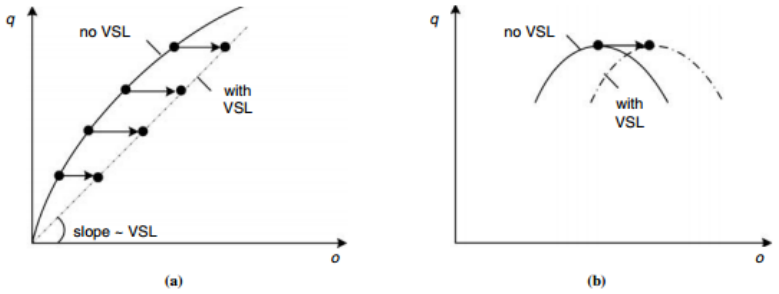

Figure 3 (a) Potential VSL impact on under-critical mean speed and (b) cross-point of diagrams with and without VSL (Papageorgiou et al., 2008)**.**

Recent studies have empirically discovered the relationship between the VSL and lane flow distribution (LFD) or traffic flow characteristics between lanes (Duret, Ahn, & Buisson, 2012; Knoop, Duret, Buisson, & Van Arem, 2010; Soriguera, Martinez, Sala, & Menendez, 2017). From empirical data, Duret (2014), Duret et al. (2012), and Knoop et al. (2010) showed that the VSL homogenizes the speed between lanes so that should lanes can be used; Soriguera et al. (2017), however, presented evidence that the VSL may not reduce the flow of the mainline, and for moderate demand, lower speed limits increase speed differences across lanes, thus increasing the incidence of lane-changing.

Kinematic Wave Theory and VSL

Several studies have explained the effectiveness of the VSL system by kinematic (shock) wave theory (Chen & Ahn, 2015; Chen, Ahn, & Hegyi, 2014; Hadiuzzaman & Qiu, 2013; Han et al., 2017; Hegyi & Hoogendoorn, 2010; Hegyi et al., 2008; H. Y. Jin & Jin, 2015; Schelling, Hegyi, & Hoogendoorn, 2011; Yang & Rakha, 2017). The earliest proposed VSL algorithm based on shock wave theory was SPECIALIST (SPEed ControllIng ALgorIthm using Shock wave Theory), a method of resolving the moving jam (Figure 4). In the figure, when the VSL system detects a shock wave (state 2), the VSL is on at the upstream of the shock wave (state 3) and then relaxes the VSL to the higher speed limit (states 4, 5) to the following vehicles. As a result, the shock wave is not propagated to the upstream. Later, this research was extended to recurrent and non-recurrent bottlenecks situations.

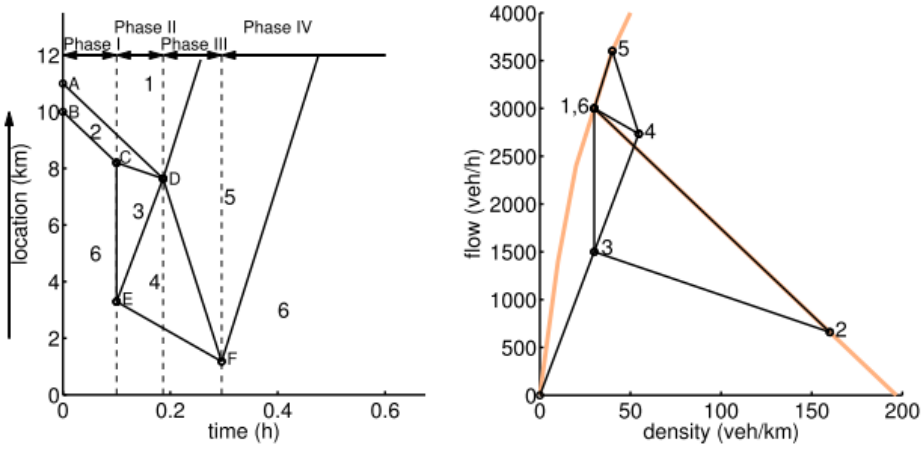

Figure 4 Four phases of the SPECIALIST algorithm (Hegyi & Hoogendoorn, 2010)**.**

Capacity drop and VSL

Although Hadiuzzaman and Qiu (2013) and Hadiuzzaman, Qiu, and Lu (2012) proposed a cell transmission model (CTM) (Daganzo, 1995)-based analytical model to understand the effectiveness of VSL control that incorporates capacity drops, this study did not explain the mechanism of the VSL as the solution of the capacity drop.

As noted in (Yang & Rakha, 2017), two VSL pioneer studies presented the mechanism of the capacity drop at bottlenecks and the VSL as a solution. Jin and Jin (2013) presented a VSL control strategy based on a proportional-integral (PI) controller to effectively mitigate traffic congestion (the capacity drop) and reduce travel time at a lane-drop bottleneck. In their study, the VSL regulated the upstream inflow, and the authors used a controller to maintain stability in a zone between the VSL zone and the lane-drop bottleneck, which prevented a capacity drop.

Several studies proposed VSL control for fixed and non-recurrent freeway bottlenecks (Chen & Ahn, 2015; Chen, Ahn, & Hegyi, 2014; Han et al., 2017) and further developed it using connected vehicles. These studies, basing VSL strategies on the kinematic wave theory, starve inflow to the bottleneck to dissipate the upstream queue (see Figure 5). After clearing the queue, the VSL continues to regulate inflow to the bottleneck, maximizing the discharge rate and preventing a capacity drop.

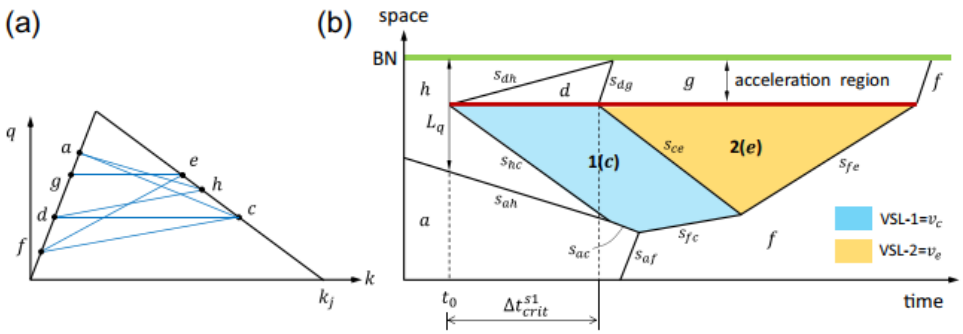

Figure 5 VSL strategy for a steady queue (a) FD with VSL (b) a time-space diagram of VSL(Chen, Ahn, & Hegyi, 2014)

Recently, Yang & Rakha (2017) proposed a bang-bang feedback VSL (i.e., speed harmonization) algorithm that controls the mainline freeway to prevent or delay a capacity drop. Using a microscopic simulation, this study demonstrated their algorithm and showed an increase in the bottleneck discharge rate and reductions in emissions and fuel consumption.

Simulation Modeling of VSL

For safety reasons, directly implementing traffic flow models in the real world is difficult without prior scrutiny. The most popular methods of proving the effectiveness of traffic flow models are simulation modeling and experiments. Simulation methods of traffic can be categorized into micro and macro simulation. Researchers who have studied the safety benefits of VSL used off-the-shelf micro-simulation software such as VISSIM or PARAMICS (Abdel-Aty et al., 2006; Abdel-Aty, Pande, Lee, Gayah, & Dos Santos, 2007; Lee et al., 2006). Other researchers who presented the traffic flow efficiency of VSL used the macroscopic traffic flow model (e.g., the cell transmission model, METANET (see Figure 6) (Carlson, Papamichail, & Papageorgiou, 2011, 2014; Carlson et al., 2010b; Hadiuzzaman et al., 2012; Hegyi, De Schutter, & Hellendoorn, 2005a; Hegyi et al., 2005b; Lu, Qiu, Varaiya, Horowitz, & Shladover, 2010)).

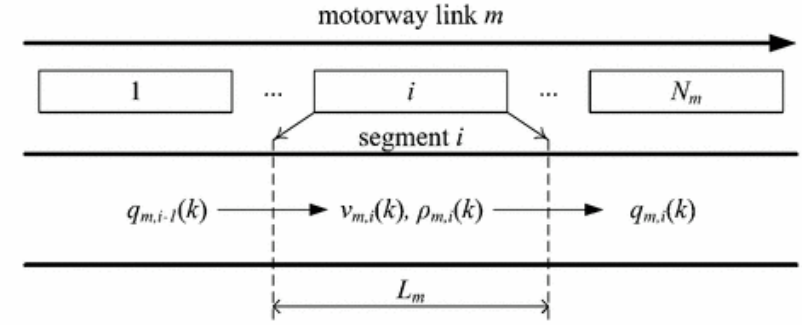

Figure 6 Discretized motorway link (Carlson et al., 2010b)

2.3.2. Variable Speed Limit Algorithm

Rule-based Algorithm

VSL algorithms can be classified into reactive rule-based or proactive algorithms. The rule-based algorithm determines the speed limit based on traffic coefficients: speed, flow, density (occupancy) threshold (see Figure 7) (Allaby, Hellinga, & Bullock, 2007; Chang, Park, & Paracha, 2011; Kang, Chang, & Zou, 2004; Lin, Kang, & Chang, 2004; Talebpour, Mahmassani, & Hamdar, 2013). The main objective of such VSL systems is to harmonize the speed between upstream and downstream (vertically) traffic or between lanes (laterally). Studies have shown that rule-based algorithms are effective at harmonizing traffic and improving safety; one study of their efficiency in traffic flow and travel time savings, however, differs from locations based on congestion levels (Khondaker & Kattan, 2015b).

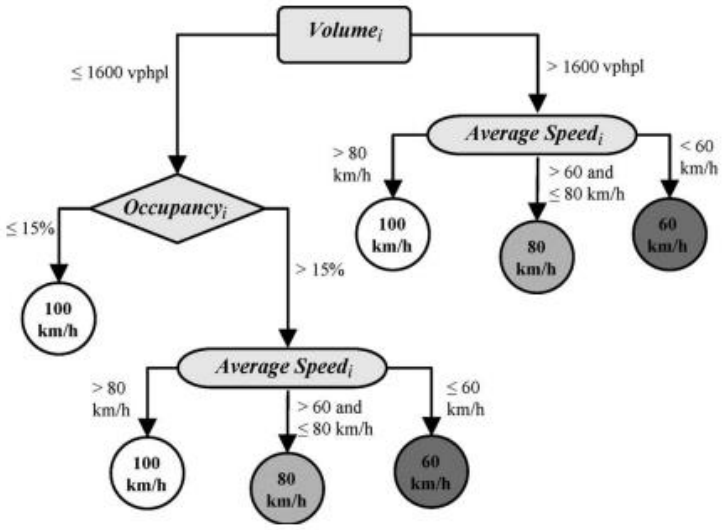

Figure 7 Example of rule-based VSL algorithm (Allaby et al., 2007)

For the rule-based algorithm, setting conservative threshold values might reduce the risk of a crash, but it would exacerbate traffic. Also, because of the time lag between

current traffic and future controlled traffic, if incautious threshold values were chosen, future traffic could not take advantage of the VSL system (Khondaker & Kattan, 2015b). It is also worth mentioning that the location of VSLs and durations or update periods of the control of VSLs are important factors related to the effectiveness of a rule-based VSL algorithm.

Proactive Algorithm

The proactive algorithm, which does not have the limitations of the rule-based algorithm, adopts a rolling horizon system (see Figure 8), control theory approaches, and a METANET model, all of which have been explained in previous studies (Fang, Hadiuzzaman, Karim, Luo, & Qiu, 2014; Hadiuzzaman et al., 2012; Hegyi et al., 2005a; Lu, Qiu, et al., 2010; Lu, Varaiya, Horowitz, Su, & Shladover, 2010). For example, Model Predictive Control (MPC) predicts future traffic based on traffic state and control input and computes optimal control values (speed limits). METANET, used in MPC modeling, discretizes distance and time so that it can easily calculate the optimal location and time period of the VSL system. However, the MPC approach, because of its complexity, has not been implemented in the real world.

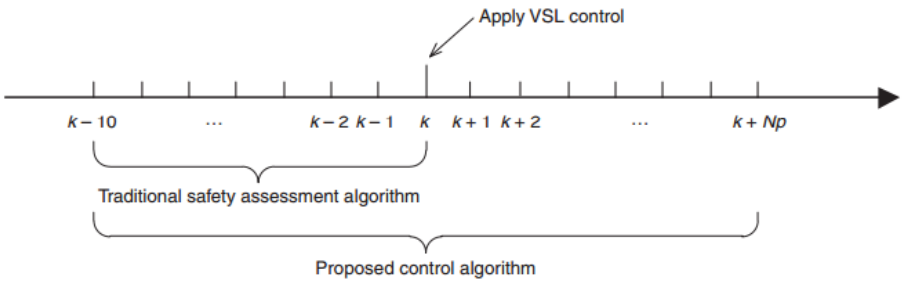

Figure 8 Rolling Horizon system and control algorithm (Fang et al., 2014)

2.3.3. Variable Speed Limit and Ramp Metering

Ramp Metering ALINEA

As previously mentioned, ramp metering (RM) has been shown to be effective at increasing mainstream outflow by controlling the inflow of the on-ramp. One of the most popular algorithm of ramp metering is ALINEA, a local feedback strategy that calculates metering rates $r(t)$ using past time-step metering rates $r(t-\Delta t)$ and differences between current and target occupancy $(\hat{o} - o_{out}(t))$ (Papageorgiou et al., 1997) (see equation (1), Figure 9).

$$r(t) = r(t-\Delta t) + K_R\big(\hat{o} - o_{out}(t)\big) \qquad (1)$$

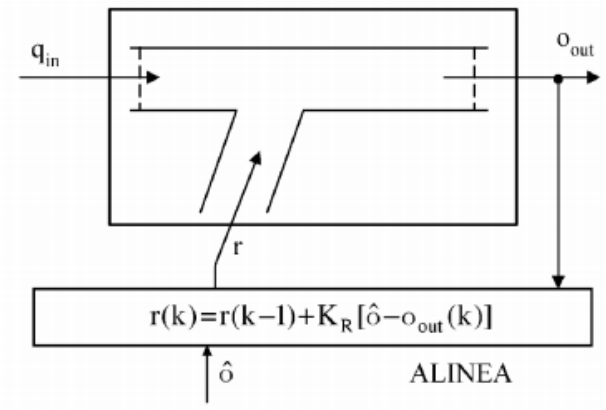

Figure 9 ALINEA: local ramp metering strategy (Papageorgiou & Kotsialos, 2002)

Queue Flush in Ramp Metering

The ramp metering system is installed on an on-ramp that connects an arterial road and a freeway. The restrictive metering rate of an on-ramp induces a queue to spill back to the upstream arterial road. To prevent this situation from occurring, an operator of a ramp metering system adopts a queue flush system (Chilukuri, 2015; Chilukuri, Laval, & Chen, 2013), which turns off the ramp meter signal when a loop detector installed at the end of the queue storage detects a queue spillback. Chilukuri et al. (2013) found that although a queue flush resolves the queue of the on-ramp, it decreases flow on the mainline freeway (see Figure 10). The queue flush algorithm consists of maximum and minimum density thresholds (k_{max}, k_{min}) of loop detectors and the number of data collecting time periods (n), shown in the following equation.

$$k_{max} \geq \frac{\sum_{i=1}^{n} k_i}{n}$$

$$k_{min} \leq \frac{\sum_{i=1}^{n} k_i}{n}$$

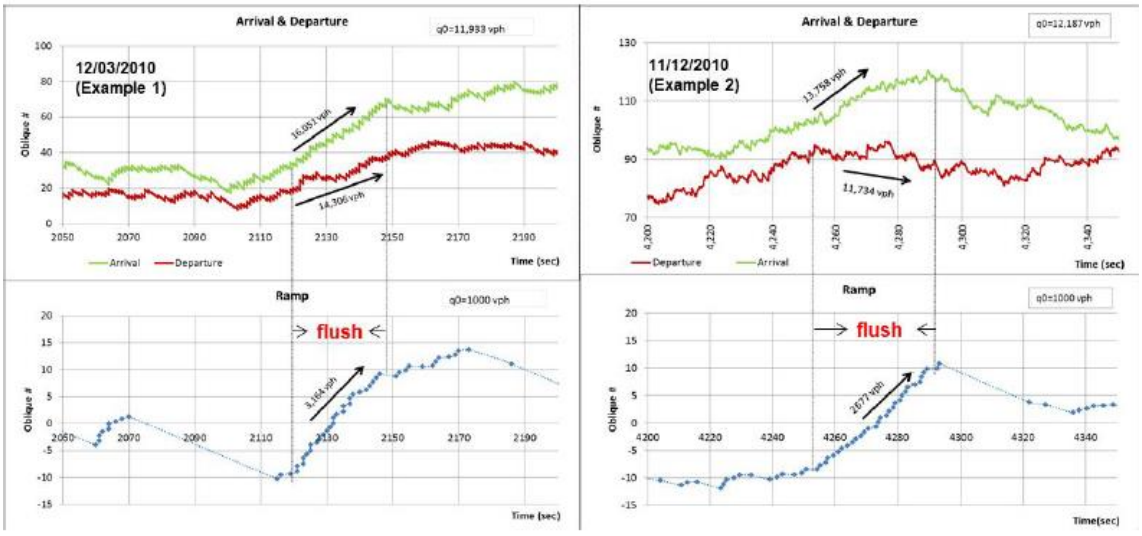

Figure 10 Increase in on-ramp flow and decrease in the mainline freeway during a queue flush(Chilukuri et al., 2013)

VSL and RM Integrated System

The research group that developed the ALINEA control strategy proposed a new viewpoint of the VSL that is similar to the RM (Carlson et al., 2010b). In their work, the VSL decreases the mainstream flow to the potential bottleneck segment, resulting in delaying bottleneck activation at under-critical occupancies (Figure 11). Their assumption of the impact of VSLs on traffic flow is based on empirical data (Papageorgiou et al., 2008).

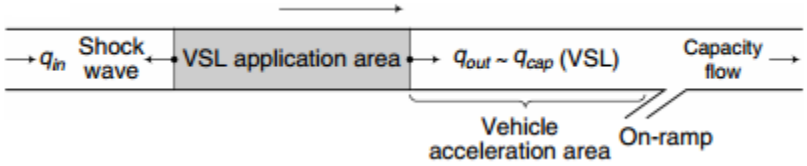

Figure 11 Persistent flow control via VSL (Carlson et al., 2010b)

Assuming that the VSL is the RM, the research team proposed the integrated optimal control system on the VSL/RM combined network using the METANET traffic flow model and expressed the VSL impact as $v(k) = v^* b_m(k)$, where $b_m(k)$ is the magnitude of limits ($b_m(k) < 1$). The main objective of the control is to find the minimum total time spent, considering VSL magnitude $b_m(k)$, the ramp queue length, and traffic oscillation costs. After comparing the results of four scenarios—No-Control, Coordinated Ramp Metering, VSL Control, and VSL and RM Integrated Control—they showed that integrated control surpasses other cases and further tested their system on large-scale networks (Carlson, Papamichail, Papageorgiou, & Messmer, 2010a). Despite the outstanding simulation results from the previous work, the VSL and RM integrated control based on the optimal control method encountered challenges in practical applications because of the limitations and restrictions related to practical traffic

systems. To overcome these challenges, Carlson et al. (2011, 2014) further proposed a feedback-based VSL and RM control in which traffic flow modeling and systems objectives were the same as those of the previous work, but instead of optimal control, they chose feedback-based control (Figure 12).

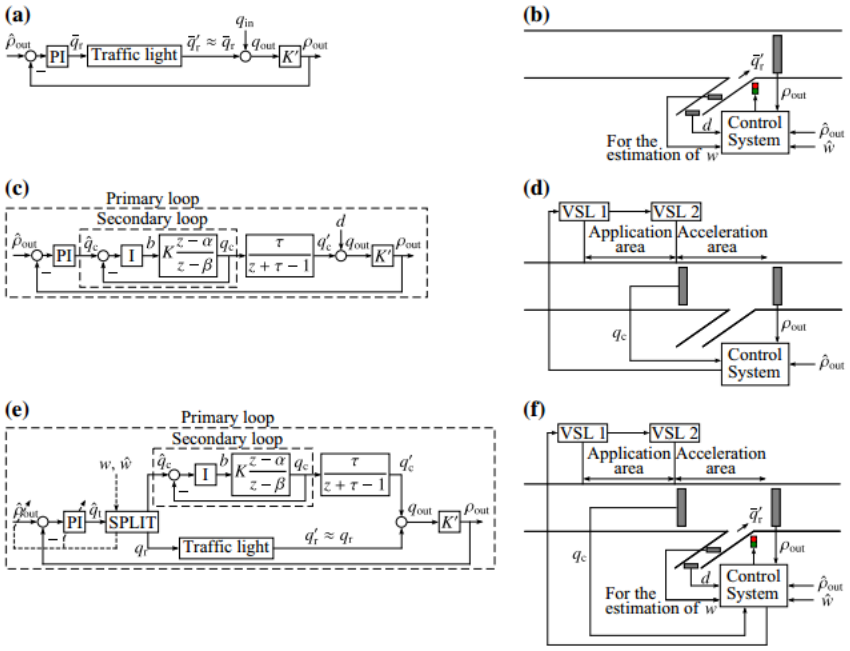

Figure 12 (a) PI-ALINEA (feedback RM); (b) RM network; (c) Feedback VSL; (d) VSL network; (e) feedback integrated control (RM and VSL); (f) RM and VSL Integrated network (Carlson et al., 2014)**.**

Using METANET simulation, the team tested the feedback-based model and compared it to optimal control and several other scenarios. They found that the integrated feedback-based model saves close to the same amount of total travel time as the optimal control model. Although the feedback-based model is not superior to the optimal control model in terms of achievements of the objectives, the authors reported that the feedback-based model is applicable in the real world because it does not use an online model or demand predictions. However, until now, field tests of the strategy have not been conducted. Therefore, to support the practical aspects of VSL, Müller, Carlson, Kraus,

and Papageorgiou (2015) proposed a micro-simulation analysis of VSL using AIMSUN. In their research, they implemented a VSL system similar to the real-world environment, such as ways of applying section-level VSL or point-level VSL, the length of the application area, and the length of the acceleration area (Figure 13). They concluded that section-VSL is preferable to point-VSL, and the shorter application and acceleration areas decrease delay.

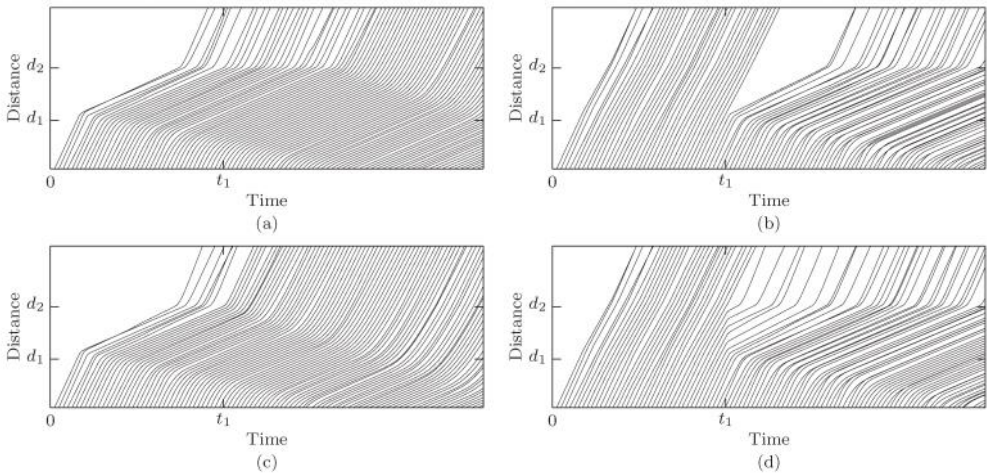

Figure 13 Time-space diagrams of point (P) and section (S) VSL application. (a) P-VSL, increase; (b) P-decrease; (c) S-VSL increase; (d) S-VSL, decrease. (Müller et al., 2015)

2.3.4. Conclusion

Most studies in the literature have found that the RM and the VSL play separate roles in resolving the capacity drop. Although the above-mentioned studied proposed combined VSL-RM, they focused on the control algorithm of the system, not the mechanism of the capacity drop and the VSL-RM. Thus, the studies fail to identify the properties of traffic flow and the practical applicability of the VSL-RM in the real world. In addition, although the VSL-RM studies referred to above includes the length of the queue on the on-ramp in the VSL-RM model, they did not incorporate the queue flush system that is currently in operation in the RM system. In addition, they did not carry out a microscopic analysis of the VSL-RM. In this dissertation, this gap has been filled.

Although several empirical studies have shown the relationship between the VSL and the lane flow distribution, their results are contradictory. These studies also did not present an algorithm of the VSL, but mentioned only that the VSL works to homogenize traffic. In this sense, this dissertation presents a microscopic VSL-RM algorithm and applies it, via experiments, to analyze various lane flow distributions and explain their mechanisms and the system.

CHAPTER III MICROSIMULATION-BASED REAL-TIME CONGESTION PRICING STRATEGY FOR MANAGED LANE

This chapter is adopted from "Hyun W. Cho and Jorge A. Laval (2016), Microsimulation-Based Real-Time Congestion Pricing Strategy for Managed Lane. *Transportation Research Record: Journal of the Transportation Research Board, 2554,* 19–26*"*

A real-time toll that accurately reflects the congestion and delays of a system enhance an HOT lane system. This paper extends an existing system-optimal real-time congestion pricing strategy by relaxing the assumption of constant capacity, which allows us to implement the strategy on a dynamic micro-simulation of the HOT lane, whose capacity and that of general purpose lanes vary because of the weaving activity at the end of the HOT lane. We found that the proposed model is superior in terms of total delay savings, particularly when bottleneck capacities vary significantly. We also found a clear linear relationship between the pricing coefficient and dimensionless delays and the pricing coefficient and revenue. These findings strengthen the system-optimum linear toll pricing strategy and suggest that DOTs can implement practical toll systems that incorporate the real-time discharge rates of bottlenecks.

3.1. Introduction

Although equity has been an issue resulting from priced managed lanes (e.g., high-occupancy toll (HOT) express toll lanes (ETL)), the necessity of express lanes has been widely accepted by users who spend a great deal of time on congested highways. The first carpool-managed (high occupancy vehicle (HOV)) lanes in the U.S. opened in 1969 in the Washington D.C. area, and they have expanded to other metropolitan areas in the country. HOT lanes were initially introduced to fill underutilized HOV lanes, and tolling agencies adopted dynamic pricing strategies based on historical or real-time traffic conditions (C.-L. Chung & Recker, 2011). In addition to these practical approaches, which have been already implemented, many novel pricing strategies have been proposed in the literature. During the last decade, studies have proposed many pricing algorithms and strategies and examined them using simulation methods. G. Zhang et al. (2008, 2009) introduced a feedback-based toll algorithm estimated by a logit model and conducted simulation tests using VISSIM. Morgul and Ozbay (2011) further developed this algorithm and applied it in PARAMICS. Yin and Lou (2009) investigated feedback-controlled and reactive self-learning controlled toll rates, determined pricing strategies based on the point-queue concept, and compared the two approaches using simulation experiments. Another study in Lou et al. (2011) further explored the self-learning approach to combine the effects of lane-changing using the hybrid traffic flow model in Laval and Daganzo (2006). In their studies of HOT lanes of the Florida I-95 express lanes Michalaka, Yin, and Hale (2013) implemented responsive pricing, a closed-loop, control-based algorithm, and time-of-day pricing strategies in CORSIM. Unfortunately, none of these studies focused on system-optimal pricing.

Laval et al. (2015) recently proposed "linear pricing strategies," a real-time system-optimum pricing strategy for toll lanes that minimizes total delay while allowing the operator flexibility to accomplish specific objectives by allocating traffic congestion to HOT or general purpose lanes. One of the principal advantages of this formulation is that main performance measures such as delays, revenues, and assignments are analytical. A stringent assumption, however, is that bottleneck capacities are constant. This study relaxes the constant capacity assumption in Laval et al. (2015) to test the hypotheses (i) that linear pricing strategies are still system optimal and (ii) that the main performance measures follow similar behaviors as in the analytical case. Toward this end, this paper is organized as follows. Chapter 3.2 presents the background and problem formulation. Chapter 3.3 presents linear tolls and new numerical estimated tolls. Chapter 3.4 explains simulation experiments, and Chapter 3.5 analyzes the results of the simulations. This paper ends with a discussion in Chapter 3. 6.

3.2. Problem Formulation

Assuming a freeway corridor with a managed toll lane (MTL) in addition to general purpose lanes (GPL) (Laval et al., 2015), let *A*(t) be the cumulative number of vehicles at time *t* that have entered the freeway segment. All vehicles are bound for a single destination past the GPL bottleneck of capacity μ_0, which may be bypassed by paying toll $\pi(t)$ to the MTL with a bottleneck of capacity μ_1 (see Figure 14).

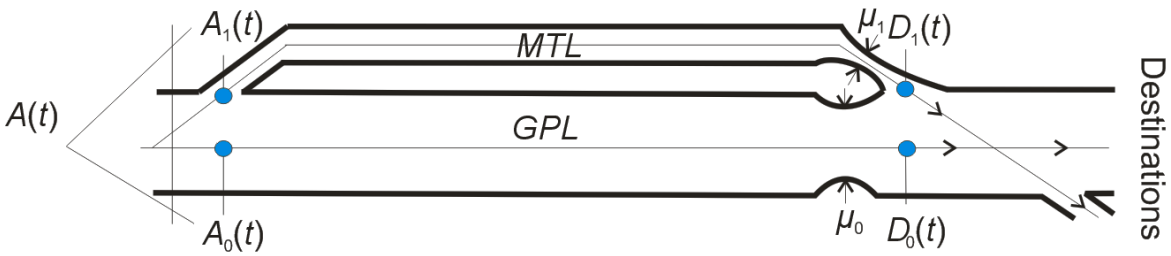

Figure 14 Schematic representation of the network

The cumulative count curve of vehicles using route r (r=0 for the GPL and r = 1 for the MTL) is denoted A_r (t) and the flow, $\lambda_r(t) = \dot{A}_r(t)$. Similarly, the cumulative count curve of vehicles arriving at a destination at time t is denoted D_r (t). Thus,

$$\lambda(t) = \lambda_0(t) + \lambda_1(t), \tag{1}$$

and $\lambda(t)$ is assumed unimodal. Let τ_r (t) be the travel time in route r experienced by a user arriving at time t:

$$\tau_r(t) = \tau_r + w_r(t), \tag{2}$$

where τ_r is the free-flow travel time and w_r (t) the queuing delay, which can be expressed as

$$w_r(t) = \frac{A_r(t) - D^*_r(t)}{\mu_r}. \tag{3}$$

The bottleneck is located at the end of the network near the destination. The virtual departure number of vehicle $D^*_r(t)$ can be obtained as follows:

$$D^*_r(t) = \mu_r \cdot \tau_r + D_r(t), \tag{4}$$

when first-in-first-out is assumed. Later, we will relax the assumption that bottleneck capacity μ_r is constant. In Laval et al. (2015), $\Delta = \tau_0 - \tau_1$; the extra free-flow travel time for using the free alternative GP lanes is assumed to be non-zero for maximum generality. However, for simplicity, in this paper, we focus on a case when $\Delta = 0$.

3.2.1. User-Equilibrium Condition with Pricing

According to (Laval et al., 2015), the user-equilibrium condition, in which the costs of the travel times on both routes are the same, can be expressed as

$$\rho_0(t) = \rho_1(t) + \dot{\pi}(t), \tag{5}$$

where we have defined demand-capacity ratios $\rho_r(t) = \frac{\lambda_r(t)}{\mu_r}, r = 0,1$. Note that (5) is applicable only when the initial condition is in the UE. Substituting (1) into (5) generates the UE assignment when both alternatives are used:

$$\rho_0(t) = \rho(t) + \bar{\mu}_1\dot{\pi}(t), \tag{6a}$$

$$\rho_1(t) = \rho(t) - \bar{\mu}_0\dot{\pi}(t), \tag{6b}$$

where $\bar{\mu}_r = \mu_r/\mu$ and $\mu=\mu_0+\mu_1$, and $\rho(t) = \lambda(t)/\mu$, the demand-capacity ratio. The equation shows that for constant tolls ($\dot{\pi}(t) = 0$), the UE condition implies that each alternative and the system have the same demand-capacity ratio.

3.2.2. System Optimum

For the present problem, the system-optimum solution for this type of network, which minimizes the total system delay, was first introduced in Muñoz and Laval (2005) and specialized in Laval et al. (2015). If we let t_0 and T_0 be the time when the system begins and ends congested, then the SO solution reads (see Figure 3 in Laval et al. (2015))

1) $t < t_0, t > T_0$; both lanes at free-flow: $\pi(t) = 0, \rho_0(t) = \rho_1(t)$
2) $t_0 < t < T_0$; $\pi(t) = \tau_0(t) - \tau_1(t),\ \rho_0(t) \geq 1,\ \rho_1(t) \geq 1.$

Note that this solution says nothing about the alternative-specific arrivals during the interval time of t_0 and T_0, which suggests that they are not unique in this time range. This

indicates that as long as the system maintains the maximum bottleneck capacity during congested periods, queues can be stored in either alternative.

3.2.3. Linear Tolls

Like Laval et al. (2015), we propose linear tolls defined with constant parameter *a*, called the pricing coefficient, such that

$$\dot{\pi}(t) = (\rho(t) - 1)a, \quad t_0 \le t \le T_0, \tag{7}$$

or equivalently (letting t_0=0),

$$\pi(t) = \frac{(A(t)-\mu t)a}{\mu}, \quad t_0 \le t \le T_0, \tag{8}$$

which suggests that the toll is proportional to the system delay. Under linear toll pricing, the flow assigned to each alternative (ρ_0, ρ_1), delays (W_0, W_1), and revenue (R) are linear functions of the pricing coefficient, *a*; that is,

$$\rho_0(a,t) = (1 + a\bar{\mu}_1)\rho(t) - a\bar{\mu}_1, \qquad t_0 \le t \le T_0 \tag{9a}$$

$$\rho_1(a,t) = (1 - a\bar{\mu}_0)\rho(t) + a\bar{\mu}_0, \qquad t_0 \le t \le T_0 \tag{9b}$$

$$\frac{W_0(a)}{W} = (1 + a\bar{\mu}_1)\bar{\mu}_0, \tag{9c}$$

$$\frac{W_1(a)}{W} = (1 - a\bar{\mu}_0)\bar{\mu}_1, \tag{9d}$$

$$\frac{R(a)}{W} = a\bar{\mu}_1, \tag{9e}$$

Note that all performance measurements (i.e., assignments, delays, and revenue) in our problem are not only linear functions of pricing coefficient *a* but also linear functions of all the constants that define the problem. (For a proof of equations 9a-9e, see Results 4.1. in Laval et al. (2015).)

3.3. Linear Tolls and Variable Bottleneck Capacity

Although bottleneck capacity might be assumed constant in some cases (Cassidy & Bertini, 1999), the proportion of exiting vehicles can drastically change freeway discharge flows (Muñoz & Daganzo, 2002). Therefore, we explore the scenario in which bottleneck capacities in our system vary with the dynamics of traffic congestion. Assuming that the bottleneck capacity is a time-dependent variable, we calculate the predictive travel time based on the bottleneck capacity at current time *t*, $\mu(t)$, as in Figure 15.

$$\tau(t) = \frac{A(t)-D(t)}{\mu(t)}. \quad (10)$$

Although the predicted travel time is the simplest estimation for vehicles arriving at time *t*, it has an obvious prediction error because of the variation in time-dependent bottleneck capacity (see Figure 15):

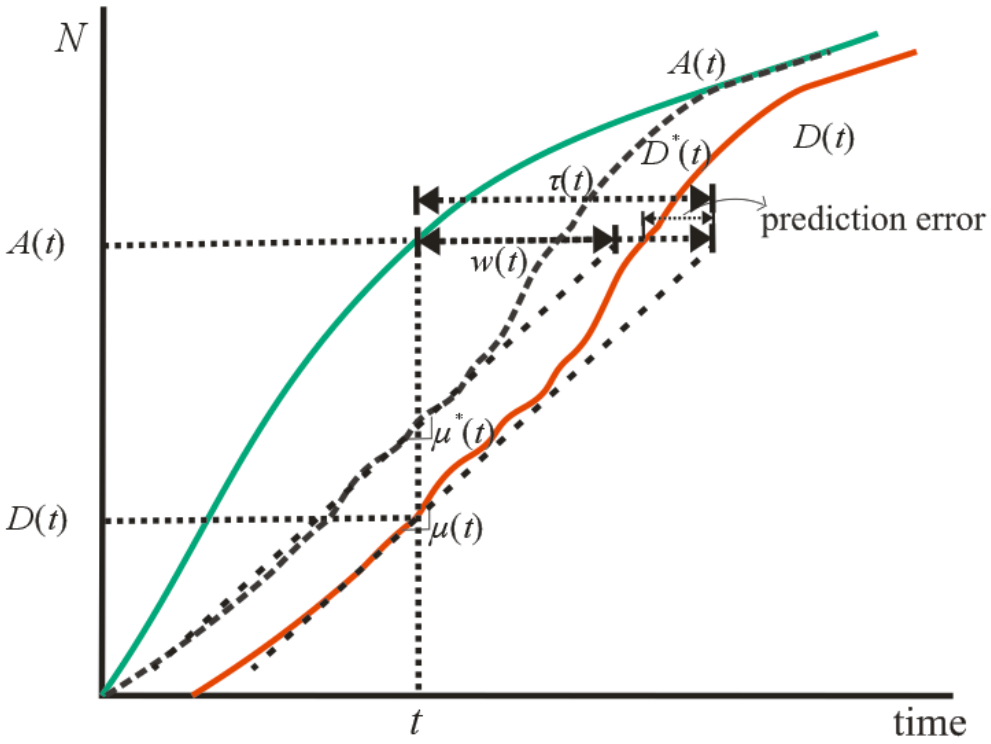

Figure 15 Input-output diagram of the linear toll pricing strategy of the variable bottleneck capacity model

In the variable bottleneck capacity model, we express the real-time linear toll (8) as

$$\pi(t) = aw(t) = a\frac{A(t)-D^*(t)}{\mu^*(t)}, \tag{11}$$

where $D^*(t)$ is the virtual departure curve at the entrance of the bottleneck (i.e., a shift of the original departure curve, $D(t)$, to the left with the amount of free-flow travel time) and $\mu^*(t) = \frac{dD^*(t)}{dt}$. Under the assumption that $\mu(t) \approx \mu^*(t)$, the toll is proportional to the predicted delay at time *t*. Incorporating (10) and (11) into the UE condition (5) yields

$$\rho_0(t) = \rho(t) + \bar{\mu}_1(t)\dot{\pi}(t) + \frac{\tau_0(t)}{\mu_0(t)}\bar{\mu}_1(t)\dot{\mu}_0(t) - \frac{\tau_1(t)}{\mu(t)}\dot{\mu}_1(t) \tag{12a}$$

$$\rho_1(t) = \rho(t) - \bar{\mu}_0(t)\dot{\pi}(t) + \frac{\tau_1(t)}{\mu_1(t)}\bar{\mu}_0(t)\dot{\mu}_1(t) - \frac{\tau_0(t)}{\mu(t)}\dot{\mu}_0(t) \tag{12b}$$

where $\dot{\pi}(t) = \frac{a\left(\left(\lambda(t)-\mu^*(t)\right)\dot{\mu^*}(t)-\left(A(t)-D^*(t)\right)\dot{\mu^*}(t)\right)}{\mu^*(t)^2} = a(\rho^*(t)-1) - \pi(t)\frac{\dot{\mu^*}(t)}{\mu^*(t)}$ (12c)

Unfortunately, unlike the equations in (9), the derivations of the analytical solutions for delay, $\int\left(A(t) - D^*(t)\right)dt$, and revenue, $\int A_0(t)\pi(t)\,dt$, quickly become intractable. To observe such intractability, note that $A_0(t) = \int \rho_0(t)\,\mu_0(t)\,dt$. In the following section, to analyze the quantities of the variable bottleneck capacity real-time linear toll model, we use simulation that incorporates a numerical approach.

3.4. Simulation Experiments

In this section, we compare the following real-time strategies using the simulation model *GTsim* (Chilukuri, Laval, & Guin, 2014a):

- CLT: Constant bottleneck capacity Linear Toll pricing strategy, i.e., eqn. (8) and (9a,b) with $\mu_r = \mu_r(t)$
- VLT: Variable bottleneck capacity Linear Toll pricing strategy, i.e., eqn. (11) and (12a,b)

In both cases, bottleneck capacities $\mu_r(t)$ at every time step are calculated as a three-minute moving average of the discharge flow immediately downstream of the weaving section provided that the density is overcritical (see Figure 16). In the figure, traffic demand heads eastbound, the top lane is the MTL (in blue), and other lanes are GPL (in red). From equations (8b) and (12b), the calculated number of MTL vehicles is directly inserted into the beginning of the MTL section of the diagram, which prevents the formation of bottlenecks upstream because of the lane-change behaviors of vehicles. The MTL ends 1 km upstream of an exit ramp, creating bottlenecks. Note that we assume that the MTL is barrier-separated, so we neglect the effects of friction, enabling the exit flow from both lanes to be the main parameter of the formation of congestion.

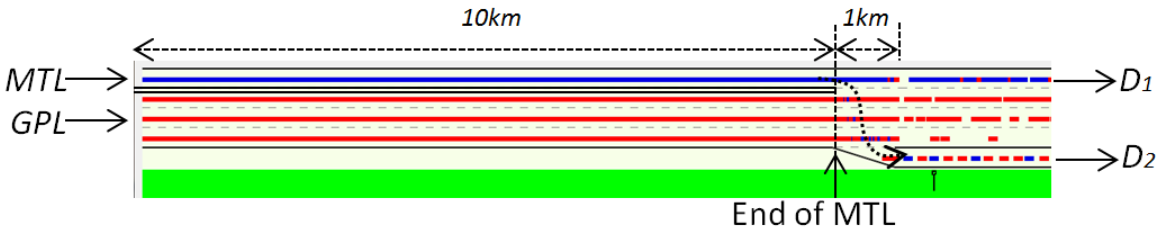

Figure 16 Diagram of the simulation model

We set traffic demand as follows: $\lambda(t)$ is 7,500vph in t < 4,200s, and 4,000vph in $t \geq$ 4,200s. Note that ideal capacity (without capacity drop) is 2,500$vph/lane$. If p represents the exit proportion of both the MTL and GPLs, which varies according to Figure 17, in $t \geq$ 4,200s, we set p at 0.25 to dissipate congestion in a timely manner.

Figure 17 Variability of exit proportion (p) according to changes in time

We simulated two-hour experiments that include the formation and the dissipation of queues in all lanes and update tolls and vehicle assignments to lanes every two minutes; that is, in both cases, the same toll lasts for a two-minute period. Under the CLT, we set the toll using (8) by changing the pricing coefficient, *a*, which determines the weighted value of a toll with delays in the range of 0.4~ 1.4 at intervals of 0.2, and calculate traffic assignments using (9a, b). Although the bottleneck capacity $\mu_r(t)$ can change in time at every time step, we assume a strategy in which the bottleneck capacity is constant ($\mu_r = \mu_r(t)$) for a two-minute period in equations (8) and (9a, b). In the VLT, we determine the toll by (11), also by changing the pricing coefficient *a* as in CLT, and allocate traffic using (12). This method requires the time derivative of the bottleneck capacity $\mu_r(t)$, which we approximate using Euler's method, that is, the rate of change of the bottleneck capacity within two consecutive time steps:

$$\mu_r(t_j) = \mu_r(t_{j-1}) + \Delta t \dot{\mu}_r(t_{j-1}). \quad (13)$$

In the following, we will investigate the performance of each strategy in terms of social costs (delays) and benefits to the operator (revenue) and verify our results with analytical equations whenever possible.

3.5. Results

3.5.1. Delays

The total delays (in units of *veh·hr*) of the CLT and VLT pricing strategies, the sum of GPL delay (W_0) and MTL delay (W_1) are summarized in Figure 18 (a), (b). The total delay appears to be independent of pricing coefficient *a*, which is consistent with our theoretical results indicating that the total delay, *W*, is a constant, independent of the pricing coefficient. The average values of the total delay of the CLT and the VLT were 1,053 and 1,027, respectively. We found that VLT is superior to CLT with an average of 3% savings in the total delay. Specific proportions of savings of the VLT are displayed in Figure 18 (b).

Interestingly, MTL delay decreases, and GPL delay increases as the pricing coefficient *a* increases in the CLT and VLT strategies. This tendency reminds us of equation (9d) of the linear tolls strategy.

$$\frac{W_1(a)}{W} = (1 - a\bar{\mu}_0)\bar{\mu}_1 = ac_1 + c_0. \quad (14)$$

To verify (14) with our results, we extracted the values of $\bar{\mu}_0, \bar{\mu}_1$ of each strategy from the simulation when the pricing coefficient $a = 1$, as in Figure 19. Note that these values are measured only when the bottleneck is active. The figure shows that the bottleneck capacity of the MTL μ_1 remains nearly constant for both cases, but the bottleneck capacity of the GPL μ_0 fluctuates responding to the changes in the exit proportion (*p*). In this sense, obtaining a representative value of bottleneck capacity of GPL is difficult. However, Figure 20 shows that the ratio of MTL delay to total delay has a linear relationship with the pricing coefficient *a*.

(a) CLT Delays

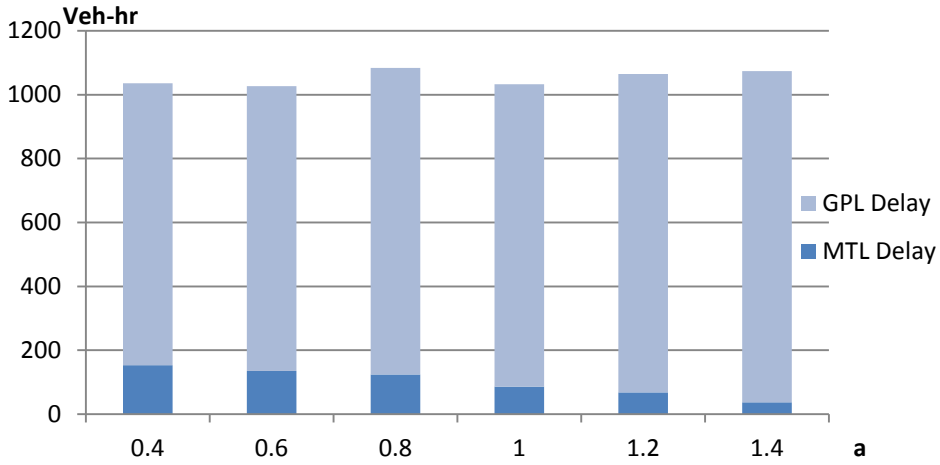

(b) VLT Delays

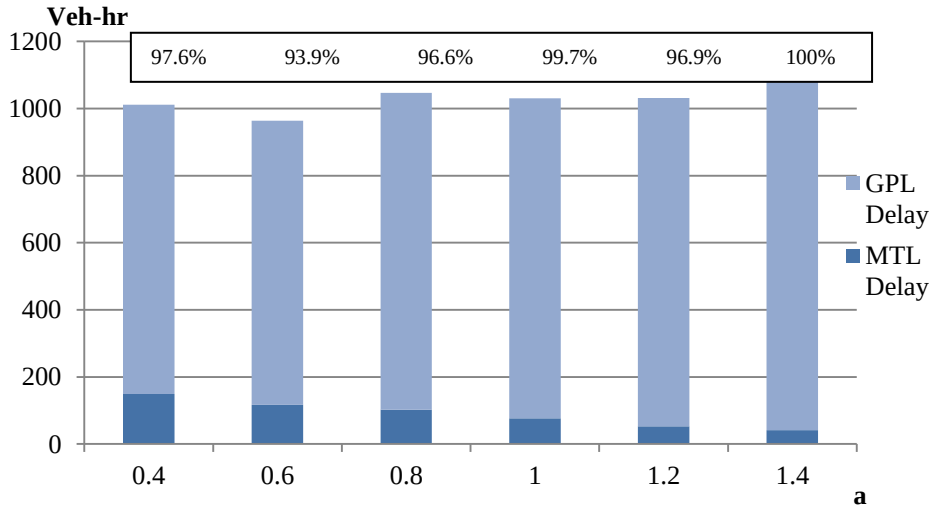

Figure 18 Total delays of pricing strategies (a) CLT and (b) VLT

(a) CLT bottleneck capacity **(b) VLT bottleneck capacity**

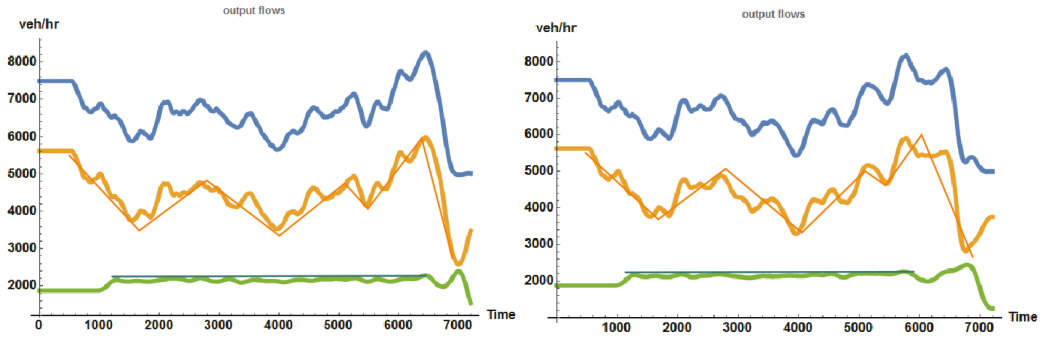

Figure 19 Bottleneck capacity as time changes for all lanes (blue), GPL (yellow), and MTL (green); (a) CLT (b) VLT, *a*=1.0

(a) CLT W_1/W **(b) VLT W_1/W**

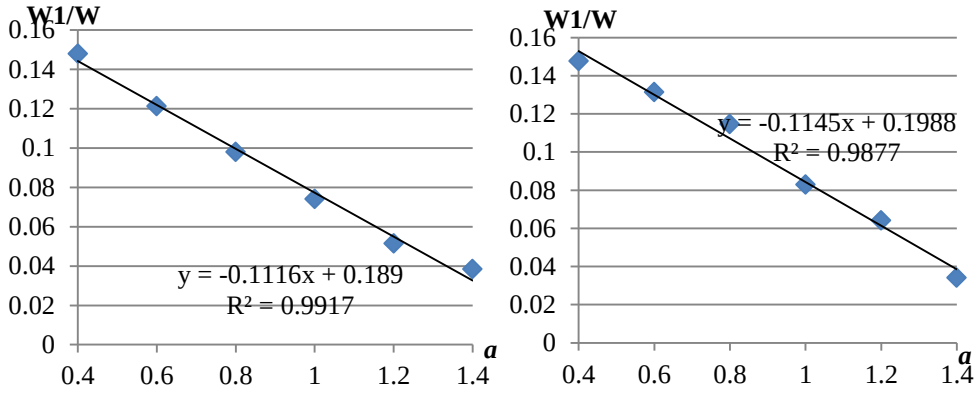

Figure 20 Relationships between W_1/W and *a* in (a) the CLT and (b) the VLT

3.5.2. Revenues

The revenue for each pricing strategy is summarized in Figure 21.

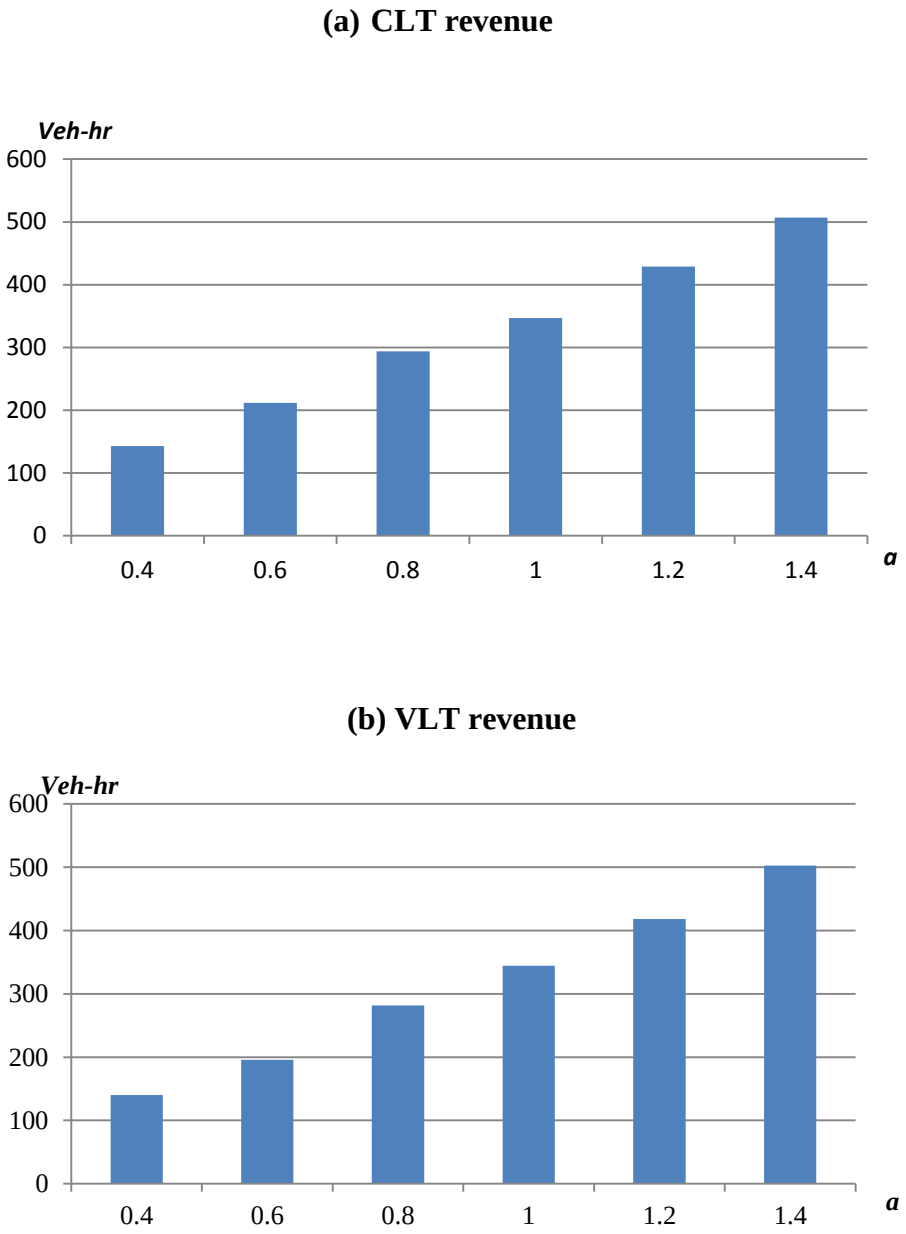

Figure 21 Revenue of pricing strategies in (a) the CLT and (b) the VLT

One can examine the benefit-cost ratio in our experiments by interpreting total delay (W) as a social cost and revenue (R) as a private benefit to the operator. In the case of linear toll pricing, this ratio is given by equation (9e):

$$\frac{R(a)}{W} = a\bar{\mu}_1 = ac_1 + c_0. \tag{15}$$

From the simulation results, coefficients c_1 and c_0 of (15) are estimated by the linear regression equations in Figure 22 (a) and (b).

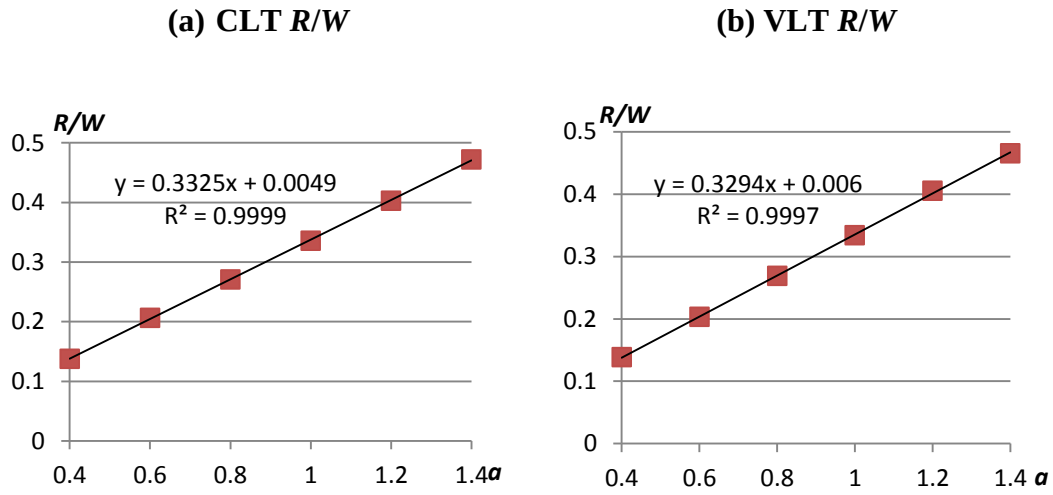

Figure 22 Relationships between $R(a)/W$ and a in (a) the CLT and (b) the VLT

In addition, we directly extracted the 1- σ range and the average value of $\bar{\mu}_1$ of CLT and VLT (see Figure 23).

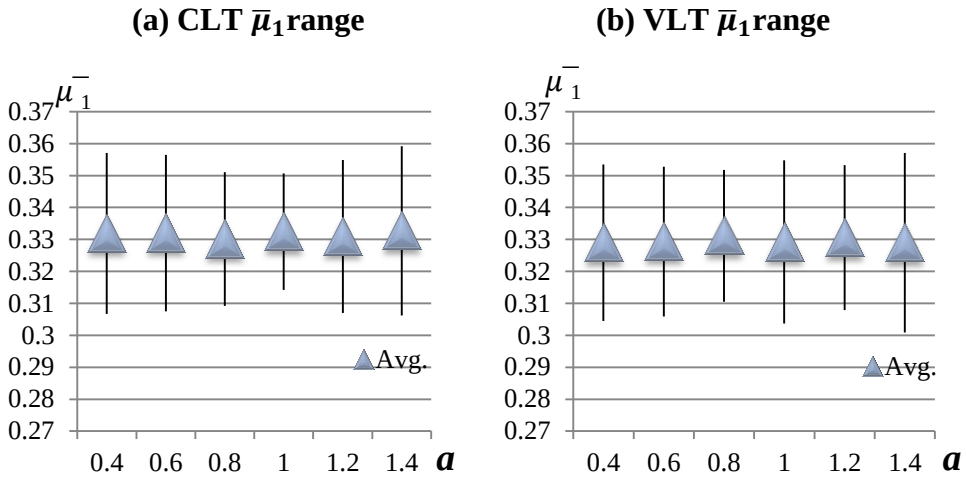

Figure 23 Averages and 1-σ ranges $\bar{\mu}_1$ of the CLT and the VLT

We compared the 95% confidence intervals of these coefficients, presented in Table 1. The table shows the 1-σ range of $\bar{\mu}_1$; it also shows that c_1 covers the confidence intervals of the coefficients of the CLT and VLT regression equations, which indicates that our simulation results partially comply with the analytical expression (9e).

Table 1 Comparison of the regression equation (15) and the coefficients of the simulation results

		c_1	c_0
CLT	Reg. eq.(15)	(0.3231, 0.3414)	(-0.004, 0.015)
	Simulation	(0.3085, 0.3549)	0
VLT	Reg. eq.(15)	(0.3166, 0.3439)	(-0.009, 0.019)
	Simulation	(0.3056, 0.3538)	0

3.5.3. Constant Exit Proportion

In experiments, we examined three cases with constant exit proportions p=0.2, 0.25, and 0.30. As in the previous cases, we found that delays and revenue follow a linear relationship with the pricing coefficient a. However, compared to the CLT strategy, the

VLT strategy did not show any meaningful improvement in savings of delay. As expected, this finding comes from equation (13), in which the rate of change $\dot{\mu}_r(t_{j-1})$ is nearly zero, resulting in virtually the same VLT and CLT.

3.6. Discussion

To develop a toll strategy that more accurately predicts the status of traffic when bottleneck capacity changes, we proposed and simulated a variable bottleneck capacity model and compared it to the constant bottleneck capacity model. The proposed model showed a greater savings in the total delay than the latter model. Interestingly, we found that equation (8) implied that the toll was proportional to the total system delay, which we observed in a real system in California. The California Department of Transportation (DOT) has applied dynamic congestion pricing to SR-91 Express Lanes under a time-of-day setting for maintaining traffic flow at free-flow speeds. The Orange County toll authority has monitored hourly traffic volumes and adjusted the toll every six months if traffic volumes consistently exceeded a given threshold. Figure 24(a) depicts the weekday toll rate for eastbound traffic on July 2014. Using the California DOT's Performance Measurement System (PeMS) data, we found that the SR-91 toll rate was similar in shape to the total delay experienced by users. The average delay of the weekday on July 2014 for the tolled section of SR-91(27~37 Postmile range) is shown in Figure 24 (b). A comparison of Figure 24 (a) and (b) show similar time range and peak amplitude, suggesting that linear pricing strategies proposed in this paper are not only theoretically appealing but also spontaneous in real systems. Implementing the linear pricing strategy and variable bottleneck capacity model in the real world requires further study such as an analysis of the price elasticity of HOT lane demand, data that include the proportions of exit traffic to all traffic in HOT lanes, and other valid data.

(a) SR-91E Toll Rate

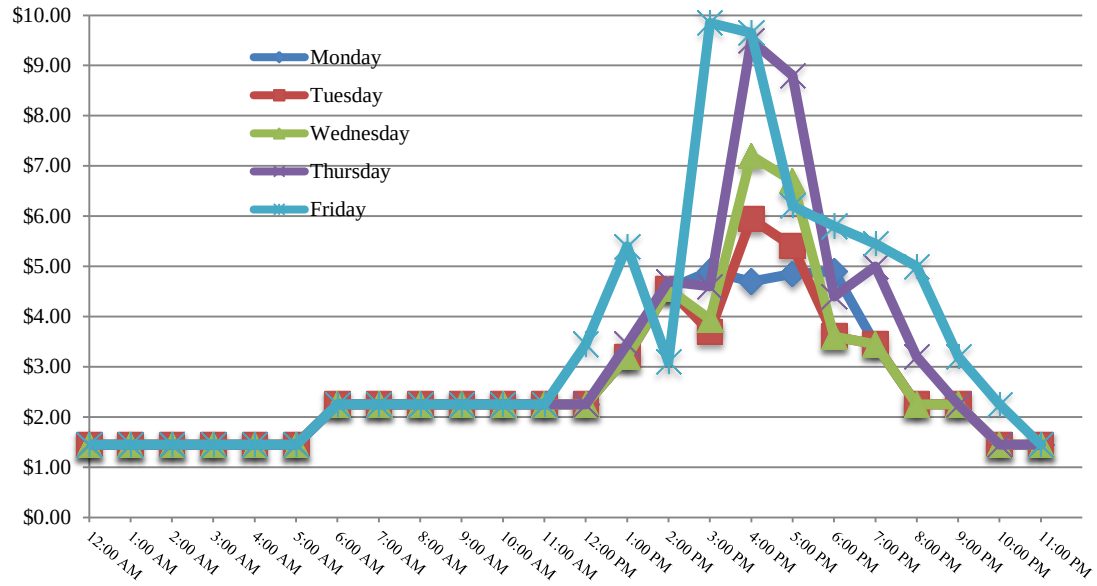

(b) Delay ($V_{threshold}$ = 60*mph*)

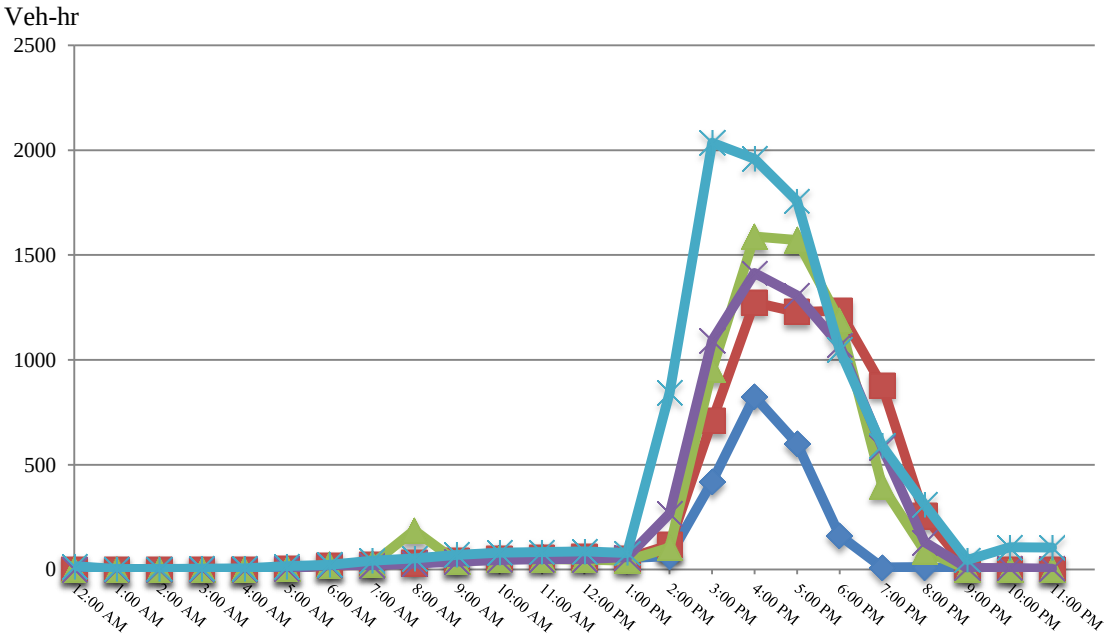

Figure 24 (a) toll rate of SR-91 eastbound on weekdays (July 2014); and (b) average delay of SR-91 eastbound on weekdays (July 2014)

CHAPTER IV COMBINED VARIABLE SPEED LIMIT AND RAMP-METERING SYSTEM FOR CAPACITY DROP CONTROL AT MERGE BOTTLENECK

This chapter investigates the effectiveness of a variable-speed-limit and ramp-metering (VSL-RM) control strategy that prevents and promotes recovery from capacity drops at freeway merge bottlenecks. By combining both kinematic wave theory and the RM concept, this study fills the gap between the two approaches by designing a VSL system that acts as a mainline RM. Toward this end, this chapter is organized as follows. Chapter 4.1 presents the problem formulation. Chapter 4.2 presents the VSL system model that prevents and recovers capacity drop, and Chapter 4.3 discusses one-lane merge and three-lane merge networks' simulation experiments and their results, and Chapter 4.4 concludes.

4.1. Problem Formulation

Consider an isolated merge bottleneck as illustrated in Figure 25, with λ_0 and λ_1, representing the demands of the mainline and the on-ramp, respectively, and μ_2, representing the capacity of the bottleneck, located in the merge area. Because of the capacity drop phenomenon, when queues form, the bottleneck capacity drops from μ_C to μ_2 (see Figure 26). According to Newell-Daganzo's merge model (Daganzo, 1995, 1996), traffic transitions at the merge depend on supply (μ_2, μ_C) and demand (λ_0, λ_1) (Figure 27). Our model assumes that total demand ($\lambda_0 + \lambda_1$) exceeds bottleneck capacity μ_2 so that current traffic is located in areas $A_2, A_3,$ and A_4 in Figure 27. In these areas, only flows q_0 and q_1 can enter the bottleneck, and queues form if these amounts exceed $(\lambda_0 - q_0, \lambda_1 - q_1)$.

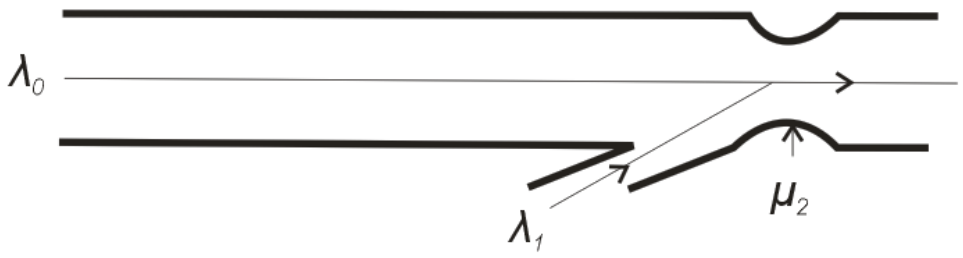

Figure 25 Isolated bottleneck at a merge area

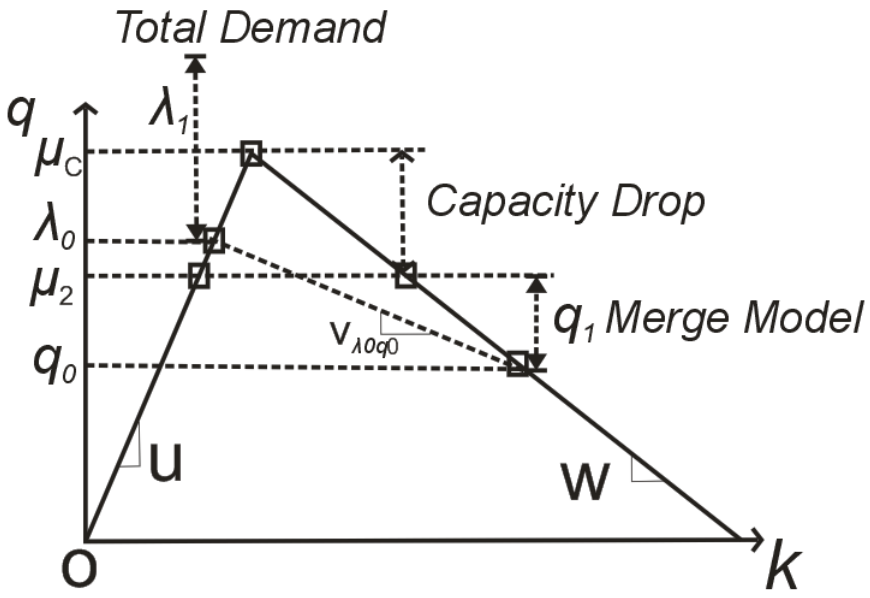

Figure 26 Capacity drop at a merge area

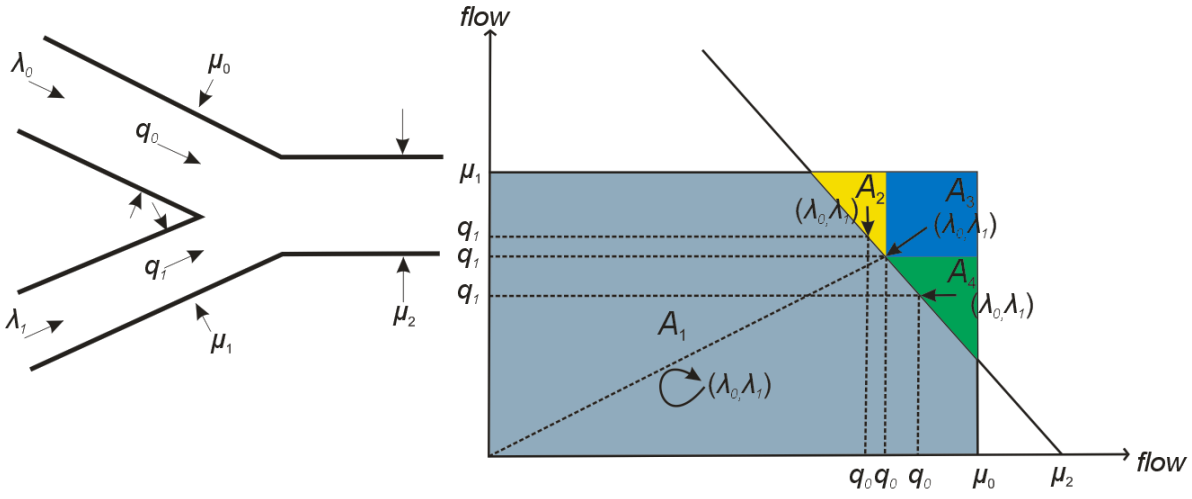

Figure 27 Newell-Daganzo merge model

4.2. Model

This section presents a VSL and ramp-metering strategy that controls traffic upstream of the merge area so that the traffic status switches from areas A_2, A_3, A_4 to area A_1, shown in Figure 27, and results in increasing the bottleneck capacity of μ_2 to μ_c.

4.2.1. Preventing capacity drop using VSL

The VSL section, located upstream of the merge bottleneck (see Figure 28), is composed of two zones: a speed limit zone and an acceleration zone. The vehicles follow the posted speed limit when they travel within the speed limit zone and accelerate to free-flow after they pass the acceleration zone. Without RM, one scenario that could prevent capacity drop is to assign priority to the on-ramp flow, thereby preventing a queue from forming in the on-ramp (see Figure 29). The figure presents an initial traffic condition A_1 of a merge model showing that the initial total demand is less than the freeway capacity, and a queue has not yet formed and a capacity drop has not occurred. After some time, suppose that the on-ramp flow demand increases and that the total demand exceeds the freeway capacity. At this point, we activate the VSL zone, with l_1 representing the length of the VSL zone and l_2 the length of the acceleration zone.

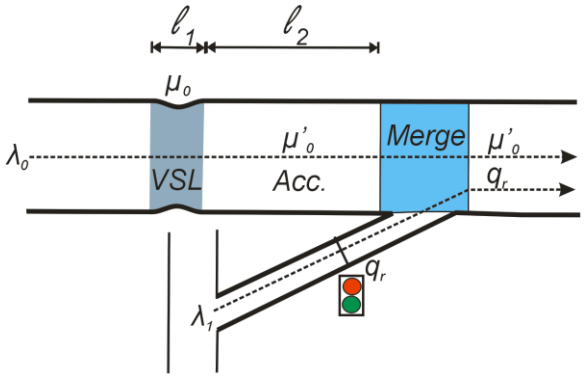

Figure 28 VSL upstream of the merge area

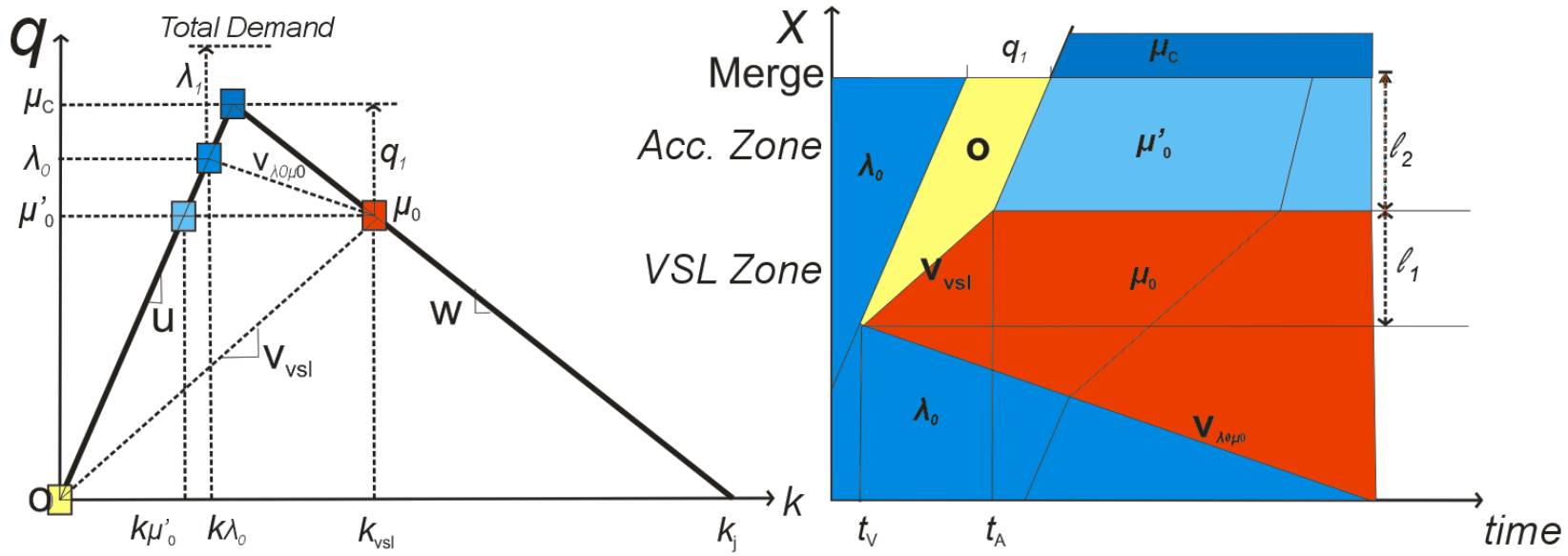

Figure 29 Mainline fundamental diagram and time-space diagram representation of a strategy for eliminating on-ramp queues

As illustrated in the fundamental diagram in Figure 29, the speed in the limit zone, v_{vsl}, is given by

$$\mu_c - q_1 = w(k_j - k_{vsl}) = v_{vsl}k_{vsl}. \quad (1)$$

where μ_c is the maximum flow without a breakdown and q_1 (= λ_1) is the on-ramp flow. Note that $\mu_c, w,$ and k_j are constants, and k_{vsl} is determined by the selection of q_1.

Let t_v and t_A represent times when the first VSL-applied vehicle enters the VSL zone and the acceleration zone, respectively. At time t_v the flow in the VSL zone becomes μ_0, and the density of the VSL zone becomes k_{vsl}. After t_A, the flow of the acceleration zone becomes μ'_0 because VSL-applied vehicles do not begin to accelerate after the lead vehicle accelerates, but instead, they exit the VSL zone and enter the acceleration zone. Assuming that vehicles accelerate to a free-flow speed quickly, the density of the acceleration zone decreases from k_{λ_0} to $k_{\mu'_0}$. This decrease creates more space for lane changing for the on-ramp flow, reducing the probability of a capacity drop.

We found two possible by-products of this system. When VSL is activated, the state of the traffic downstream of the first VSL-applied vehicle becomes the void state (*O* in the figure). Although this void induces a loss of capacity for a moment, it is useful, a topic that will be discussed in the next section. The potential drawback is that the queue forms upstream of the VSL zone in state μ_0 with shock speed $V_{\lambda 0 \mu 0}$. We will show that as long as this shock does not reach the upstream ramp, benefits can be expected. To clarify this point, we illustrate the cumulative counts of vehicles at the beginning and end of the network in Figure 30. Solid lines represent the demand for each route, dashed lines depict the capacity drop situation (without the VSL), and dotted lines show the

application of the VSL system. When VSL is applied, the slopes of the departure rate become steeper than they do when it is not applied, so the total travel time decreases.

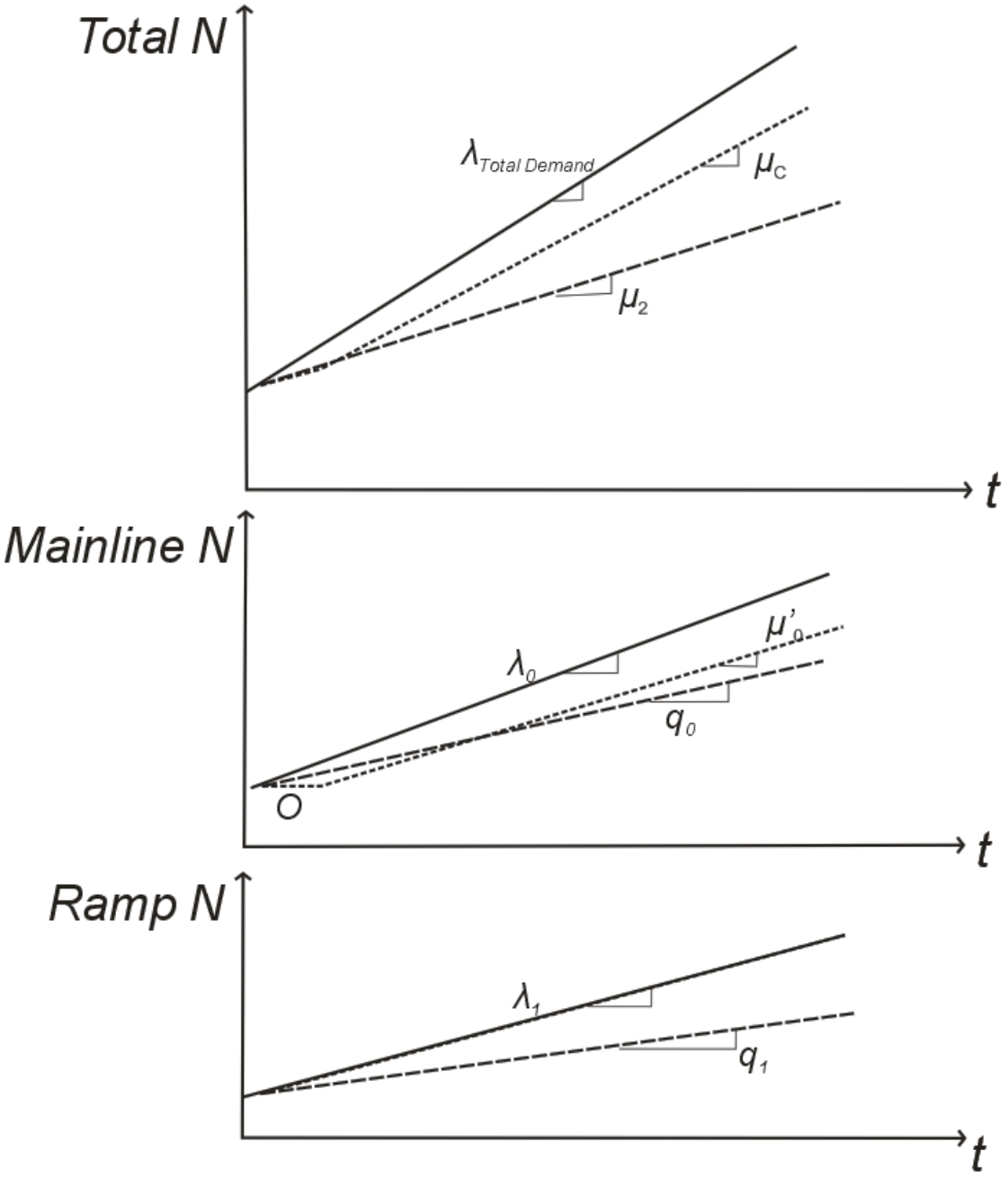

Figure 30 Cumulative count curves of the capacity drop and the VSL

4.2.2. Combined VSL and RM Model

In the previous section, we presented a VSL model that assigns priority to on-ramp traffic flow. However, this model may deteriorate mainline flow when on-ramp flow is abnormally high. To compensate for this problem, we propose a method combining RM and the VSL that provides more flexibility in operation than the previous VSL system alone. Let us assume that $q_{1'\,RM}$ is the ramp metered rate; we then calculate the speed of the VSL and other corresponding traffic parameters from the following equation, which is similar to equation (1); that is,

$$\mu_c - q_{1'\,RM} = w\left(k_j - k_{vsl}\right) = v_{vsl}k_{vsl}. \tag{2}$$

The ramp-metering flow can be determined by the following methods:

Method 1: This method enhances mainline safety by maintaining speed v_{vsl} only slightly less than the previous mainline travel speed. This method predetermines v_{vsl} (e.g., $v_{vsl} = v_{free-flow} - 10_{mph}$) and then calculates ramp flow $q_{1'\,RM}$.

Method 2: This method uses the RM algorithm ALINEA (Papageorgiou et al., 1990, 1997) (see Chapter 2):

$$r(t) = r(t - \Delta t) + K_R\left(\hat{o} - o_{out}(t)\right), \tag{3}$$

where $r(t)$ and $r(t - \Delta t)$ are the metering flow rates of the current and previous time steps (Δt is the length of the time period of updates), respectively, $o_{out}(t)$ is the occupancy of the current time step, and K_R is the constant defined by the operator.

In addition to enhancing flexibility and safety, the combined RM and VSL method fills the void (*O*) upstream of the first VSL-applied vehicle, explained in the previous section, by controlling on-ramp flow. If we assume a given low metering rate

and the formation of a queue behind the ramp signal, then both period (*T*) and maximum length (*L*) of void *O* are given by

$$T = l_1(\,{}^{1}\!/_{v_{vsl}} - {}^{1}\!/_{v_f}) \tag{4}$$

$$\mathrm{L} = \begin{cases} l_2, & v_f \cdot T = l_2 \\ v_f \cdot T, & v_f \cdot T < l_2 \\ l_2 + \ (l_1 - v_{vsl} \cdot {}^{(l_1 + l_2)}\!/_{v_f}), & v_f \cdot T > l_2 \end{cases} \tag{5}$$

The number of free-flow accelerated vehicles from the queue at the on-ramp that can fill void *O* is $Q(t_{b'} - t_{a'})$, where *Q* is the capacity of the lane, $t_{b'}$ is the time that the first VSL-applied vehicle passes the merge line, and $t_{a'}$ is derived by $\frac{w}{w+v_{free-flow}} t_{b'}$, where the time that the last free-flow vehicle passes the merge is zero without loss of generality; see Figure 31.

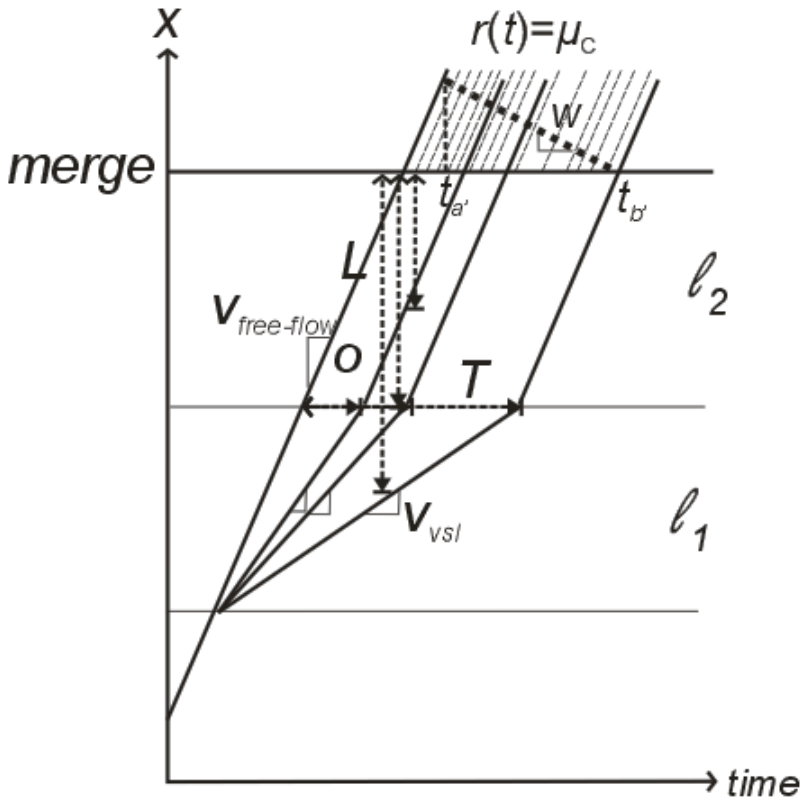

Figure 31 Time-space diagram of metering rate during the void period

Method 3: This method, which uses the maximum metering rate of the ramp, $r(t)$ during period *T*, can be expressed as

$$r(t) = \mu_c, \tag{6}$$

We extend our problem to the recovery of the capacity drop. Assume that abrupt high demand of on-ramp traffic induces a capacity drop, illustrated in Figure 26. To resolve the capacity drop, an RM system restricts on-ramp flow up to the lowest metering rate, which is sufficient not to interrupt mainline flow at time t_{min_R}. As the mainline flow is protected from the on-ramp flow, the capacity is recovered to μ_c (Cassidy & Rudjanakanoknad, 2005), and the queue in the mainline diminishes and clears. When the

mainline queue clears, we activate the VSL at time $t_{VSL_{On}}$, as in Figure 29, to prevent the recurrence of the capacity drop. Also, using Method 3, we impose the metering rate of the ramp during the void period, $r(t) = \mu_c$, which flushes the on-ramp queue. Figure 32 illustrates a time-space diagram of the integrated system. The figure shows that the entrance of the VSL zone meets the back of the queue at time VSL activation $t_{VSL_{On}}$. With current technology, the VSL zone, or speed limit signs, are prefixed, and VSL activation time $t_{VSL_{On}}$ is determined from RM activation time t_{min_R}.

The corresponding cumulative count curves of Figure 32 are illustrated in Figure 33. The solid and dashed lines are similar to those in Figure 30; dash-dotted lines depict the combined RM and VSL strategy. As expected, while the mainline flow rate increases after the ramp flow is metered, the ramp flow rate decreases until the queue clears and initiates the VSL. However, the total flow rate increases significantly so that the total travel time decreases. The following section presents a simulation approach that verifies the proposed strategy.

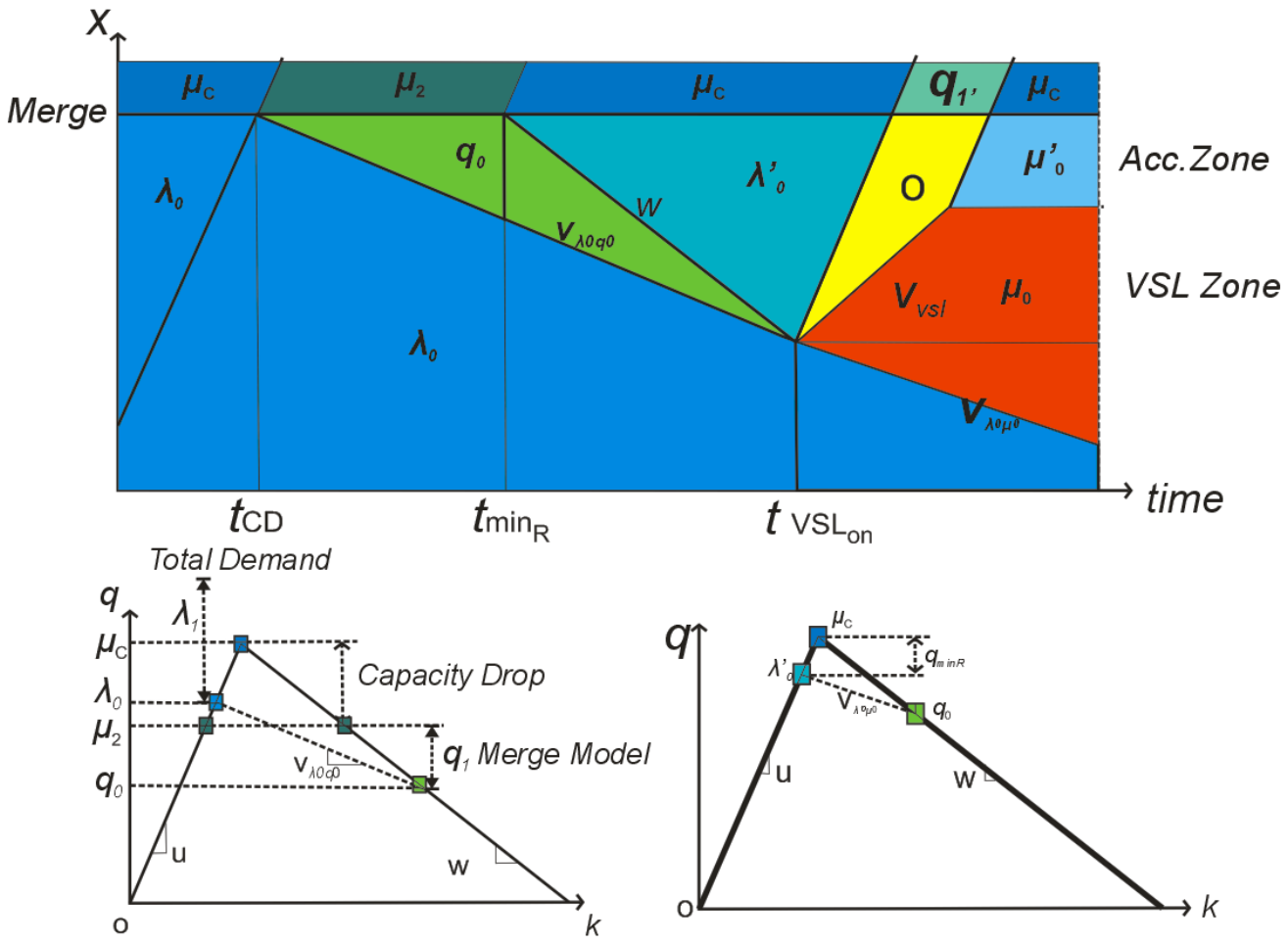

Figure 32 Time-space diagram of the recovery of the capacity drop using the integrated RM and VSL model for mainline traffic

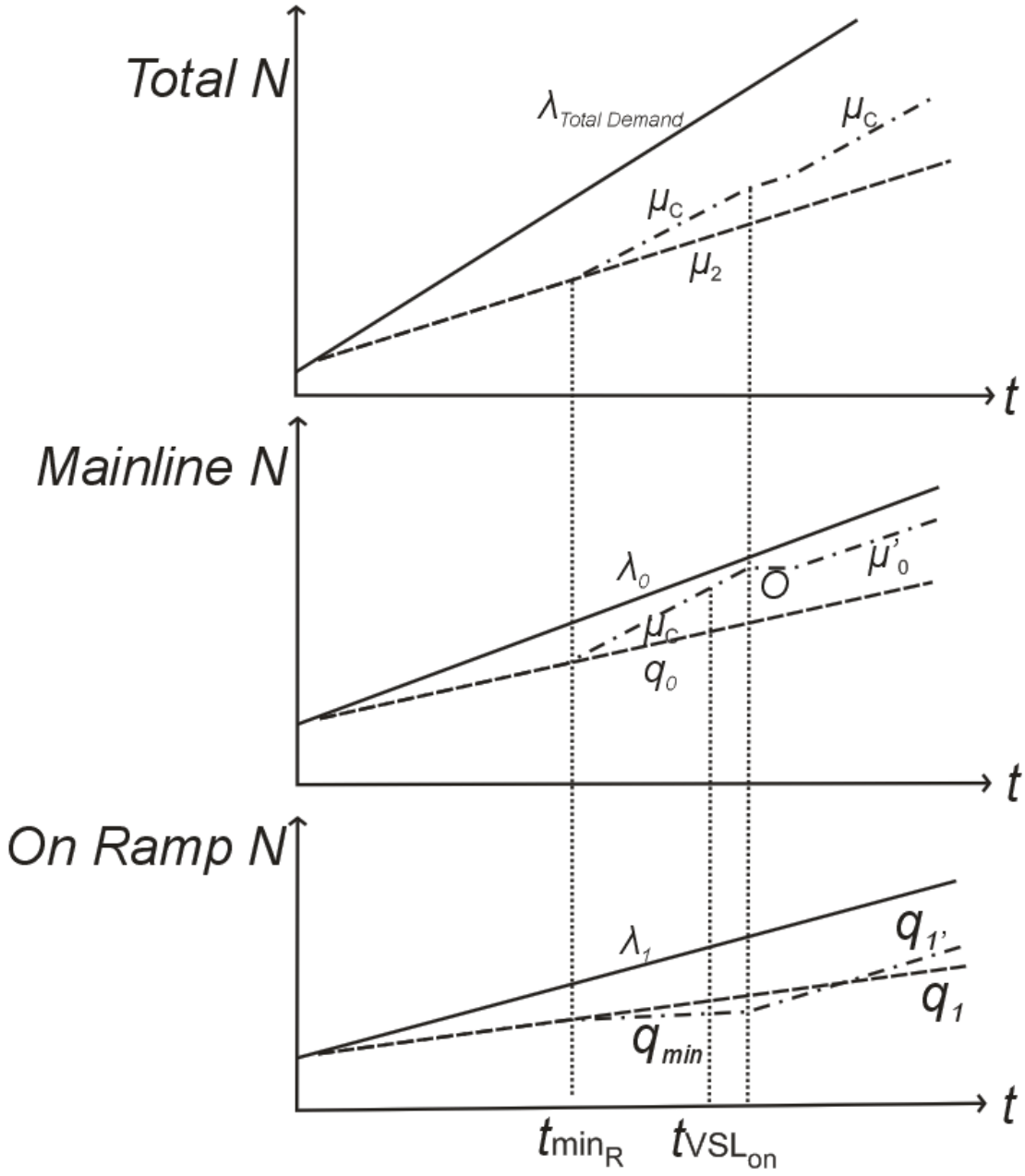

Figure 33 Cumulative count curve of Figure 32

Method 4: This method always uses only the ramp metering system and activates the VSL only when the queue flush system becomes activated. This method incorporates equation (2) into modified method 3.

In most cases, the ramp metering system is accompanied by a queue flush system that prevents the queue from spilling back to an arterial road. When the queue flush is activated, a ramp-metering signal is turned off, and the flow rate of ramp $r(t)$ becomes μ_c, as in method 3. However, although in the queue flush situation, we can control the ramp flow within the range of the demand of ramp $\lambda_1(t)$ and capacity μ_c,

$$\lambda_1(t) \le r(t) \le \mu_c.$$

The speed of the VSL follows $\mu_c - r(t) = w(k_j - k_{vsl}) = v_{vsl}k_{vsl}$.

To utilize the queue flush and the VSL system, we further analyze the design of the combined system. The objective of this specific design is to fill void *O* of the VSL with queued vehicles in the ramp. We assume that the on-ramp is composed of the ramp acceleration zone and a queue storage, that l_{RS} is the length of the queue storage, and that the on-ramp is located parallel to the mainline, shown in the time-space diagram of the on-ramp and the mainline freeway in Figure 34. Then we let t_{vsl} be the time of the VSL activation after queue detection on the ramp. However, we fill void *O*, but we do not insert flow μ_c of the ramp before t_m (shown in the figure), so the queue flush is turned on at time $t_{QueueFlush}$. Then we let Δt_v be the time difference between t_{vsl} and $t_{QueueFlush}$, which is derived from the following equation:

$$\Delta t_v = \frac{l_{RS}}{v_f - v_{vsl}}. \quad (7)$$

Note that v_f can be replaced by the speed of the VSL of the previous period if it is greater than that of the current period.

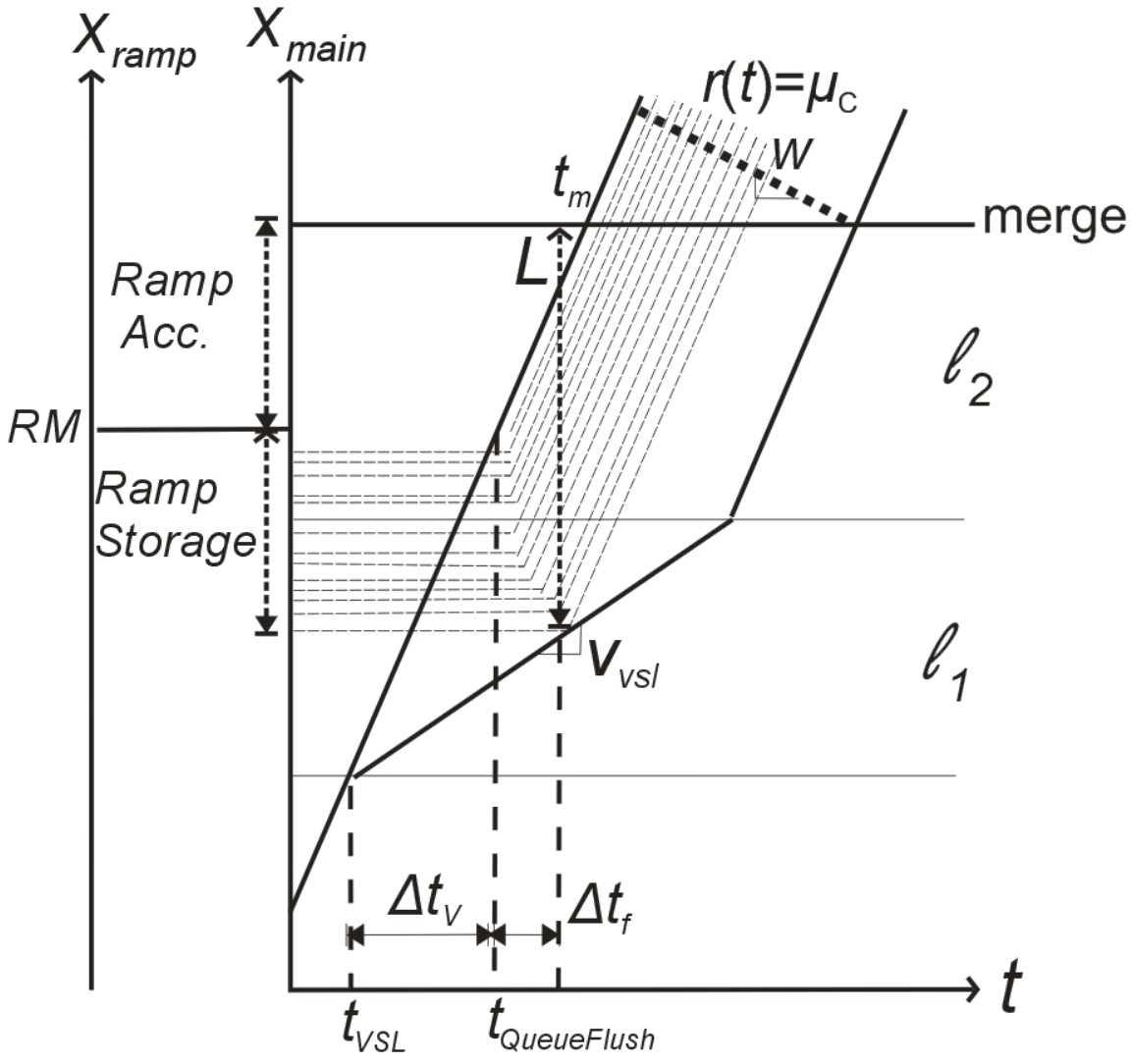

Figure 34 Time-space diagram

In the figure, Δt_f is the duration of the queue flush time that can fill void *O*. This duration is calculated from the length of the queue storage, a spacing of vehicles d_j, and a spacing time τ_j as proposed and verified in (Ahn, Cassidy, & Laval, 2003; Newell, 2002); see Figure 35. Assuming that vehicles in the queue storage stop, and that time τ_j is a constant, Δt_f is calculated from the following equation:

$$\Delta t_f = \sum_{j=1}^{l_{RS}/d_j} \tau_j. \tag{8}$$

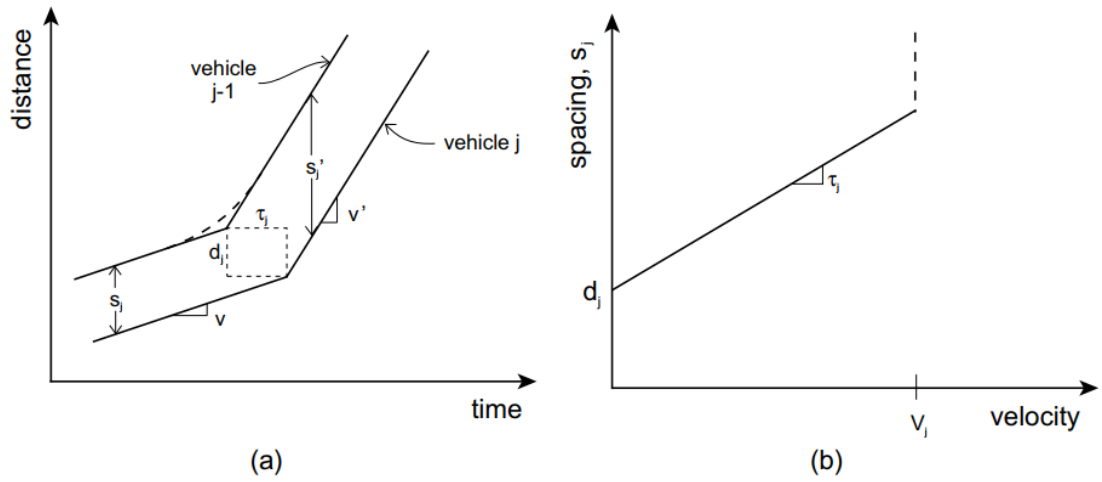

Figure 35 (a) Piecewise linear vehicle trajectories, (b) relation between velocity and spacing for an individual driver (Ahn et al., 2003; Newell, 2002)

4.3. Simulation Experiments

This section presents simulation experiments of the proposed VSL-RM model using a micro-simulation application, GTsim (Chilukuri, Laval, & Guin, 2014b; Cho & Laval, 2016).

4.3.1. One-Lane Merge Network

Simulation Settings

We designed a one-lane mainline and a one-lane on-ramp that merges into the one-lane mainline (see Figure 36). In the figure, traffic demand heads eastbound, and the VSL zone is located upstream of the merge. The length of the VSL zone, l_1, is set to 100 m. The solid line on the left side of the network (in brown) shows a vehicle decreasing speed because of the VSL.

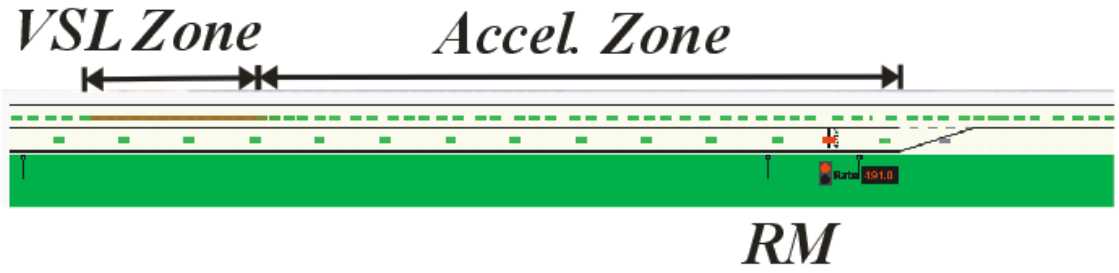

Figure 36 VSL network in GTsim

The length of the acceleration zone, l_2, in Figure 36 is set to 1,000 m upstream of the merge, which is large enough to recover the free-flow speed for VSL-applied vehicles. GTsim adopts the free-motion model for cars that are introduced by the FHWA, (2000) and Laval & Daganzo (2006). In this model, the acceleration of a vehicle follows equation $a = a_0\left(1 - {}^{v}/_{v_f}\right) - gG$, where $g = 9.81\,\frac{m}{s^2}$ and $v_f = 100\,\frac{km}{h}$. Parameter a_0 is

chosen as a random value between 2 to 4, considering mixed vehicle type circumstances. Figure 37 describes the trajectory of the free-motion model from zero-speed when $a_0 = 2.3\ m/s^2$, which is the acceleration of recreational vehicles. It shows that a vehicle must travel a distance of about 110 to increase speed from zero to 60 *km/h*, about 260 meters to increase speed from zero to 80 *km/h*, and about 460 meters to increase from zero to 90 *km/h*. Therefore, it must travel about 350 (=460-110) meters to increase from 60 to 90 *km/h*.

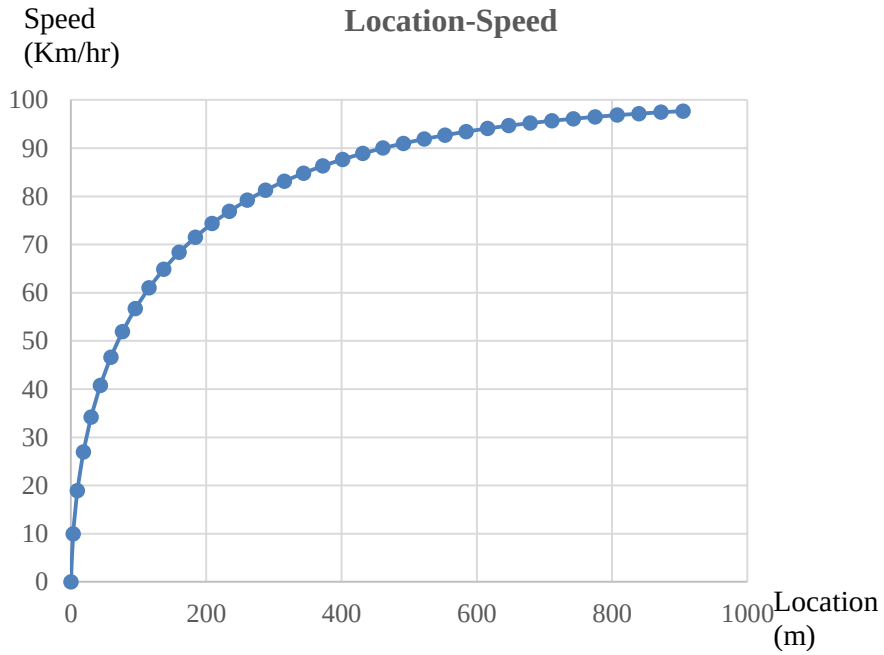

Figure 37 Trajectory of the free-motion model

The RM system is installed at the on-ramp. We set the origin-destination (O-D) traffic demand as shown in Table 2. Note that the ideal capacity, μ_c (without the capacity drop), is 2,500 $vph/lane$. We simulate 30-minute experiments that include the formation and backup of the queue in the mainline to the beginning of the network and update VSLs every two minutes.

Table 2 O-D table of one-lane merge network experiment

TIME / **DEMAND**	**0 – 600 *SEC.***	**600 – 1800 *SEC.***
λ_0	2000 *vph*	2300 *vph*
λ_1	200 *vph*	400 *vph*
λ_{total}	2200 *vph*	2700 *vph*

We compare the following four cases of traffic control strategies.

a) No control

b) VSL control only (using equation (1))

c) RM control only (using equation (3))

d) VSL and RM (using equation (1) first, then (3) from Method 2)

For case *d*, we first apply VSL equation (1) and supplement it by ALINEA-RM (equation (3)).

Results

The cumulative count curves at the entrance and the exit of the network for the four cases are summarized in Figure 38. The figure presents an oblique coordinate (Muñoz & Daganzo, 2002) to illustrate the differences among the count curves; the background flow is 2,200 (*vph*). It is important to note that this figure is a particular realization of a stochastic process whose purpose is to illustrate the findings of the proposed methodology, which have been verified with many other realizations.

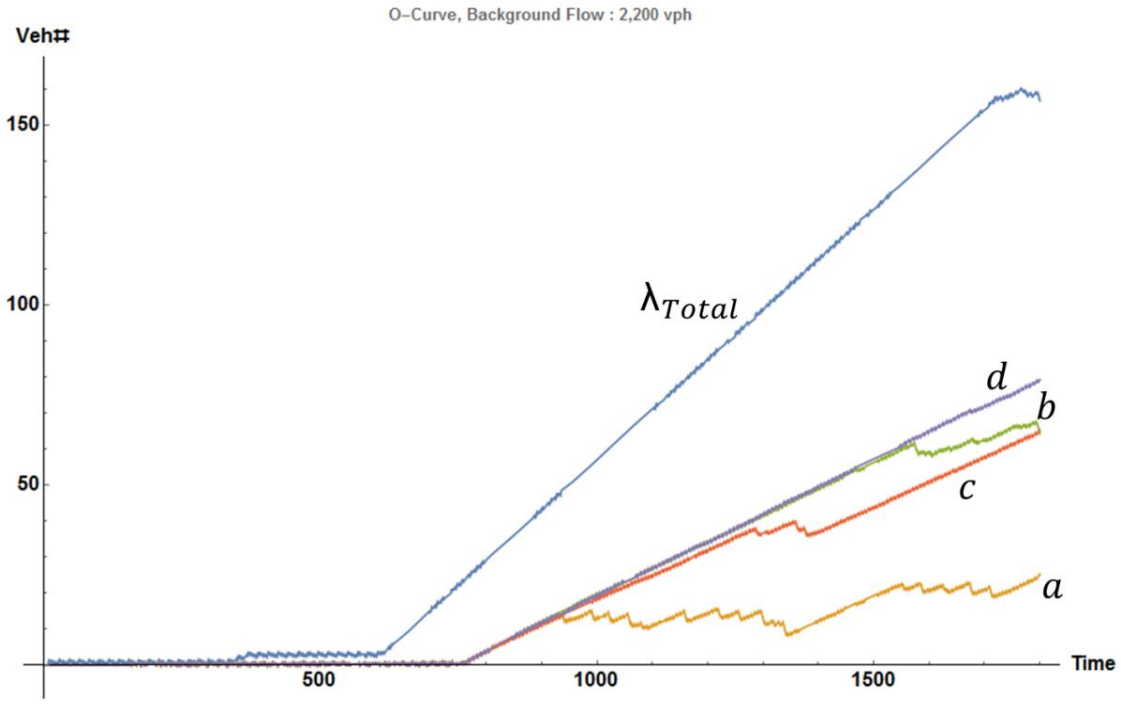

Figure 38 Oblique count curves of the simulation results

The figure shows that with no control (case *a*), the capacity drops early in the simulation, and therefore, the smallest number of vehicles arrive at the exit point during the simulation time. VSL control only (case *b*) and RM control only (case c) are similar, but VSL control maintains capacity longer than RM control, and the latter recovers from the capacity drop quickly while the VSL control does not. The results show that the combined VSL and RM system outperforms other methods. Not only does it prevent a capacity drop, but it also does not break down. We conducted more experiments by changing the proportions of O-D demand while maintaining total demand at a constant level. The results are summarized in Figure 39.

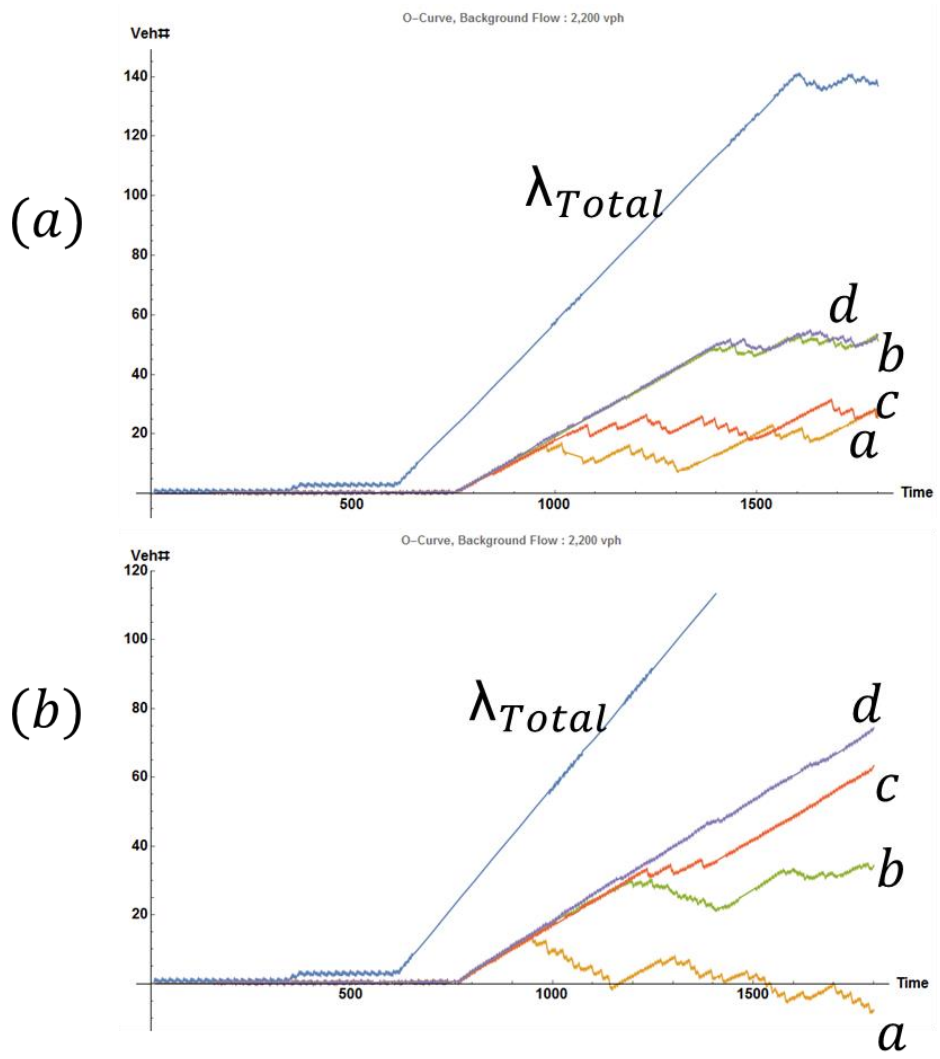

Figure 39 Oblique curves of varied O-D demand flow (a) 2400/300 and (b) 2200/500

In Figure 39 (a), the performance of the only VSL (case *b*) and integrated VSL and RM (case *d*) are almost the same, and only RM (case *c*) is not as effective as in Figure 38. A possible explanation for this finding is that when on-ramp flow is low, the RM system underperforms. However, as shown Figure 39 (b), VSL only (case *b*) does not perform as well as RM only (case *c*), and it delays a capacity drop for a long period.

4.3.2. Three-Lane Merge Network

Simulation Settings

We design a three-lane mainline and a one-lane on-ramp that merges into a three-lane mainline (see Figure 40).

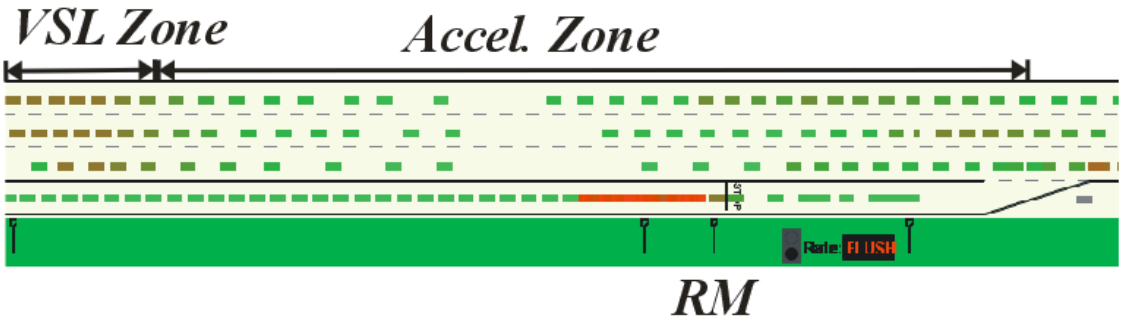

Figure 40 VSL network in *GTsim*

The length of the acceleration zone in Figure 40 is set to 1,000 *m* upstream of the merge, and the length of the VSL zone is set to 100 *m*. The RM system is also installed at the on-ramp. The RM signal is also located 1,000 *m* upstream of the merge. (Note that whereas the length of the ramp shown in Figure 40 is 4 *km*, the length of the mainline shown in Figure 40 is 1 *km*.) The length of the queue storage is set to 500 *m*, and a vehicle detection system is installed at the end of the queue storage. In addition, a new queue warning detection system is installed 300 *m* upstream of the RM signal.

We set the O-D traffic demand as shown in Table 3. To create congestion, we designed 25-minute high traffic demand. After 25 minutes in the simulation, we starve the flows to clear the congestion. We simulate 30-minute experiments that include the formation and the backup of a queue in the mainline to the beginning of the network and update the queue flush and VSLs every two minutes.

Table 3 O-D table of three-lane merge network experiment

TIME DEMAND	0-1500 (*SEC.*)	1500-
λ_0 (vph)	6600	0
λ_1	1100	0
λ_{total}	7700	0

We compare the following five cases of traffic control strategies.

a) No control

b) RM-ALINEA control only without Queue Flush System

c) RM-ALINEA control only with Queue Flush System

d) Combined RM with a new queue warning and VSL (Method 4) on all lanes

e) Combined RM with a new queue warning and VSL (Method 4) on only the shoulder lane

While Case *b* is the same strategy as case *c* in Chapter 0, case *c* implements the queue flush system, the metering rate of which is a saturated flow if the queue flush detector (500 *m* upstream from the RM signal) recognizes the queue backed up to the detector.

For cases *d* and *e*, the VSL is activated if the queue warning detector (300 *m* upstream from the RM signal) recognizes that the queue is backed up to the detector. If the queue arrives in the queue flush detector, the metering rate is set to the real-time traffic demand of the ramp. The speed of the VSL in cases *d* and *e* are calculated from equation (1). In this experiment, we inserted two parameters, α and β, in the equation to analyze the sensitivity of the VSL system (see Figure 41, equation (9)).

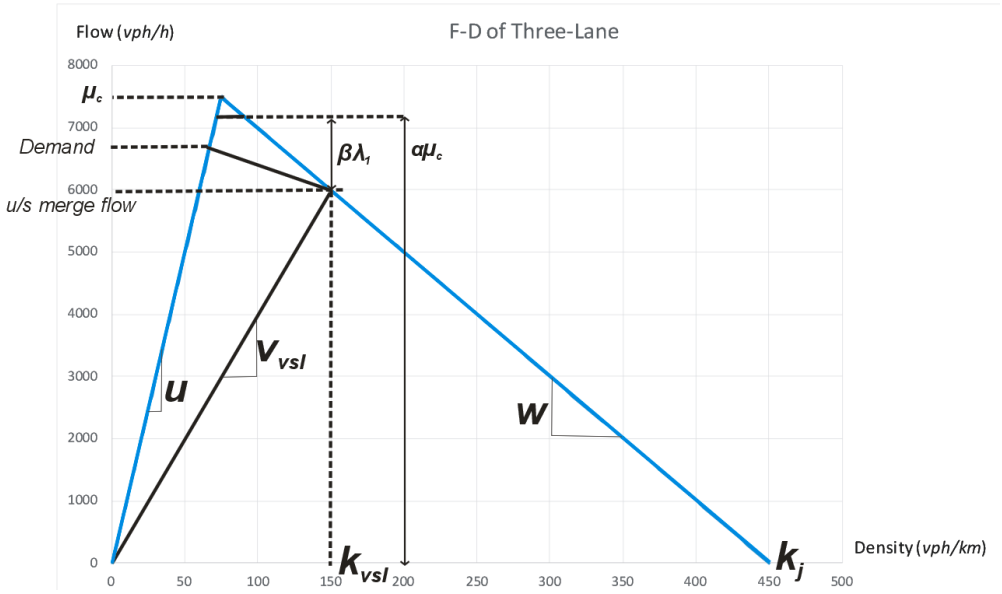

Figure 41 Fundamental Diagram of the three-lane freeway

$$\alpha\,\mu_c - \beta\,q_1 = w\left(k_j - k_{vsl}\right) = v_{vsl}k_{vsl} \tag{9}$$

In equation (9), $\alpha\,\mu_c$ is the target freeway capacity of the VSL system, and $\beta\,q_1$ is the new metering rate during the queue warning period, where q_1 is the real-time traffic demand of the ramp. Not to overflow the queue storage, β becomes 1 during the queue flush period. We conducted experiments with sixteen combinations of four of each value of α (1, 0.98, 0.96, and 0.94) and β (1.2, 1, 0.8, and 0.6). Table 4 summarizes the flows downstream of the VSL that correspond to parameters α and β. Table 5 shows the speed of the VSL, which corresponds to the cases of Table 4, which is calculated from equation (9). Note that the speed in Table 5 is applied before the queue flush.

Table 4 Flow (*vph*) downstream of the VSL of parameters α and β

α \ β	**1.2**	**1**	**0.8**	**0.6**
0.94	5730	5950	6170	6390
0.96	5880	6100	6320	6540
0.98	6030	6250	6470	6690
1	6180	6400	6620	6840

Table 5 VSL Speed (*km/h*) of parameters α and β

α \ β	**1.2**	**1**	**0.8**	**0.6**
0.94	35	39	44	49
0.96	38	42	47	53
0.98	41	45	51	58
1	44	49	55	63

For case *e*, the VSL system is applied only to the shoulder lane (see Figure 42). This shoulder lane speed limit is being used in some sections of the freeway in the state of Georgia in the United States. They operate flex shoulder lanes, where the speed limit for the shoulder lane is 45 *mph*, but the speed limit for general purpose lanes is 65 *mph*.

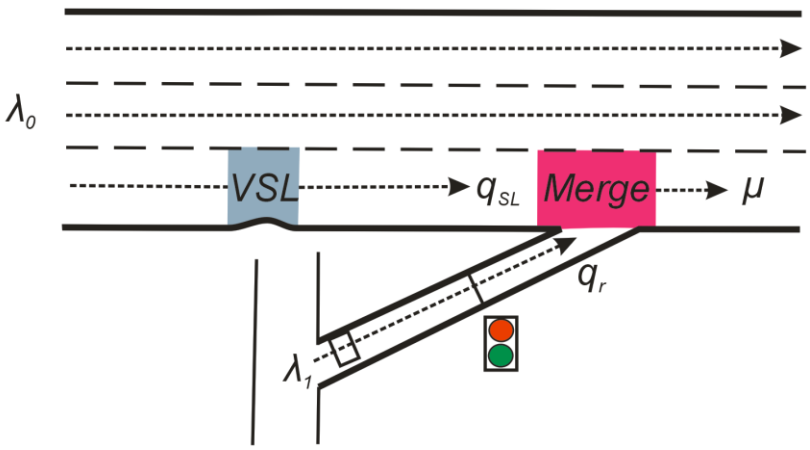

Figure 42 Diagram of the shoulder lane VSL

Recent studies (Duret et al., 2012; Knoop et al., 2010; Soriguera et al., 2017) empirically discovered a relationship between the lane flow distribution (LFD) and the VSL, but they did not present an algorithm of the VSL. To analyze this relationship, we conducted experiments with six cases of LFDs:

- 1/3, 1/3, 1/3 (Evenly distributed)
- 0.34, 0.34, 0.32 (Median lane, center lane, shoulder lane)
- 0.35, 0.35, 0.3 (Median lane, center lane, shoulder lane)
- 0.36, 0.36, 0.28 (Median lane, center lane, shoulder lane)
- 0.37, 0.35, 0.28 (Median lane, center lane, shoulder lane)
- 0.37, 0.36, 0.27 (Median lane, center lane, shoulder lane)

Note that the mainline traffic demand λ_0 is 6,600 *vph,* so the maximum ratio of one lane is 0.379, because the ideal capacity of one lane in GTsim is 2,500 *vph*.

Results

The results of the simulation experiments for each LFD are summarized in Figure 43 - 48. The measurement of effectiveness (MOE) of the experiment is the total vehicle delay that has a unit of *Veh-hr*. In the figure, the delays of each mainline, ramp, and total system are presented. For cases *d* and *e*, the average values of sixteen experiments are presented. (All results of the simulation experiments are shown in Appendix A.1.)

We found that for both control cases *d*) and *e*), VSL strategies outperform control case *c*) (RM only with the queue flush). However, the effectiveness of the VSL varies in the LFD. The shoulder lane VSL was the most effective in the (0.37, 0.36, 0.27) LFD (see Figure 48), where the shoulder lane allows more space for merging vehicles. In this LFD, the shoulder lane VSL was even superior to that of control case *b* (RM only without the queue flush). The best scenario of the shoulder lane VSL on this LFD was when $\alpha = 0.94$ and $\beta = 1$. This scenario showed a total delay of 37 *veh-hr* (20 *veh-h*r for the ramp and 17 *veh-hr* for the mainline), which was 22% less than that of the control case *b*), and 43% less than that of the no control case *a*).

Results of statistical tests (*t*-test) of simulation experiments are also summarized in Table 6-9. From the *t*-test, we found that only control case *b*) significantly differed from the no-control case in terms of the total delay, but all control cases significantly differed in terms of the mainline delay. In a comparison of case *c*) and the average value of delay of the VSL, these controls were not significantly different. However, in a comparison of case *c*) to a specific LFD (0.37, 0.36, 0.27) VSL, they were significantly different (p-value < 0.000001). Also, in a comparison of control cases *d*) and *e*) using th paired *t*-test, the two methods were significantly different. As the VSL affects the delay

of the mainline, the *p*-value of the mainline delay was always lower than the *p*-value of the total delay.

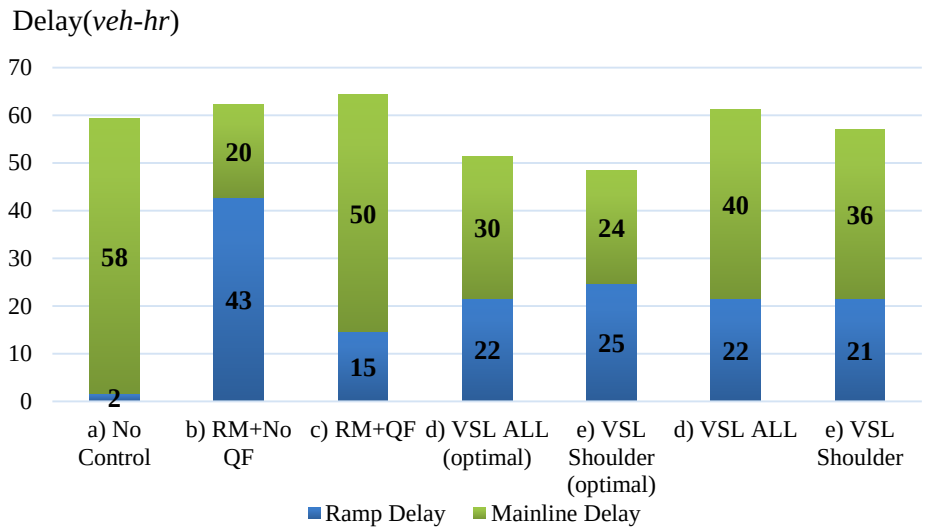

Figure 43 Delays (*Veh-hr*) of control strategies of the (1/3, 1/3, 1/3) LFD

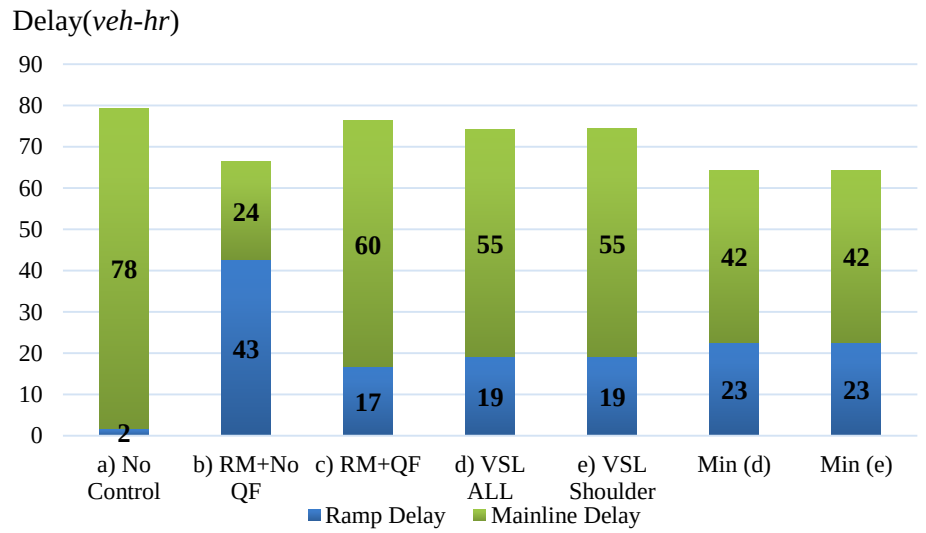

Figure 44 Delays (*Veh-hr*) of control strategies of the (0.34, 0.34, 0.32) LFD

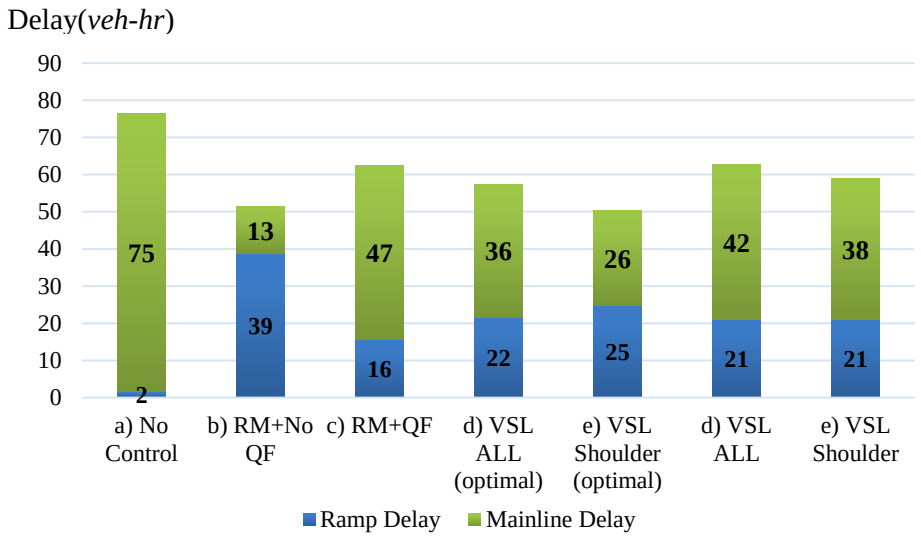

Figure 45 Delays (*Veh-hr*) of control strategies of the (0.35, 0.35, 0.3) LFD

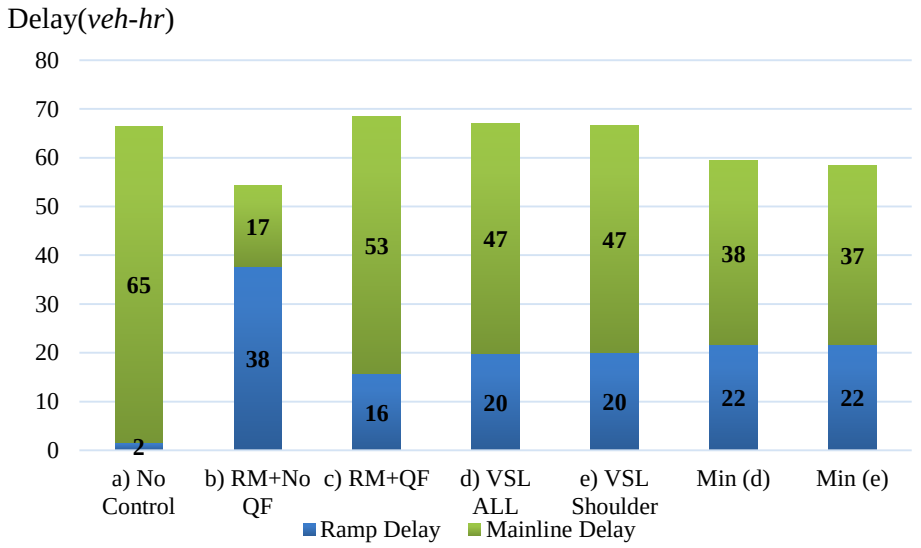

Figure 46 Delays (*Veh-hr*) of control strategies of the (0.36, 0.36, 0.28) LFD

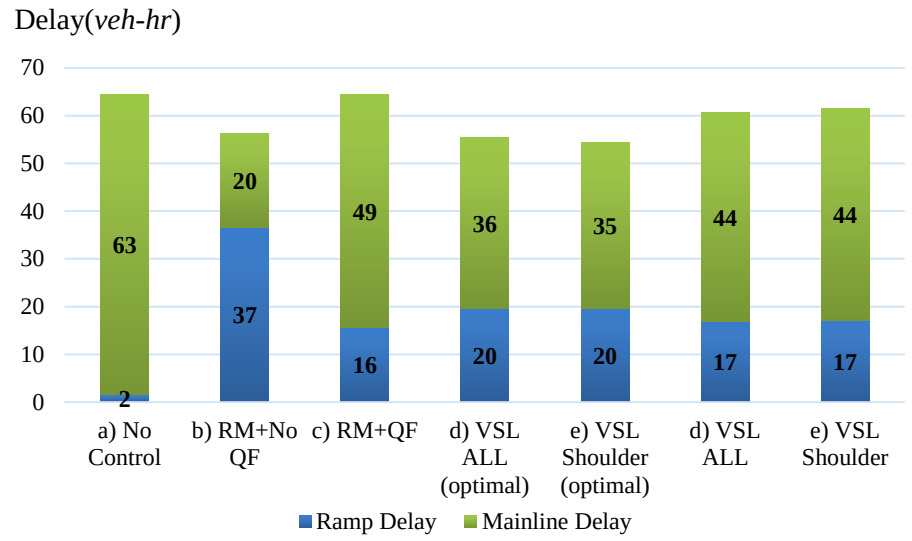

Figure 47 Delays (*Veh-hr*) of control strategies of the (0.37, 0.35, 0.28) LFD

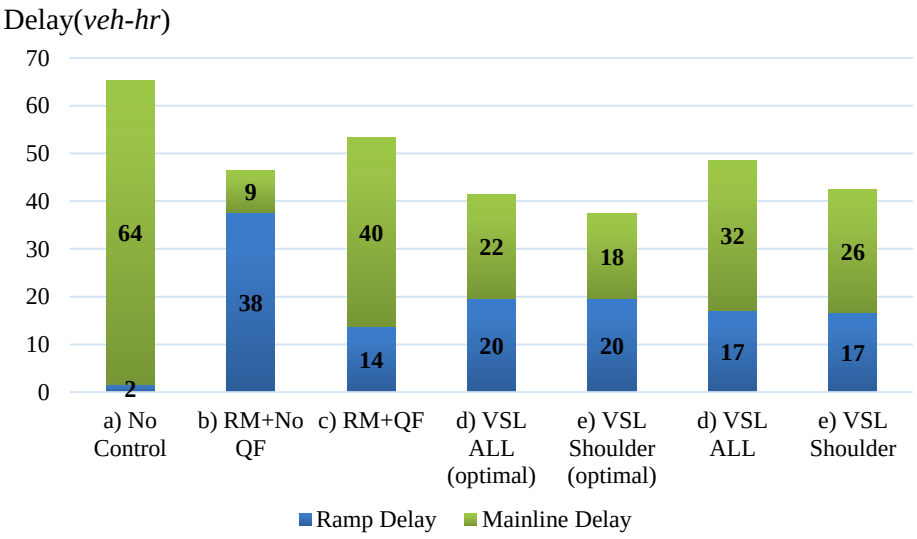

Figure 48 Delays (*Veh-hr*) of control strategies of the (0.37, 0.36, 0.27) LFD

Table 6 T-test of no control and other controls (μ_0=μ_1)

μ_0	σ_0	n_0	μ_1	σ_1	n_1	*p-value*
No Control (All Delay)			RM no Queue Flush (All Delay)			Paired t-test
68.51	7.68	6	56.17	7.28	6	0.025
(Mainline Delay)			(Mainline Delay)			Paired t-test
66.86	7.68	6	16.86	5.42	6	0.0000001
No Control (All Delay)			RM Queue Flush (All Delay)			Paired t-test
68.51	7.68	6	64.84	7.53	6	0.297
(Mainline Delay)			(Mainline Delay)			Paired t-test
66.86	7.68	6	49.52	6.62	6	0.002
No Control (All Delay)			VSL All Lanes (All Delay)			
68.51	7.68	6	62.39	8.99	96	0.107
(Mainline Delay)			(Mainline Delay)			
66.86	7.68	6	43.147	9.28	96	0.00000002
No Control (All Delay)			VSL Shoulder Lane (All Delay)			
68.51	7.68	6	60.13	10.76	96	0.064
(Mainline Delay)			(Mainline Delay)			
66.86	7.68	6	40.92	11.30	96	0.0000003

Table 7 T-test of controls (μ_0=μ_1)

μ_0	σ_0	n_0	μ_1	σ_1	n_1	*p-value*
RM Queue Flush (All Delay)			VSL All Lanes (All Delay)			
64.84	7.53	6	62.39	8.99	96	0.516
(Mainline Delay)			(Mainline Delay)			
49.52	6.62	6	43.15	9.28	96	0.101
RM Queue Flush (All Delay)			VSL Shoulder Lane (All Delay)			
64.84	7.53	6	60.13	10.76	96	0.295
(Mainline Delay)			(Mainline Delay)			
49.52	6.62	6	40.92	11.30	96	0.069
VSL All Lanes (All Delay)			VSL Shoulder Lane (All Delay)			Paired t-test
62.39	8.99	96	60.13	10.76	96	0.0002
(Mainline Delay)			(Mainline Delay)			Paired t-test
43.15	9.28	96	40.92	11.30	96	0.0001

Table 8 T-test of controls (μ_0=μ_1)

μ_0	σ_0	n_0	μ_1	σ_1	n_1	*p-value*
RM Queue Flush (All Delay)			VSL All Lanes LFD **(0.37,0.36,0.27)** (All Delay)			
64.84	7.53	6	48.53	5.64	16	0.00002
(Mainline Delay)			(Mainline Delay)			
49.52	6.62	6	31.50	4.92	16	0.000001
RM Queue Flush (All Delay)			VSL Shoulder Lane LFD **(0.37,0.36,0.27)** (All Delay)			
64.84	7.53	6	42.47	3.01	16	0.005
(Mainline Delay)			(Mainline Delay)			
49.52	6.62	6	25.75	4.95	16	0.00000001
VSL All Lanes LFD **(0.33,0.33,0.33)** (All Delay)			VSL Shoulder Lane LFD **(0.37,0.36,0.27)** (All Delay)			
61.28	5.05	16	42.47	3.01	16	0.005
(Mainline Delay)			(Mainline Delay)			
49.52	6.62	16	25.75	4.95	16	0.00000001

Table 9 T-test of the VSL LFD (μ_0=μ_1)

μ_0	σ_0	n_0	μ_1	σ_1	n_1	*p-value*
VSL All Lanes LFD **(0.33,0.33,0.33)** (All Delay)			VSL All Lanes LFD **(0.37,0.36,0.27)** (All Delay)			
61.28	5.05	16	48.53	5.64	16	0.0000002
(Mainline Delay)			(Mainline Delay)			
39.75	5.28	16	31.50	4.92	16	0.00008
VSL Shoulder Lane LFD **(0.33,0.33,0.33)** (All Delay)			VSL Shoulder Lane LFD **(0.37,0.36,0.27)** (All Delay)			
57.03	5.33	16	42.47	3.01	16	0.0000000001
(Mainline Delay)			(Mainline Delay)			
35.56	6.97	16	25.75	4.95	16	0.00007

For the (0.37, 0.36, 0.27) LFD, speed-contour maps (time-space diagram) and oblique count curves of all five control cases are described in Figure 49 -53. We found an obvious capacity drop for control cases *a*) (see Figure 49) and *c*) (see Figure 51). In Figure 49 (b), the slope of the departure curve (yellow, bottom line) is almost parallel to the horizontal axis, which is 6,800 *vph*. The slope of the departure curve in Figure 50 (b) is also parallel to the horizontal axis; however, its background flow is 7,200 *vph*.

In Figure 49 (a), the map shows almost no congestion on the mainline freeway, but large queues formed on the ramp, which is not shown on this map. Figure 52 and Figure 53 show the best results for control cases *d*) and *e*). They show that a capacity drop was prevented, as proposed in the model. However, speed reductions upstream of the merge (VSL zone) were found, as described in the previous chapter.

Figure 54 presents the speed contour maps and the oblique curves of only the shoulder lanes of (0.37, 0.36, 0.27) LFD cases *c*) and *e*). The figure shows that the shoulder lane only VSL restricts flow of the shoulder lane so that retards the capacity drop. Figure 55 also depicts the speed contour maps and oblique count curves of the median and center lanes. We assume that although these lanes are not directly affected by the speed of the VSL, the speed friction between lanes reduces the speed of the lane.

(a) Speed contour map

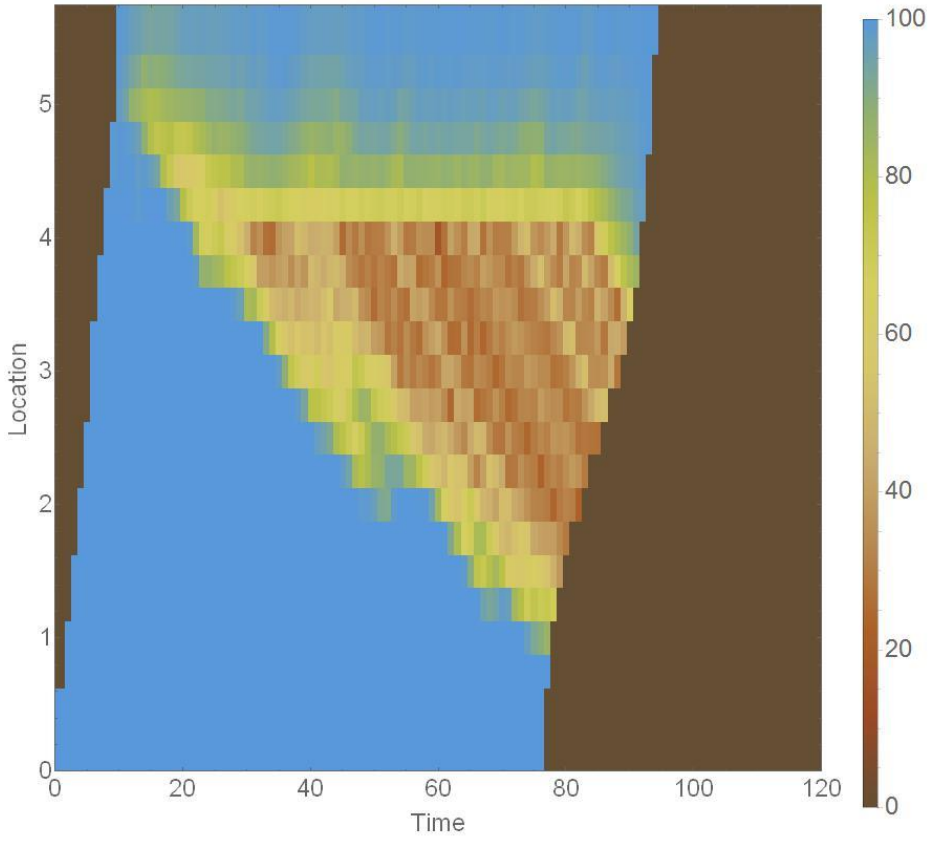

(b) Oblique count curves (background 6800 *vph*)

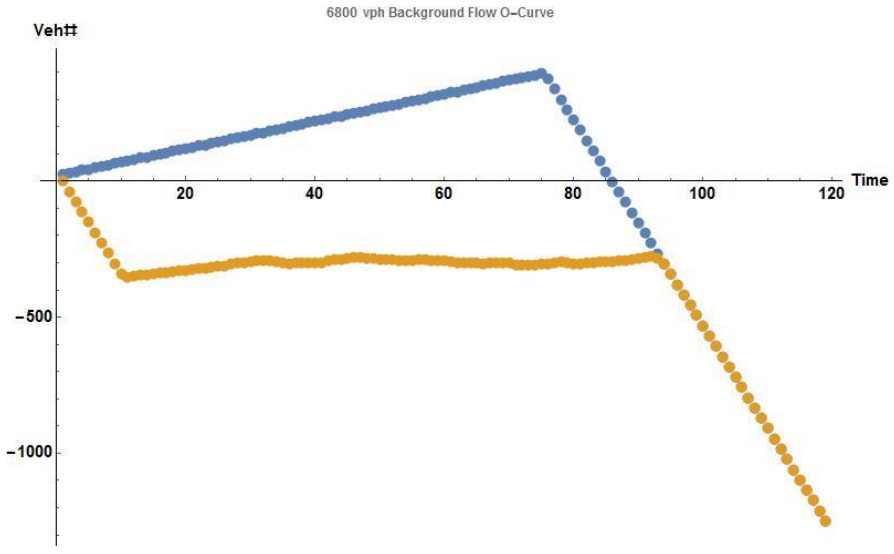

Figure 49 Case *a*) no control: (a) the speed contour map and (b) the oblique count curves of the (0.37, 0.36, 0.27) LFD

(a) Speed contour map

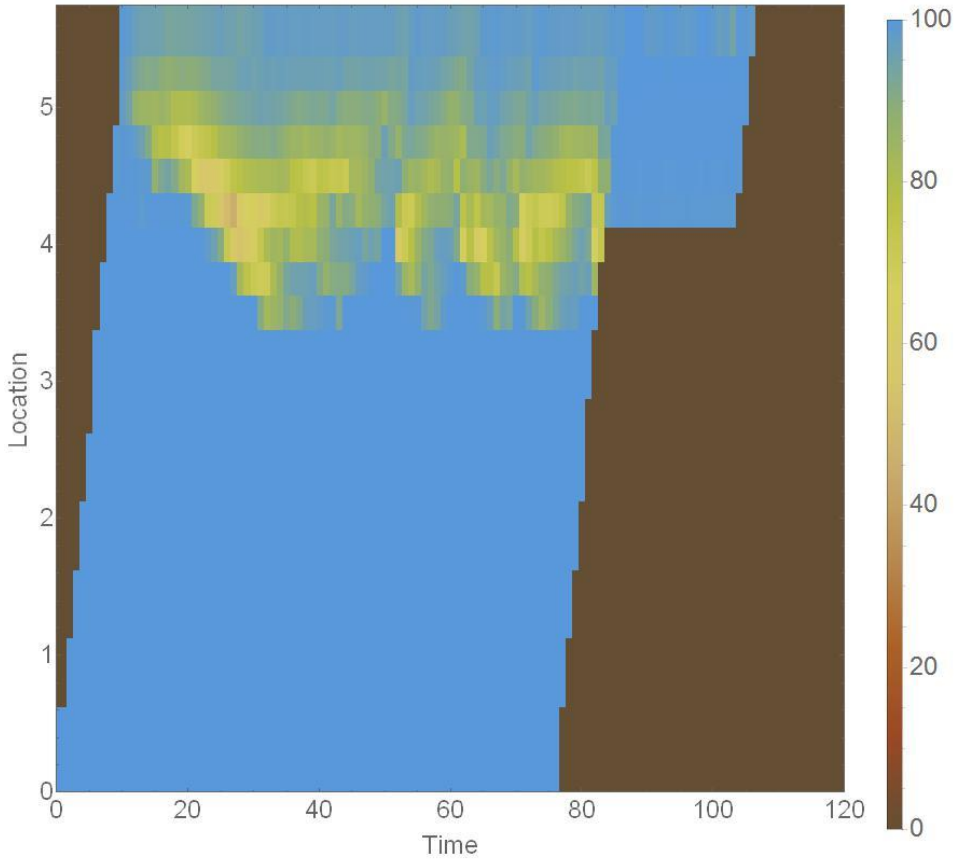

(b) Oblique count curves (background 7200 *vph*)

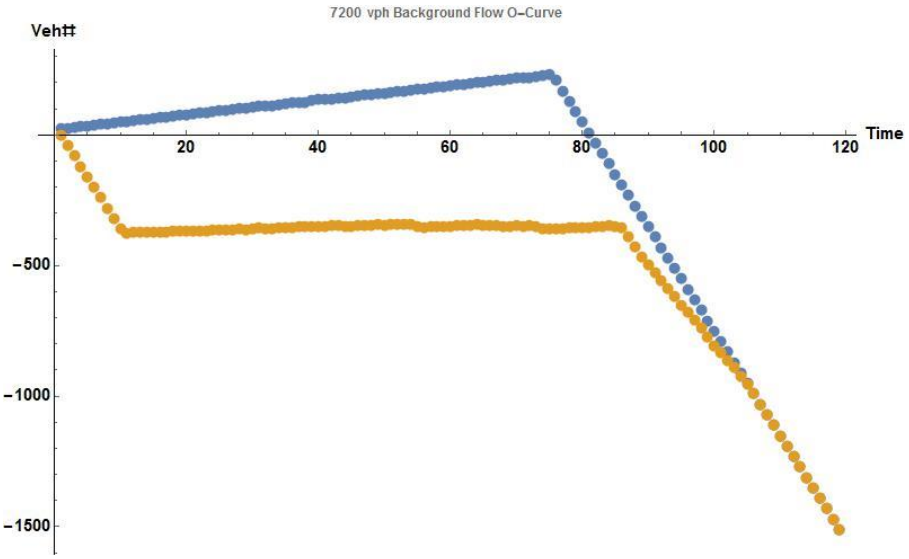

Figure 50 Case *b*) RM-ALINEA control only without the queue flush system: (a) the speed contour map and (b) the oblique count curves of the (0.37, 0.36, 0.27) LFD

(a) Speed contour map

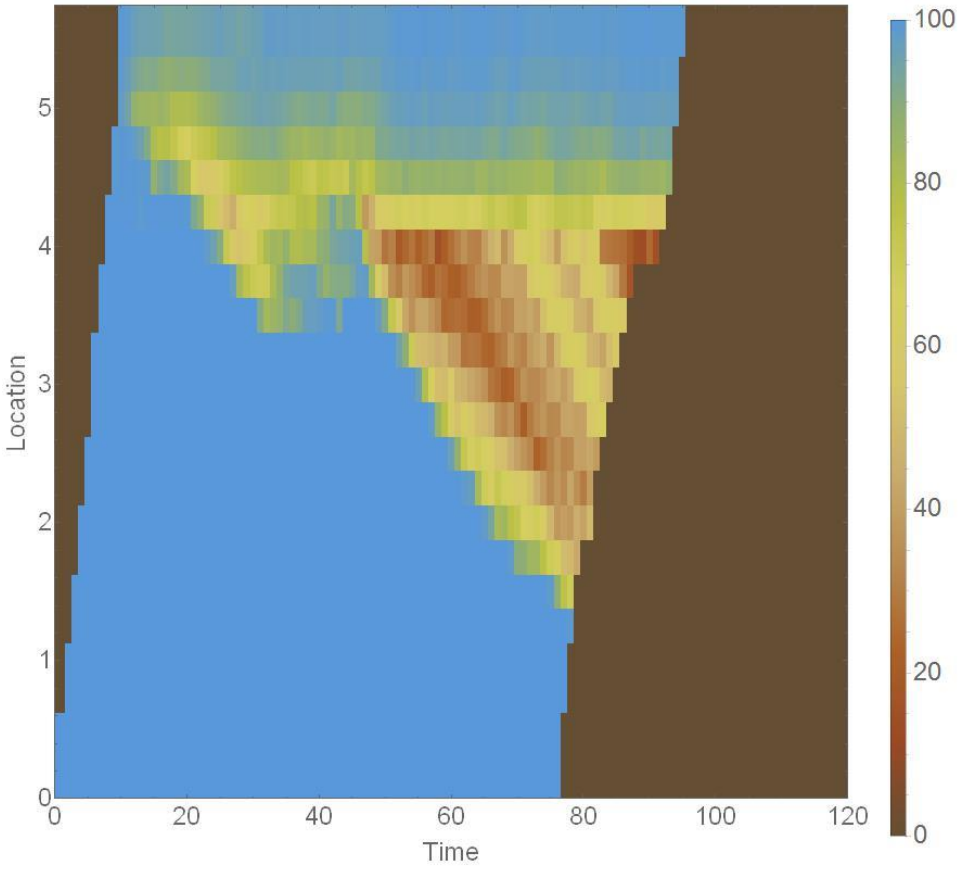

(b) Oblique count curves (background 6600 *vph*)

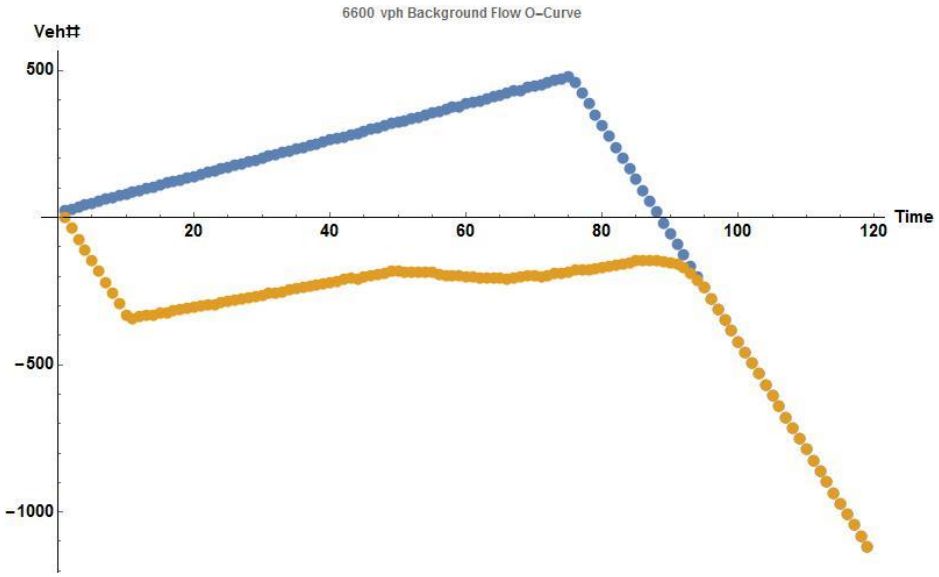

Figure 51 Case *c*) RM-ALINEA control only with queue flush system: (a) the speed contour map and (b) the oblique count curves of the (0.37, 0.36, 0.27) LFD

(a) Speed contour map

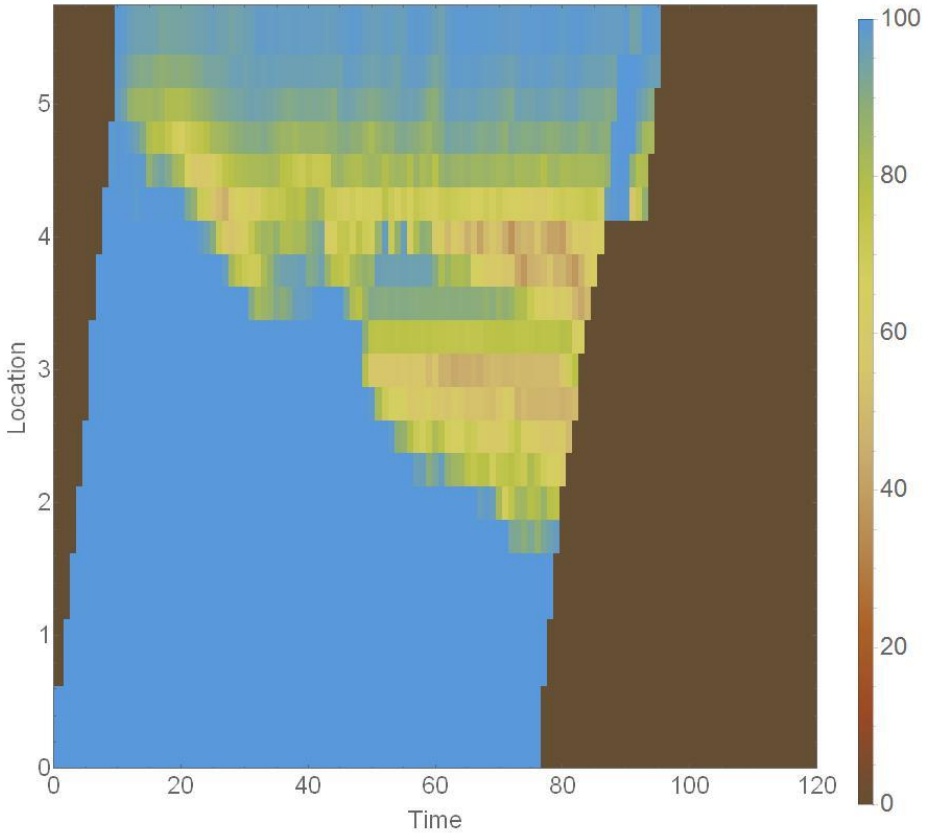

(b) Oblique count curves (background 7300 *vph*)

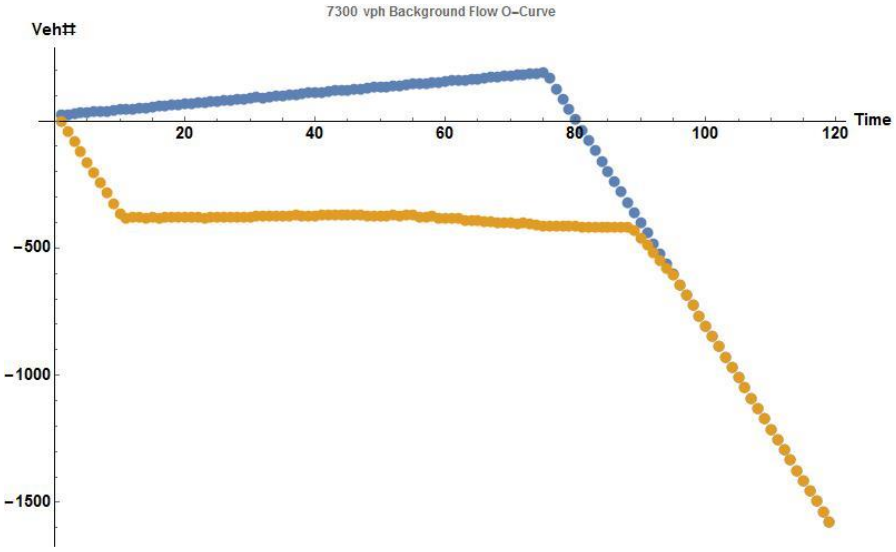

Figure 52 Case *d*) combined RM with the queue flush and VSL (Method 4) on all lanes: (a) the speed contour map and (b) the oblique count curves of the (0.37, 0.36, 0.27) LFD ($\alpha = 1, \beta = 1$)

(a) Speed contour map

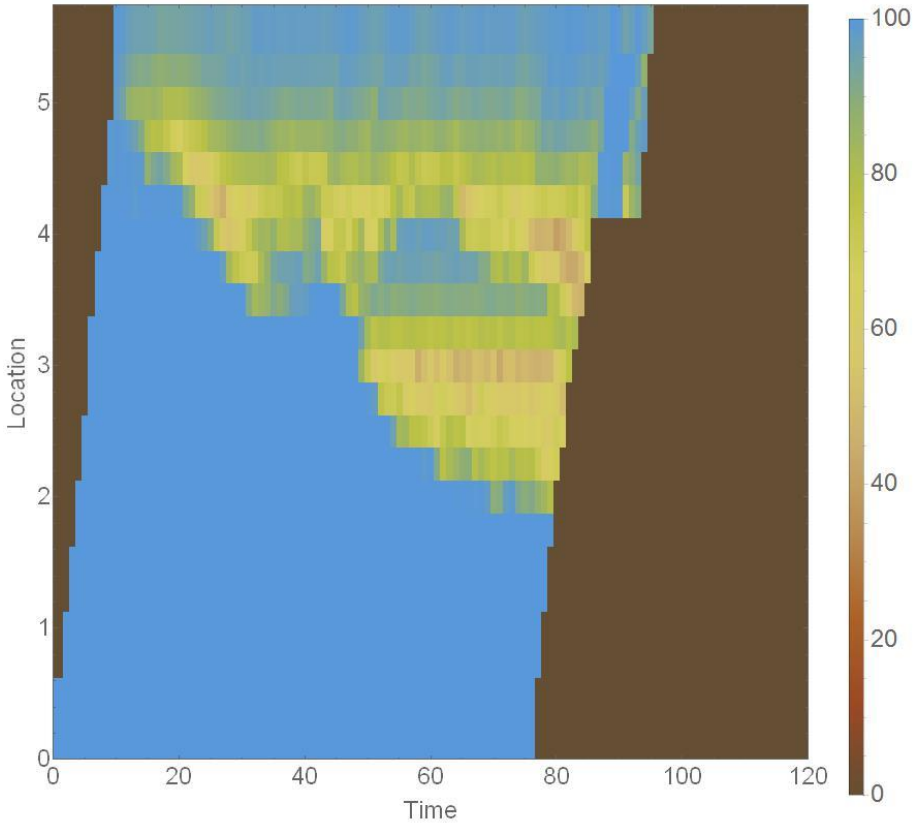

(b) Oblique count curves (background 7300 *vph*)

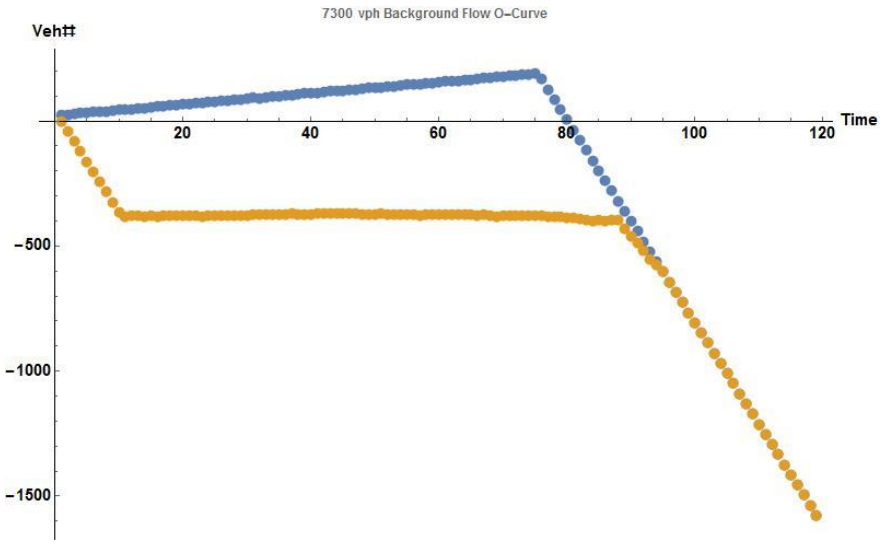

Figure 53 Case *e*) combined RM with the queue flush and VSL (Method 4) on only the shoulder lane: (a) the speed contour map and (b) the oblique count curves of the (0.37, 0.36, 0.27) LFD ($\alpha = 0.94, \beta = 1$)

(a) RM, Shoulder Lane **(b) VSLS, Shoulder Lane**

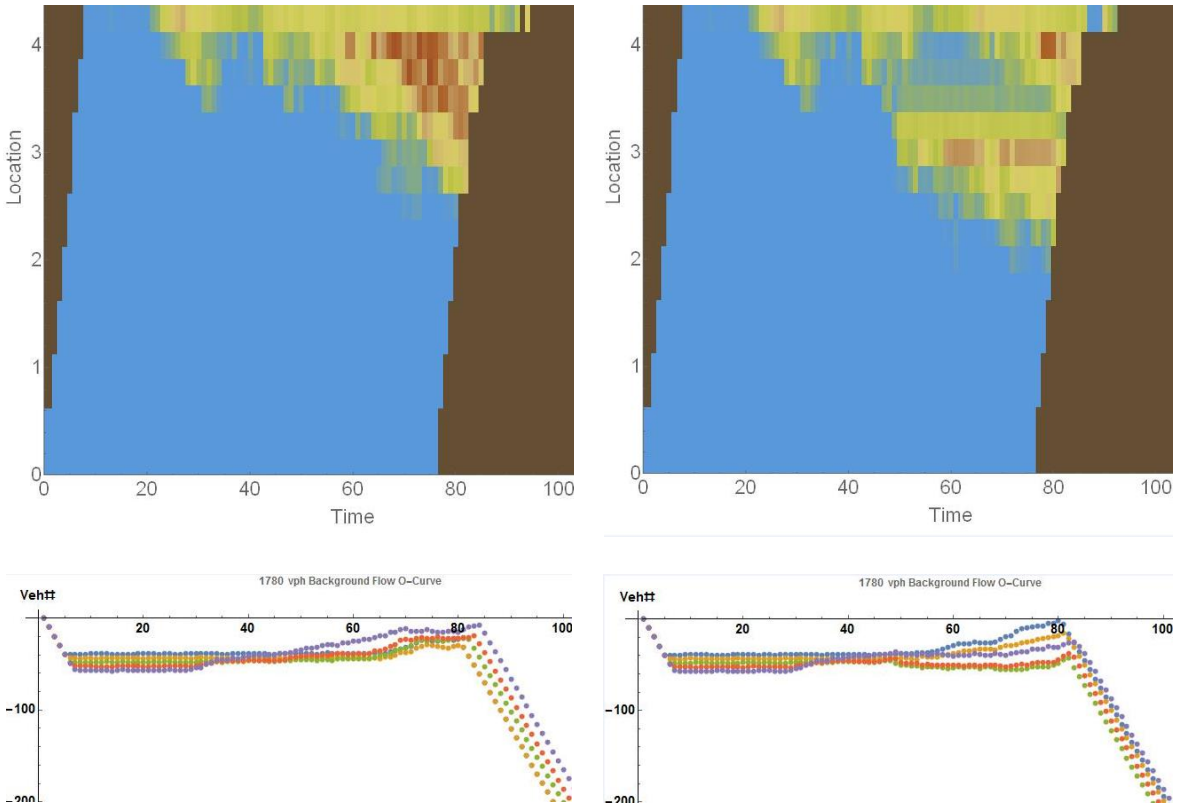

Figure 54 Speed contour map and the oblique count curves of (a) Case c) and (b) case e) of the shoulder lane (Blue: 2.75km, Yellow: 3km, Green: 3.25km, Red: 3.5km, Purple: 3.75km) of the (0.37, 0.36, 0.27) LFD (α=0.94,β=1)

(a) VSLS, Center Lane **(b) VSLS, Median Lane**

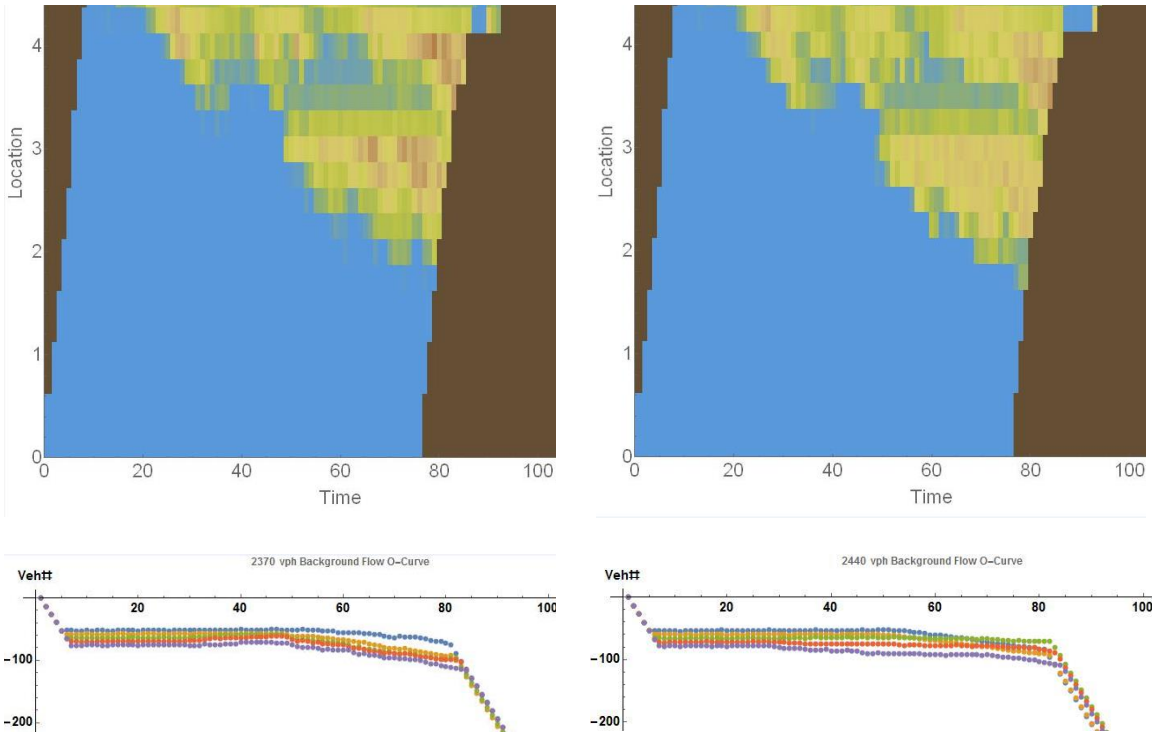

Figure 55 Speed contour maps and oblique count curves of (a) Case e) center lane and (b) case e) the median lane (Blue: 2.75km, Yellow: 3km, Green: 3.25km, Red: 3.5km, Purple: 3.75km) of the (0.37, 0.36, 0.27) LFD (α=0.94,β=1)

The results of statistical tests (*paired t*-test) of the parameter analysis, summarized in Table 10 -12, show that the scenarios using either parameter α or β significantly differ, and the difference is statistically more significant for the mainline delay. In Table 12, the scenarios of (All VSL, α=1, β=0.8) and (All VSL, α=0.94, β=1.2), which exhibited the largest discrepancies in their flows (Table 4), also significantly differed. However, the scenarios of (All VSL, α=1, β=1) and (All VSL, α=0.96, β=0.6) did not significantly differ. This finding is consistent with the assumption that the speeds of the VSLs of the two scenarios are the same (49 *km/h*; see Table 5).

Table 10 Paired T-test of VSL parameter α (μ_0=μ_1)

μ_0	σ_0	n_0	μ_1	σ_1	n_1	*p-value*
VSL All Lanes **($\alpha = 1$)** (All Delay)			VSL All Lanes LFD **(α =0.94)** (All Delay)			Paired t-test
61.30	9.56	24	63.84	8.78	24	0.01
(Mainline Delay)			(Mainline Delay)			Paired t-test
42.11	10.05	24	44.56	8.91	24	0.01
All VSL, $\alpha = 1$ (All Delay)			All VSL, α =**0.96** (All Delay)			Paired t-test
60.69	9.96	48	62.03	9.95	48	0.053
(Mainline Delay)			(Mainline Delay)			Paired t-test
41.48	10.43	48	42.77	10.43	48	0.043

Table 11 Paired T-test of VSL parameter β (μ_0=μ_1)

μ_0	σ_0	n_0	μ_1	σ_1	n_1	*p-value*
VSL All Lanes **($\beta = 1.2$)** (All Delay)			VSL All Lanes LFD **(β =0.8)** (All Delay)			Paired t-test
65.05	11.16	24	61.22	9.15	24	0.013
(Mainline Delay)			(Mainline Delay)			Paired t-test
49.77	10.09	24	40.56	8.67	24	0.0000003
VSL Shoulder Lane **($\beta = 1.2$)** (All Delay)			VSL Shoulder Lane **(β =0.8)** (All Delay)			Paired t-test
62.88	11.16	24	58.84	11.08	24	0.001
(Mainline Delay)			(Mainline Delay)			Paired t-test
47.69	10.73	24	38.27	10.42	24	0.0000000001

Table 12 Paired T-test of VSL parameters α and β (μ_0=μ_1)

μ_0	σ_0	n_0	μ_1	σ_1	n_1	*p-value*
All VSL, $\alpha = 1, \beta = 0.8$ (All Delay)			All VSL, $\alpha = 0.94, \beta = 1.2$ (All Delay)			Paired t-test
58.09	10.70	12	64.76	11.56	12	0.005
(Mainline Delay)			(Mainline Delay)			Paired t-test
37.69	10.08	12	49.44	10.56	12	0.00003
All VSL, $\alpha = 1, \beta = 1$ (All Delay)			All VSL, $\alpha = 0.94, \beta = 0.6$ (All Delay)			Paired t-test
61.09	11.50	12	60.09	7.86	12	0.711
(Mainline Delay)			(Mainline Delay)			Paired t-test
42.02	11.65	12	38.02	7.63	12	0.208

As mentioned, we found that the parameters were more sensitive to mainline delays. In this sense, we categorized the results of the parameter analysis of the mainline of the freeway in Figure 56 through 61. In these figures, the α axis shows the target capacity and the β axis shows the ramp flow parameter. The figures depict temperature maps, in which blue areas represent less total delay and red areas more total delay. For example, the area of the map in Figure 56 (b) is blue near $\alpha = 0.94$, β =0.6 and $\alpha = 0.98$, β =0.6, and its corresponding delay is the least of all of the scenarios (see Table 13).

Table 13 Mainline delays of parameter analysis of control case *e*) of (1/3, 1/3, 1/3) LFD

α \ β	**1.2**	**1**	**0.8**	**0.6**
0.94	43	41	32	***24***
0.96	34	45	32	43
0.98	39	43	37	***25***
1	41	44	34	35

The figures show that the values of parameter α=0.98 and β=0.8 (β =1 in (0.37, 0.36, 0.27 LFD)) in most scenarios show the lowest value of the mainline delay. This finding implies that the capacity without breakdown of this merge section of the freeway is close to 7,350 *vph* ($\alpha\ \mu_c$=0.98*7500). The low value of parameter β reduces the mainline delay in the early stage, but it quickly induces a queue flush situation (β =1). Therefore, it is difficult to generalize the optimum parameter set for the minimum total delay for all of the LFD scenarios.

(a) VSL ALL Lanes

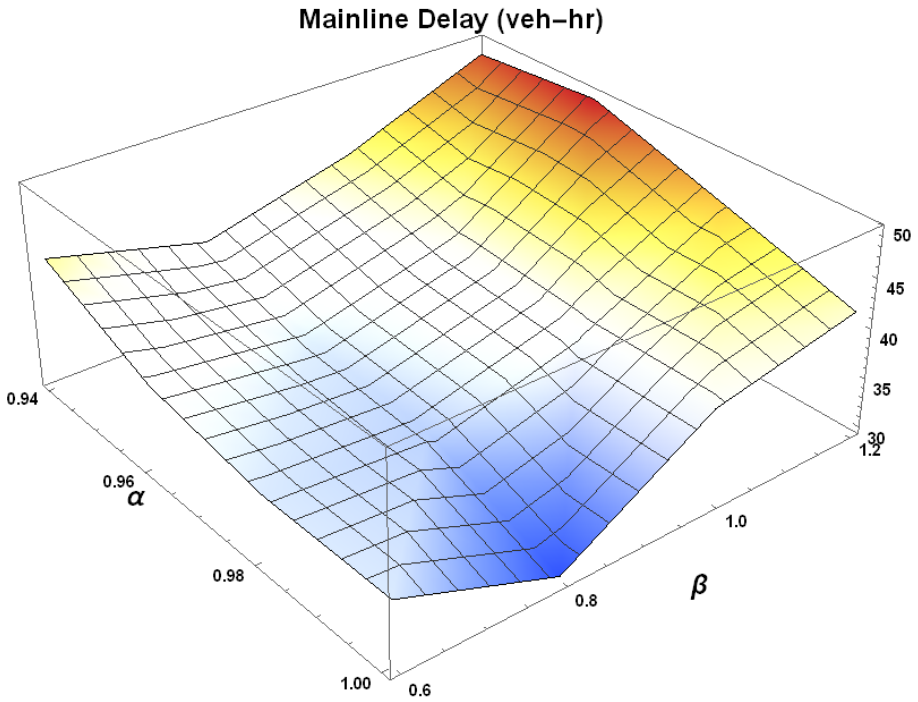

(b) VSL Shoulder Lane

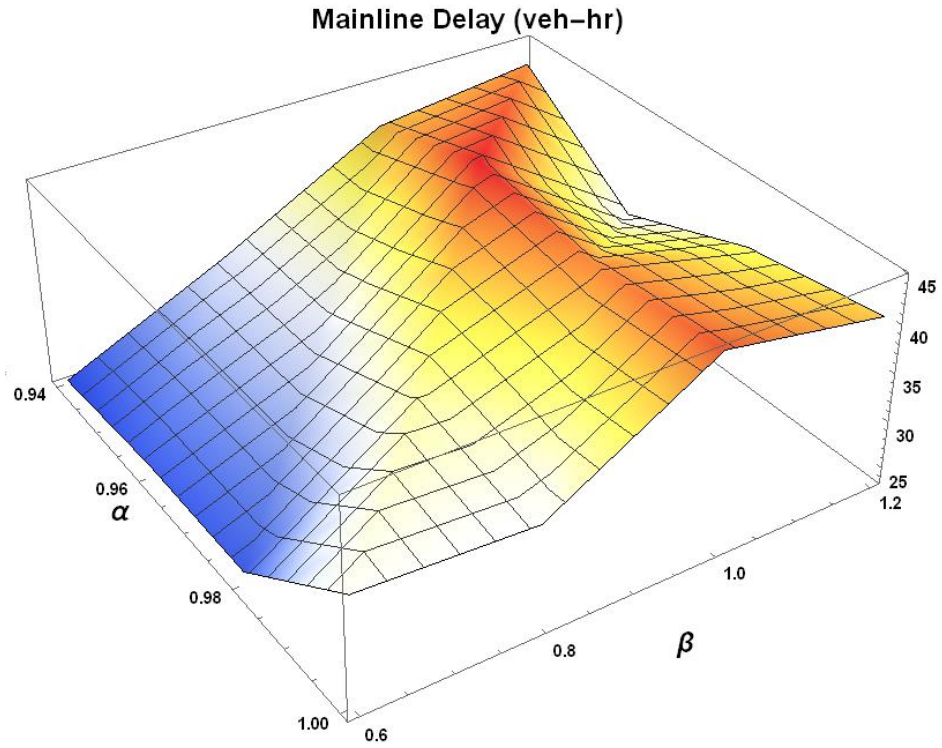

Figure 56 MOE (Mainline) contour map of parameter α (X-axis);, β (Y-axis) analysis of the (1/3, 1/3, 1/3) LFD

(a) VSL ALL Lanes

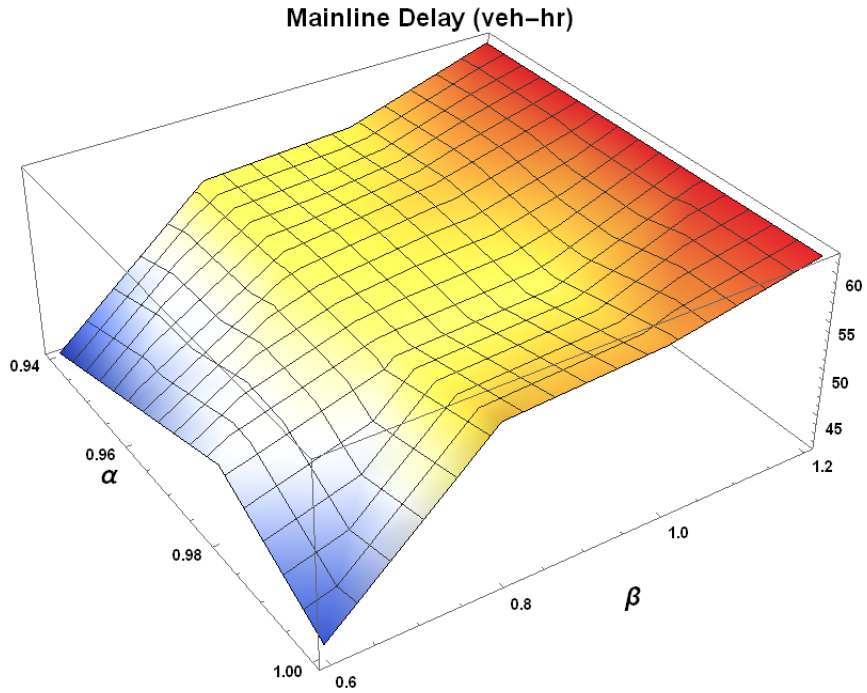

(b) VSL Shoulder Lane

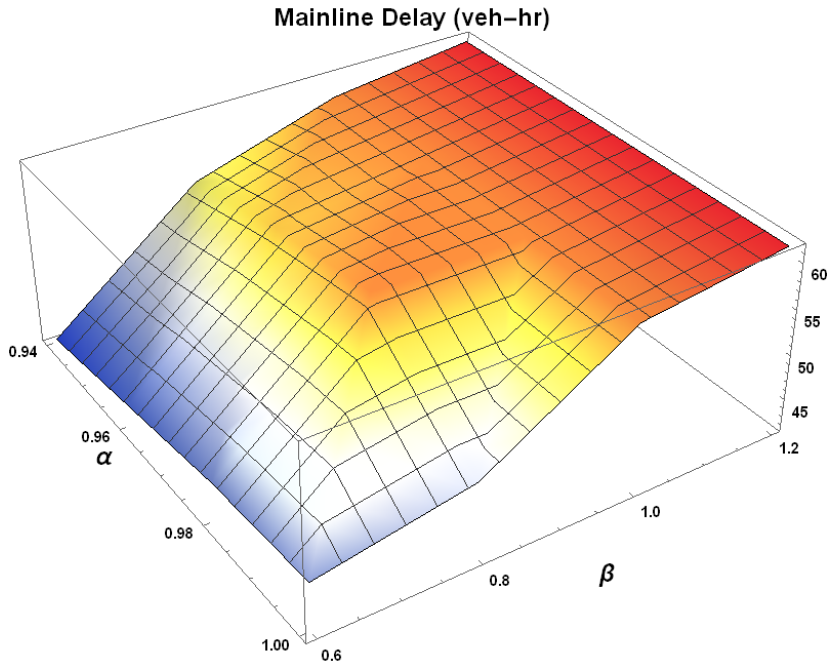

Figure 57 MOE (mainline) contour map of parameter α (X-axis); β (Y-axis) analysis of the (0.34, 0.34, 0.32) LFD

(a) VSL ALL Lanes

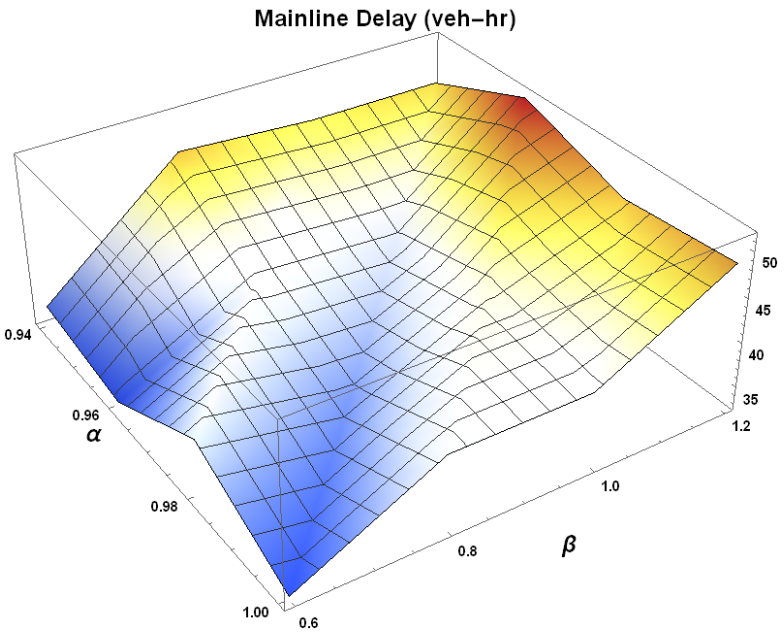

(b) VSL Shoulder Lane

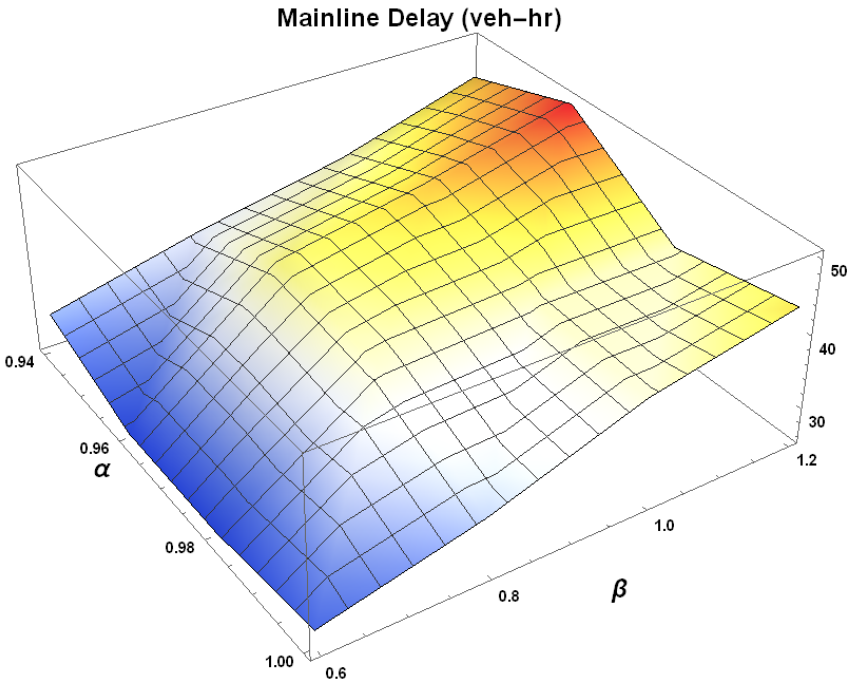

Figure 58 MOE (mainline) contour map of parameter α (X-axis); β (Y-axis) analysis of the (0.35, 0.35, 0.3) LFD

(a) VSL ALL Lanes

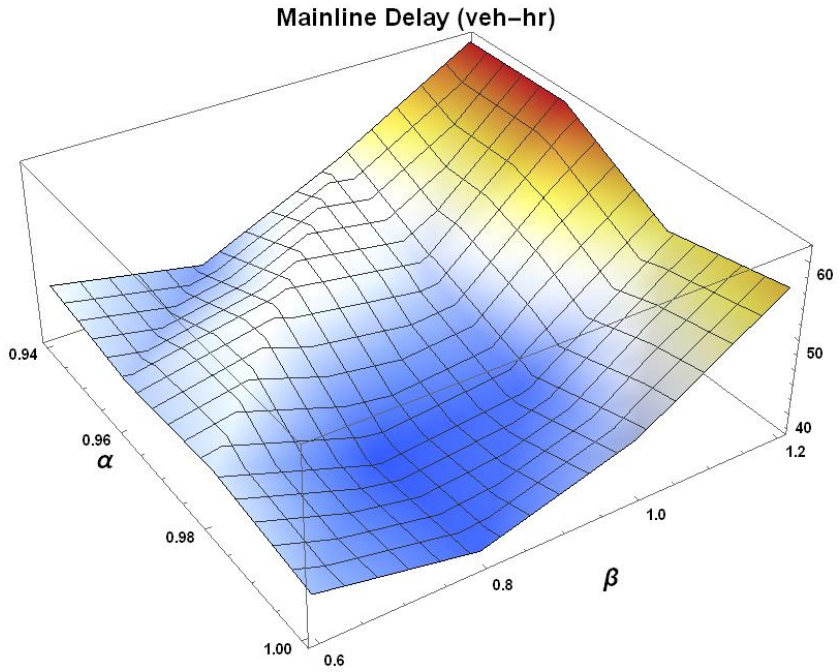

(b) VSL Shoulder Lane

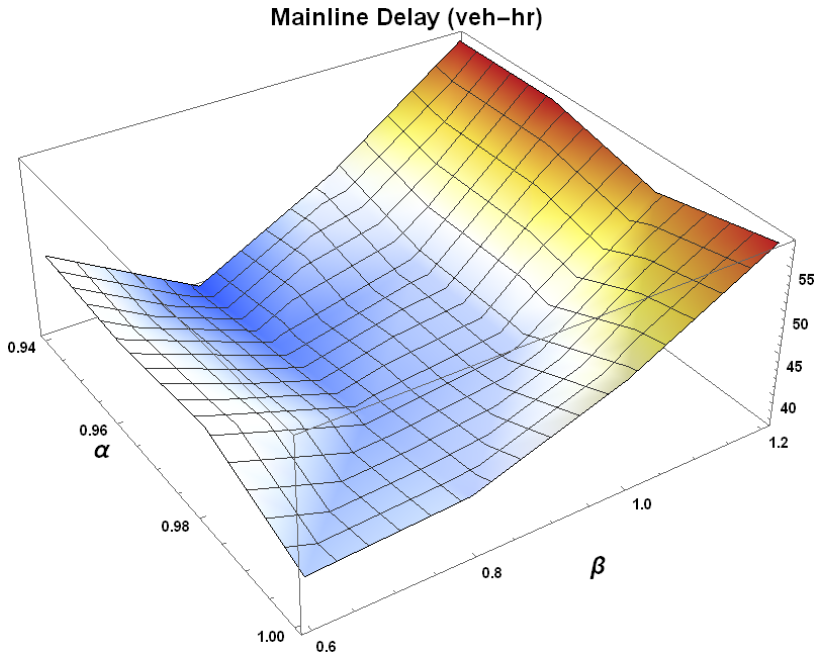

Figure 59 MOE (mainline) contour map of parameter α (X-axis); *β* (Y-axis) analysis of the (0.36, 0.36, 0.28) LFD

(a) VSL ALL Lanes

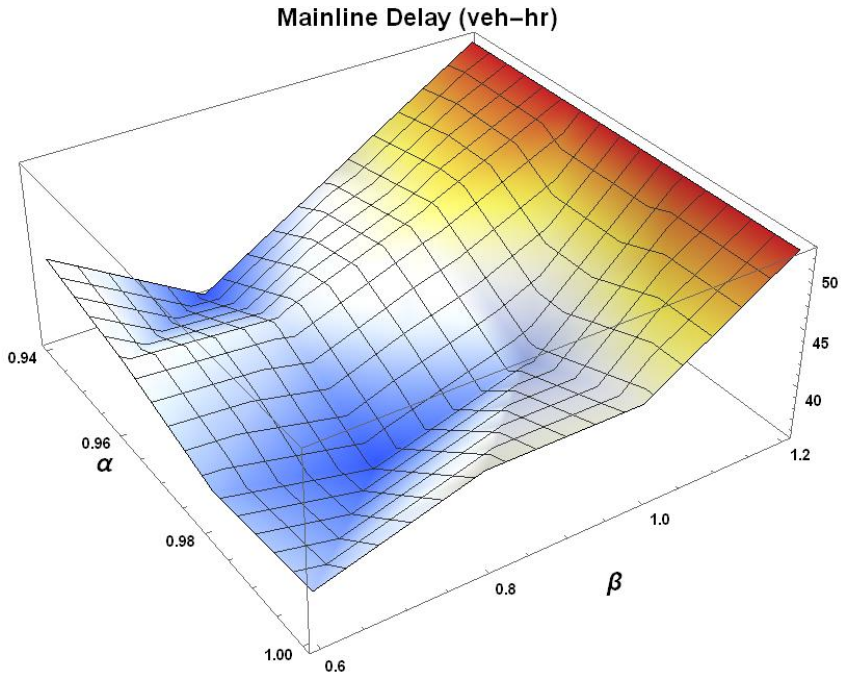

(b) VSL Shoulder Lane

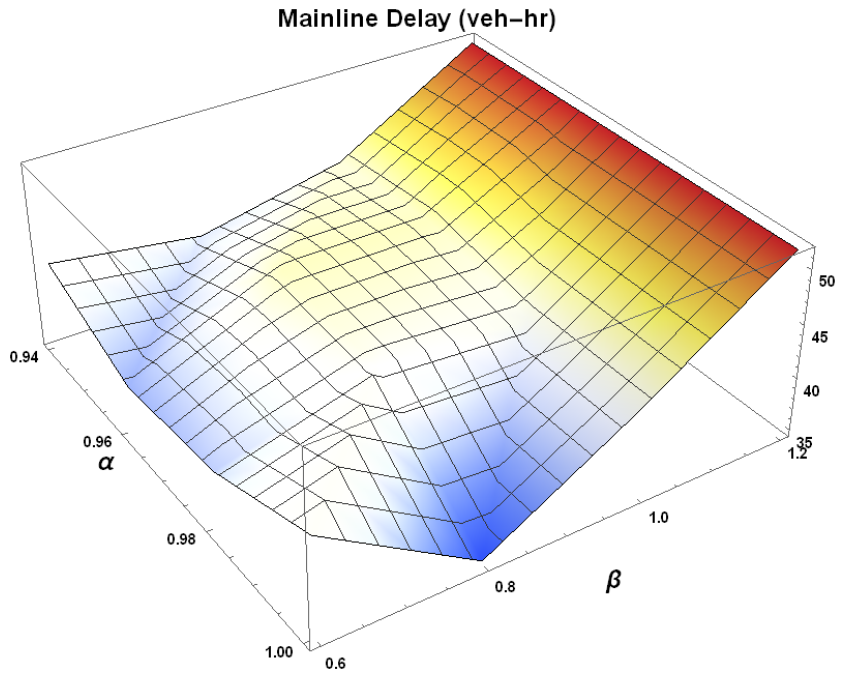

Figure 60 MOE (mainline) contour map of parameter α (X-axis); β (Y-axis) analysis of the (0.37, 0.35, 0.28) LFD

(a) VSL ALL Lanes

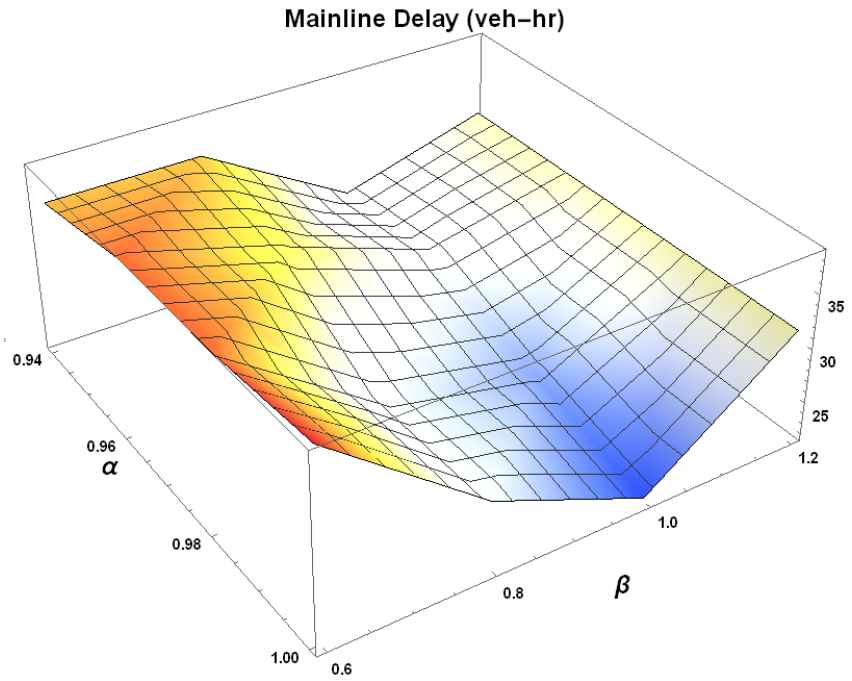

(b) VSL Shoulder Lane

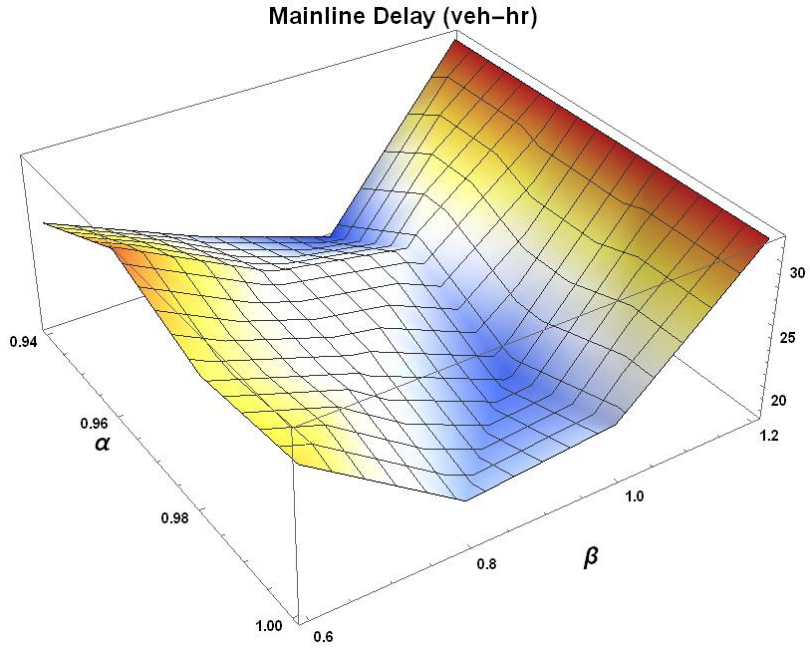

Figure 61 MOE (mainline) contour map of parameter α (X-axis); *β* (Y-axis) analysis of the (0.37, 0.36, 0.27) LFD

4.4. Conclusion

To prevent and recover from a capacity drop in a merge area, we proposed and simulated the combined VSL and RM models. Based on the one-lane merge network simulation results, we found that combining the VSL and RM models is the most effective method of maintaining maximum freeway capacity. If one is restricted to a single control strategy, however, the best choice depends on the distribution of the traffic demand. It is important to note that the simulation experiments invariably ended with a short but dense queue that propagated through the merge area, causing a queue on both the freeway and the ramp. We suspect that this situation resulted from the relaxation phenomenon after lane changing (Laval & Leclercq, 2008; Leclercq, Chiabaut, Laval, & Buisson, 2007).

From the three-lane merge network simulation results, we found that the effectiveness of the VSL is heavily related to the shoulder lane flow. In this simulation, the VSL operates as a supplement for ramp metering. If the length of the queue of the ramp is not a constraint, one may use only ramp metering. However, if it is, the VSL proposed in this study is more effective than using only ramp metering. We found that the optimal parameters of the VSL system varied among LFDs. Also, not all scenarios of the LFDs or the parameter settings of the VSL system could prevent a capacity drop. Therefore, further study of the optimal parameter of the VSL is needed if we are to apply it to the real world.

To the best of the author's knowledge, this study is the first to propose and simulate shoulder lane VSL. From the simulation results, we found that the VSL of the shoulder lane is more effective than the VSL of all lanes in terms of reducing delays in some LFDs. However, this study did not restrict the minimum speed of the VSL or the

maximum speed limit difference among lanes, which may be a critical issue pertaining to safety. Also, we minimized the length of the VSL zone in our simulation to 100 *m* to reduce the delay of vehicles that pass the VSL zone, which also poses a concern regarding the safety and stability of the system. In addition, GTsim did not incorporate a deceleration model of vehicles, which suggests another direction of research. Although the findings of this study indicate the need for further study that establishes explicit guidelines for practitioners, the findings of this research provide the groundwork for installing VSLs on mainlines at recurring merge bottlenecks.

CHAPTER V CASE STUDY: OPTIMAL COMBINED VARIABLE SPEED LIMITS AND RAMP METERING SYSTEMS

This chapter presents a case study of the optimal combined VSL and RM system model of a study corridor of the metro Atlanta freeway. Chapter 5.2 presents simulation settings, the RM, and the VSL modules in GTsim, and simulation-based optimization experiments. Chapter 5.3 describes their results, and Chapter 5.4 concludes with a discussion. The specific explanation of the study corridor and data analysis of this chapter is included in the Appendix.

5.1. Introduction

In traffic operations research, simulation-based optimization methods have been widely used (P. Li, Abbas, Pasupathy, & Head, 2010; Ma & Abdulhai, 2002; Osorio & Bierlaire, 2013; Osorio & Chong, 2015; Osorio, Flötteröd, & Zhang, 2015; Park, Yun, & Ahn, 2009; Park & Zhu, 2007; Yin, 2000; Yun & Park, 2006). Among these methods, the genetic algorithm (GA) is one of the most popular stochastic simulation-based optimization methods when solution spaces are very large. Only a few studies have adopted the GA in the ramp metering algorithm. Chu & Yang (2003) used the GA to find optimal parameters (regulator K_R, desired occupancy, update cycle of the metering rate, and location of the downstream detector) of ALINEA. The study applied ALINEA to only one on-ramp of seven entrance on-ramps, and the GA provided 2.5% improvement in the measurement of effectiveness (i.e., total vehicle travel time). Chilukuri, Laval, and Guin (2015) also used the GA to generate optimal parameters of the SWARM ramp metering algorithm for four entrance on-ramps.

In the previous chapter, we proposed the combined VSL and RM system and investigated the parameter sensitivity analysis of the system. We found that the optimal values of the parameters of the system vary in the lane flow distribution, and recommended further study to apply it to real life. This chapter presents a case study that implements the VSL-RM strategy in an actual freeway corridor in Atlanta. To find the optimal values of parameters that utilize the system, we incorporated the GA-based stochastic optimization and GTsim.

5.2. Simulation

5.2.1. **GTsim**

In this study, we developed a microscopic simulation model, GTsim (Chilukuri et al., 2014a; Cho & Laval, 2016). This application, based on the kinematic wave model, is the first of its kind proven to replicate traffic dynamics during congestion, such as capacity drop and relaxation phenomena. GTsim implements the latest lane-changing models, significantly improving our understanding of traffic congestion. Thus, in GTsim, we generated a 19.25-mile study corridor consisting of same number and lengths of lanes as the study corridor (see Appendix A.2). It also contains the exact number and location of the VDS, the ramp meter system, and the VSL (see Figure 62-63). In Figure 62, a green sign indicates an origin and red a destination. Figure 63 describes some examples of GUI of GTsim.

As input flow, we used the estimated O/D flows described in Appendix A.3. The O/D flows were automatically updated every five minutes in the simulation. The corridor was simulated for approximately 120 minutes (14:30 to 16:30) and included congestion buildup and completely congested conditions (60 minutes), and starving input flows to dissipate congestion (60 minutes). The simulation continuously stored the flow and the speed information at the detector station prescribed in the model.

The total travel time, defined as the sum of the O/D travel times of all vehicles during the simulation time, was adopted as the measure of effectiveness (MOE) to evaluate the performance of the set of RM and VSL parameters. In the case of the queue spilling back to the origin, which prevents the generation of the same input flows as other cases, we imposed an extra-large travel time penalty, which differentiated the cases.

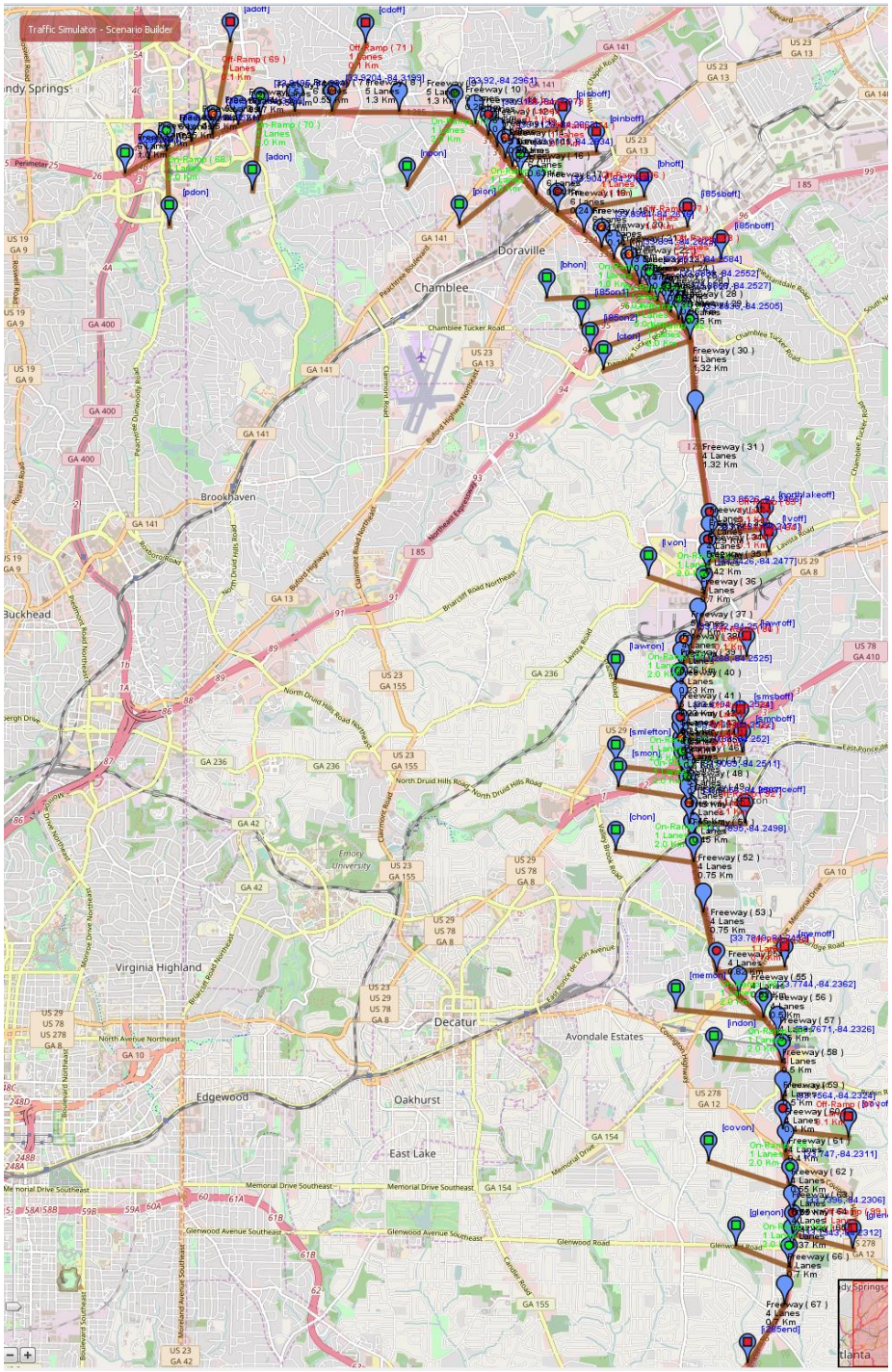

Figure 62 GTsim Corridor

(a) Two Lane Drop Geometry GUI of GTsim

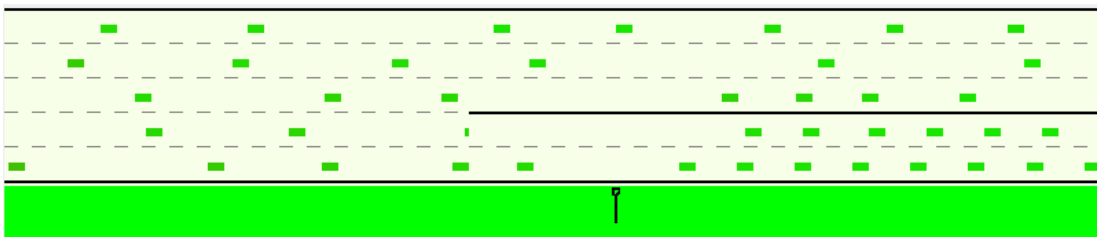

(b) Ramp Metering GUI of GTsim

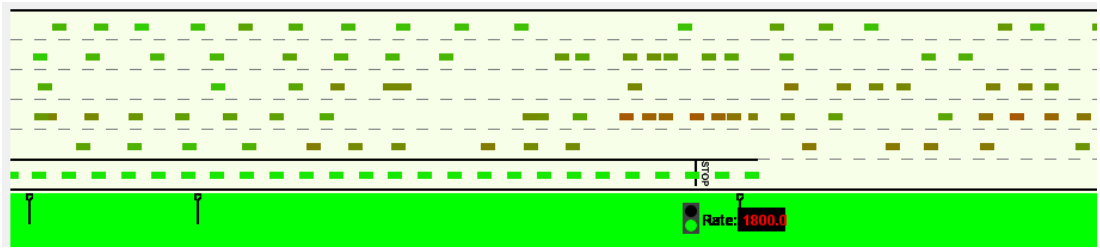

(c) Queue Flush

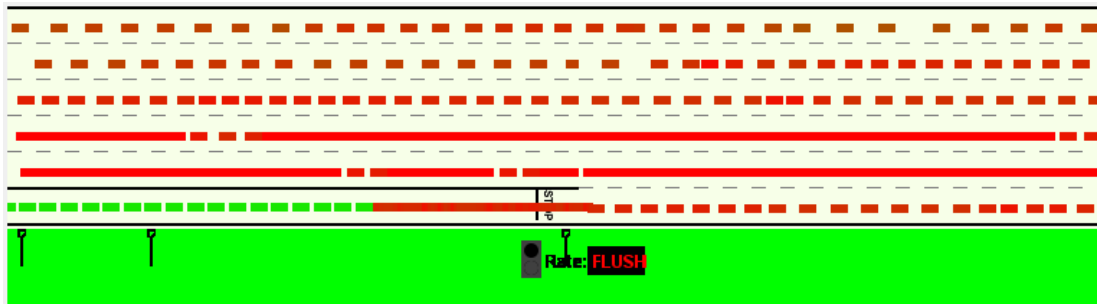

Figure 63 GUI of (a) Two-lane drop geometry, (b) ramp metering, and (c) the queue flush of GTsim

5.2.2. **RM and VSL module in GTsim**

In this study, we aim to produce optimal metering rates for each on-ramp meter system. GDOT implemented the ALINEA algorithm. Parameter K_R in ALINEA is location specific, so it will be optimized in this study. $\hat{o}$ in ALINEA represents critical occupancy (target density), which is also location specific, and the detector lies in 250 to 600m downstream of the merge location.

To obtain this value of the density for each location, we plotted flow-density (q-k) curves using NaviGAtor's VDS data (see Appendix A.5). NaviGAtor's VDS data produce flow, speed, and occupancy for 20 seconds, so we transformed the data to five-minute data. We also converted the time-mean speed to the space-mean speed. After processing, we generated the density by dividing the flow by the space-mean speed.

We adopted the VSL-RM model (method 4) from Chapter 4. In this model, the VSL is activated only when the queue flush is activated, and the speed of the VSL is calculated from equation $\alpha\ \mu_c - \beta\ q_1 = w(k_j - k_{vsl}) = v_{vsl}k_{vsl}$. The two parameters, α and β, will be optimized in this study. For the VSL-RM system model, we had no choice but to implement the model in only one merge location (see Appendix A.2) of the study corridor in GTsim. We implemented the shoulder-lane VSL to this merge location.

5.2.3. **Calibration and Validation**

GTsim has several parameters that must be calibrated. From (Chilukuri et al., 2014a). The parameters are categorized into capacity parameters (i.e., free-flow speed, jam density, and wave speed), lane-changing parameters (i.e., longitudinal distance between a vehicle and an exit ramp, tau (i.e., time to execute a lane-changing maneuver), epsilon (i.e., relaxation speed gap), and driver behavior parameters (friction speed). These calibrated parameters are summarized in Table 14. We used all parameter values in Table 14 for the entire corridor, except the value for the parameter of longitudinal distance between a vehicle and an exit ramp. For some sections of the study corridor, the higher value of this parameter was needed to replicate feasible congestion propagation.

Table 14 Calibrated Parameters

Calibrated Parameter	Parameter Value
Free-flow speed	100 *km/hr*
Jam density	150 *veh/km*
Wave speed	20 *km/hr*
Longitudinal distance between vehicle and exit ramp	2 (4) *km*
Tau (time to execute a lane changing maneuver)	4 *s*
Epsilon (relaxation speed gap)	2
Friction speed	20 *km/hr*

We validated the model by comparing the speed contour maps of (a) NaviGAtor's VDS data (2016/04/12) and (b) GTsim (see Figure 64) that use the estimated O/D flow as input flows of the same day. In Figure 64, the color legend shows the speed scale (unit: *km/hr*). Note that in the speed plot of NaviGAtor (Figure 64 (a)), vehicle speeds over 100 (*km/hr*) are capped at 100 (*km/hr*) to meet the free-flow speed of GTsim. We found that in the real-world corridor on the date (Figure 64 (a)), congestion formed around the 34-mile post area at about 2:45 PM and around the 38-mile post area at about 3:30 PM. We confirmed similar patterns in the GTsim plots (Figure 64 (b)).

(a) NaviGAtor VDS

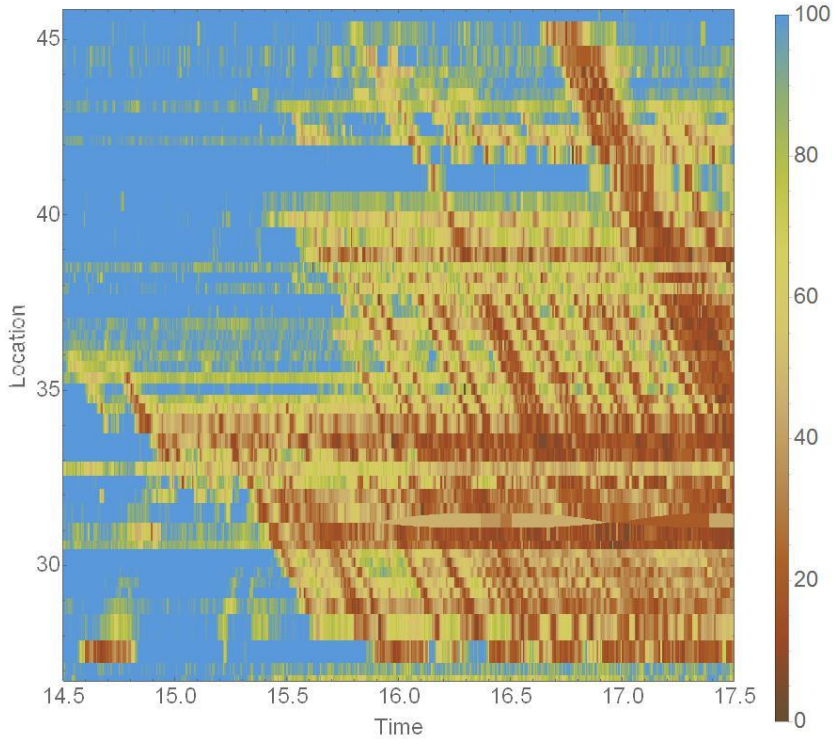

(b) GTsim

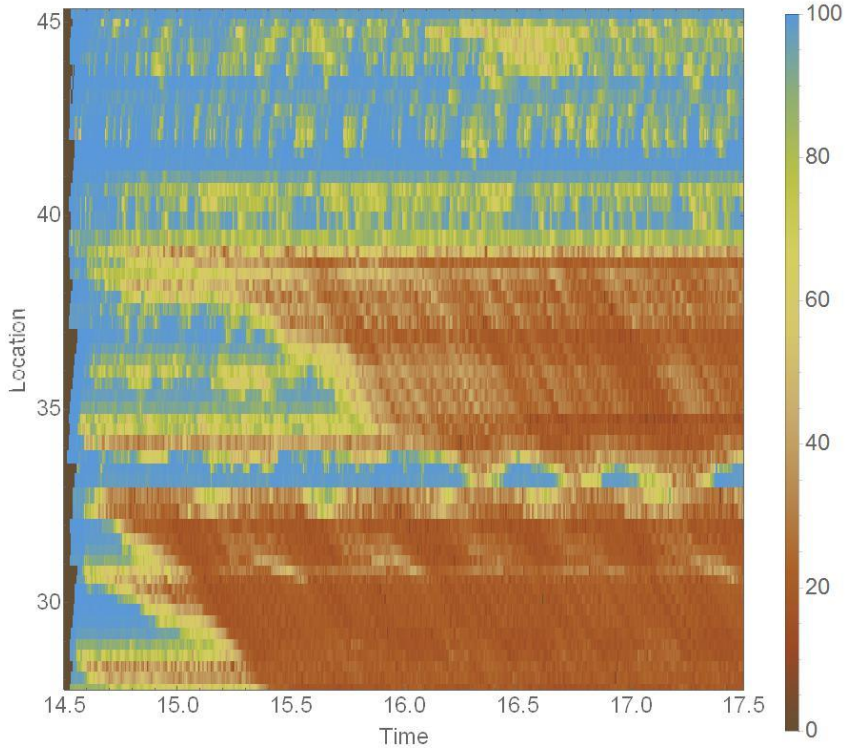

Figure 64 Speed contour map (Unit: *km*) of (a) NaviGAtor and (b) GTsim

5.2.4. **Simulation Optimization-Genetic Algorithm**

One of the most widely used stochastic simulation-optimization techniques in engineering, the sciences, and the social sciences is the genetic algorithm (GA). The evolution of the GA is successful, its method is robust to adapting to biological systems, and its parallel implementation with computer software and hardware is relatively easy. The GA searches for an optimal solution while iteratively evolving with probabilistic selection, crossover, and mutation (Mitchell, 1997).

The number of allowable values of each of the eleven K_R (or queue flush) parameters in this study correspond to a total of 85,899,300,000,000,000,000 ($\approx 80^{11}$) combinations of K_R parameter values. Not surprisingly determining the optimal set of parameter values from this huge set is extremely time consuming. The GA is known for searching "spaces of hypotheses containing complex interacting parts, where the impact of each part on overall hypothesis fitness may be difficult to model" (Mitchell, 1997).

Two main components of the optimization framework of this study are the GA optimizer and the GTsim module (Figure 65). The GA optimizer provides a set of parameter values used by the GTsim module to evaluate the total travel time sent back to the optimizer. The GTsim application continuously provides status information to the ramp-metering algorithm that calculates metering rates based on status information and the parameters provided by the GA optimizer.

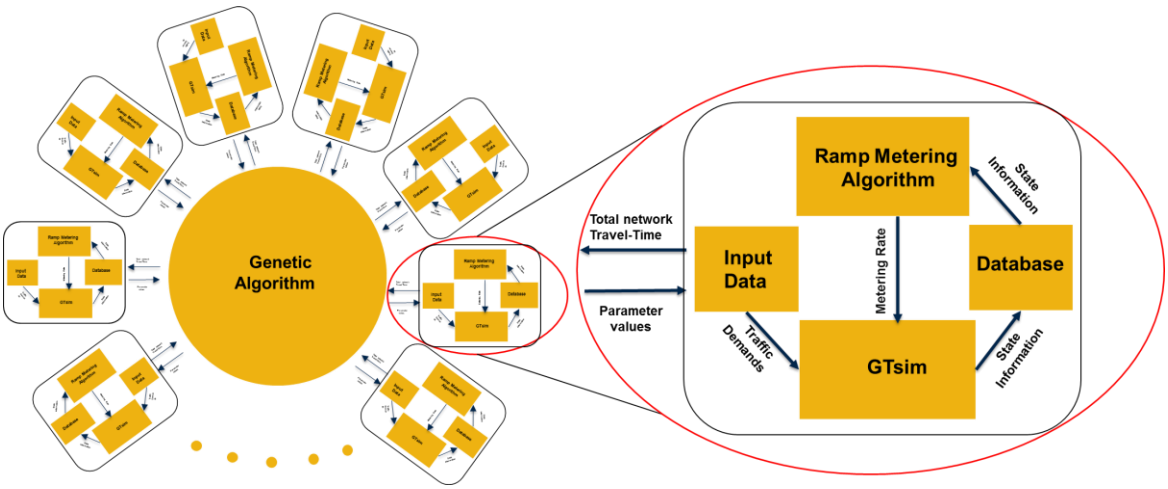

Figure 65 GA-based Optimization Scheme (Chilukuri et al., 2015)

We used 32 parallel 2.30 GHz maximum speed CPUs as the GA optimizer. Each GTsim module runs approximately two minutes to process a 120-minute simulation running time. The size of the population of each generation is set to 30. Elitism and tournament selection methods are used for the selection process. The probability of the uniform rate of crossover is set to 0.4, which indicates less than 40% parameter crossover. For mutation, the uniform probability is set to 0.5 (50% of mutation). Continuing to selection, crossover, and mutation, the GA optimizer evaluates the fitness of the output and determines whether or not to proceed (evolve) or to stop. The GA optimizer continues to evolve and iterate until it finds the optimal solution.

5.3. Results

The results of the simulation-optimization for three cases (no control, the RM control only, the VSL-RM control) are summarized in Table 15. We found that the performance of the VSL-RM with optimized parameters outperforms the RM control only model with its optimized parameters in terms of reducing total travel time.

Table 15 Travel time (vehicle-hour) comparison of No Control, the RM only, and the VSL-RM cases

Case	System	Ramp	Freeway
No Control	6561	175	6386
RM Only	6254 (4.7%)	194 (-10.9%)	6061 (5.1%)
VSL-RM	6038 (8.0 %)	192 (-9.7%)	5846 (8.5%)

Figure 66-8 show the speed contour maps of each control case. In the figure, we found that most congestion arises upstream of the 32-milepost. The VSL in this study corridor is located at the 34-milepost, and the target bottleneck location is downstream of the 35-milepost, highlighted by the red oval line in the figures. We found that both controls reduce congestion in the target area. The main benefits of the controls are that they delay the bottleneck formation time and lessen the severity of the bottleneck (passing speed).

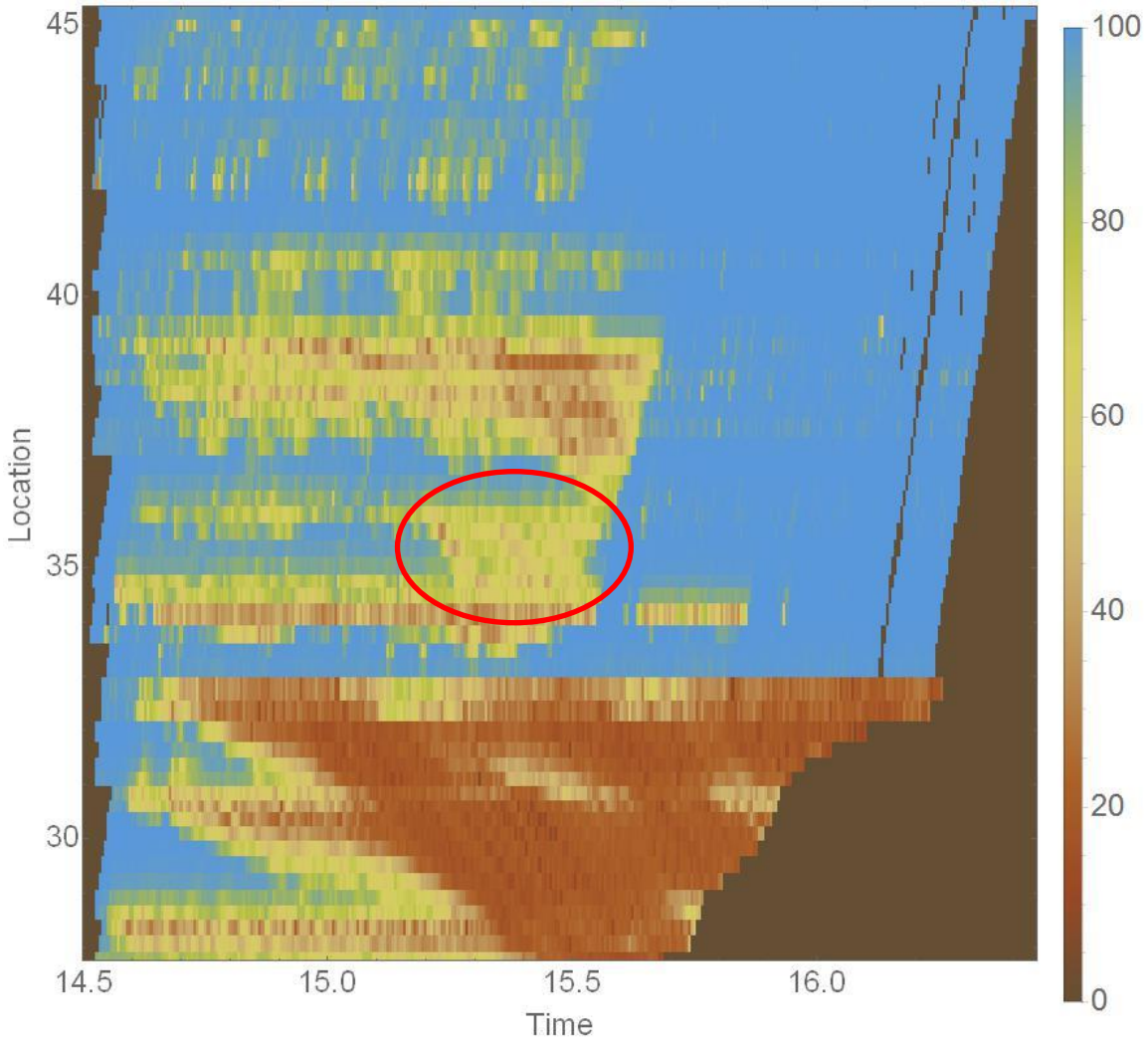

Figure 66 Speed Contour map of No control case

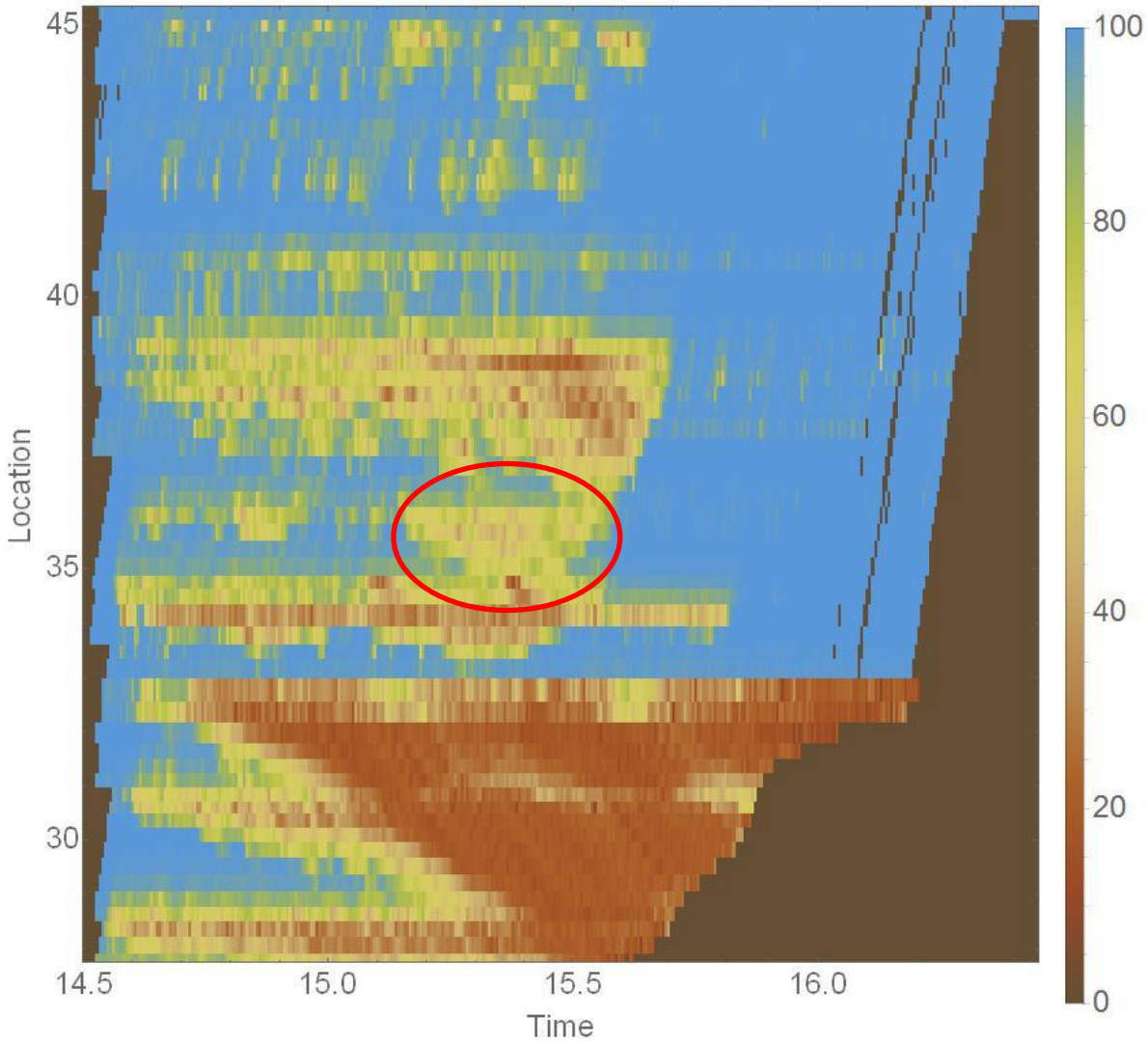

Figure 67 Speed Contour map of the RM only case

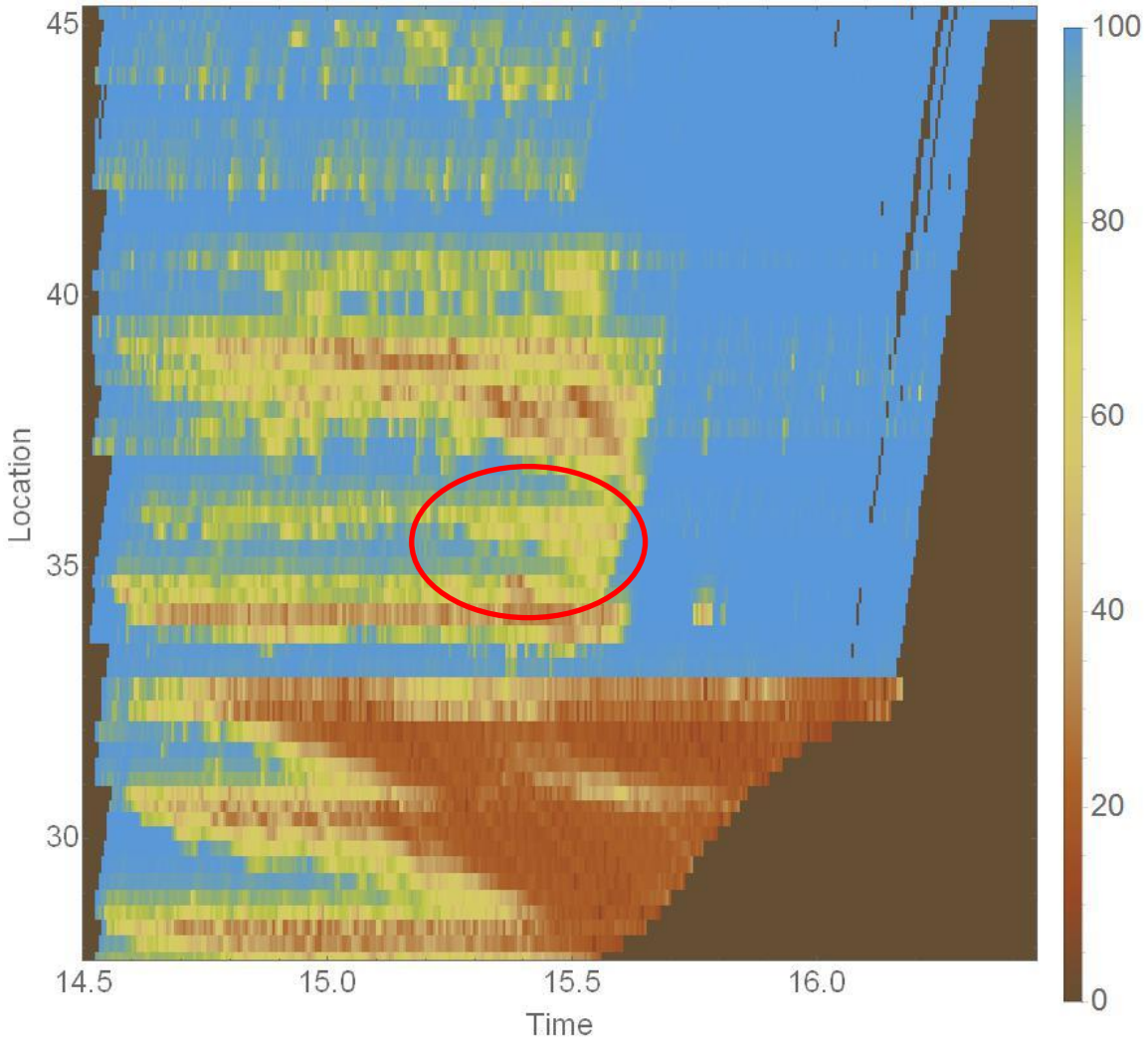

Figure 68 Speed Contour map of the VSL-RM case

As mentioned, all possible values for the K_R parameters and the solution spaces of the VSL parameters are very large. The GA ran for up to 500 generations. After 300 generations, the GA converged to a minimum. To confirm that it was truly the global minima, tens of thousands of combinations of allowable values of impact parameters were also simulated. We found that the minimum obtained from the GA after 300 generations was indeed the global minimum. Thus, it was confirmed that the GA parameters used above will converge to the global minimum. We also found that using the optimal parameter values of either model in the other model does not improve the system, rather it deteriorates it instead. This optimal parameter set, however, is very sensitive possibly because bottlenecks are correlated, not isolated. Table 16 summarizes the optimal parameter values of the RM only system and the VSL-RM system.

Table 16 Optimal parameter values of the RM only and VSL-RM models

Location	K_R (RM only)	K_R (VSL+RM)
Ashford Dunwoody Rd	118	138
North Peachtree Rd	92	103
Peachtree Industrial Blvd	95	145
Chamblee Tucker Rd	151	84
α OF the VSL	-	0.958
β of theVSL	-	1.286
Lavista Rd	120	114
Lawrenceville Hwy	106	132
Church St	124	111
Memorial Dr	106	122
Covington Hwy	142	79
Glenwood Rd	104	122

5.4. Conclusions

This study presented the stochastic simulation-based optimization framework that integrates GTsim and the GA-based optimization module to determine optimal parameter values of the combined VSL-RM and RM only systems. With these optimal parameter values, we compared the minimum total travel time of the two systems to the no control case. We found that the optimal values derived from this case study, compared to the no-metering case scenario, reduce travel times by more than 8%. The optimal parameter values derived in this case study are temporal and location sensitive and need to be optimized for other locations and time periods. However, the optimization framework developed in this study can be seamlessly used to generate optimal parameters for other locations.

CHAPTER VI CONCLUSIONS

This dissertation developed analytical and simulation models of (i) managed toll lanes (MTL) and (ii) the combined variable speed limit and ramp metering system, and using the GA-based simulation-optimization framework, it investigated (iii) a case study of the optimal VSL-RM model that implements real-world data.

When the bottleneck capacity of a freeway is unstable and changes, the variable bottleneck capacity model discussed in Chapter 3 showed greater savings in total delay than the constant bottleneck capacity model. In the variable bottleneck capacity model, the toll was proportional to the total system delay, and the model had a property that delay and revenue obtained from any traffic situation are approximately linear functions of the parameters and traffic even when the bottleneck capacity of a freeway varies.

In the real world, one of the system requirements of operating the MTL is to keep the MTL free-flow; however, we designed the MTL of the model in Chapter 3 to become congested to create a bottleneck and measure its capacity. Although the bottleneck capacity is a key variable of the model, the model is analytically valid with a constant bottleneck capacity that can be obtained from the real world (Laval et al., 2015). Maintaining the MTL at capacity without queues within the model, the operator intuitively maximizes revenue.

When the freeway is operating at capacity, it is vulnerable to breakdown and results in a capacity drop. To prevent and recover from a capacity drop, Chapter 4 presented the combined VSL and RM model. This model incorporates the kinematic wave traffic flow model and ALINEA and the queue flush ramp metering system. Based on our simulation experiments of a simple one-lane network, we found that combining

the VSL and RM models is more effective at maintaining maximum freeway capacity than using either single method alone. However, results of the three-lane merge network experiments show that the effectiveness of the VSL-RM varies with regard to the shoulder lane flow and the parameters that relate to the target capacity of the freeway and control the ramp queue.

Chapter 5 presented a case study of the VSL-RM model that incorporates the real-world network and data. The micro-simulation model GTsim was integrated into the GA-based simulation-optimization framework, which generates optimal parameters of the VSL-RM model. We found that compared to the no control and incautious set of parameters of the model, the optimal set of parameters of the model improves the system in terms of minimizing the total vehicle travel time.

The contribution of the VSL-RM model of this dissertation is its utilization of the mechanism of the capacity drop. The parameter presented in the model showed a guideline for maximum capacity without the capacity drop. The model was also the first to incorporate the queue warning and queue flush system, which had not been subject to experiments before. Another contribution is that it provided insight into the relationship between the control and the shoulder lane flow, finding that when the shoulder lane VSL is applied at the upstream of the bottleneck, lane-changing from the shoulder lane to the median lane increases. However, if there is less flow on the shoulder lane, merging onto the freeway is easier for the on-ramp flow, so the shoulder lane VSL is beneficial to the on-ramp flow and the system in terms of preventing a capacity drop.

Despite its advantages, the VSL-RM model presented in this dissertation has limitations in applications to real-world situations and demands further research. The

model assumes that the compliance rate of a vehicle is 100%, which is not realistic in real life. The model also does not account for the safety guideline of speed limits and the deceleration ability of vehicles. Experiments pertaining to the VSL-RM model in Chapter 4.3.2 entailed single demand but tested various lane flow distributions. In addition, the model does not account for the stochastic nature of capacity drops of merging. These limitations could be addressed in future studies. Finally, future connected vehicle technology will enable the adjustment of the length of the VSL zone, the on- and off-time of the VSL-RM, and the balanced lane flow distribution of the VSL and acceleration zones of the freeway.

APPENDIX

A.1. Result of Chapter 4.3.2.

Table 17 Results of simulation experiments of Chapter 4.3.2.

Cases	Median Lane	Center Lane	Shoul Lane	α	β	Total Delay	Ramp Delay	Mainline Delay
NoControl	0.333	0.333	0.333	0	0	59.34	1.65	57.69
NoControl	0.34	0.34	0.32	0	0	79.34	1.65	77.69
NoControl	0.35	0.35	0.3	0	0	76.34	1.65	74.69
NoControl	0.36	0.36	0.28	0	0	66.34	1.65	64.69
NoControl	0.37	0.35	0.28	0	0	64.34	1.65	62.69
NoControl	0.37	0.36	0.27	0	0	65.34	1.65	63.69
RMNoQF	0.333	0.333	0.333	0	0	62.34	42.65	19.69
RMNoQF	0.34	0.34	0.32	0	0	66.34	42.65	23.69
RMNoQF	0.35	0.35	0.3	0	0	51.34	38.65	12.69
RMNoQF	0.36	0.36	0.28	0	0	54.34	37.65	16.69
RMNoQF	0.37	0.35	0.28	0	0	56.34	36.65	19.69
RMNoQF	0.37	0.36	0.27	0	0	46.34	37.65	8.69
RMQF	0.333	0.333	0.333	0	0	64.34	14.65	49.69
RMQF	0.34	0.34	0.32	0	0	76.34	16.65	59.69
RMQF	0.35	0.35	0.3	0	0	62.34	15.65	46.69
RMQF	0.36	0.36	0.28	0	0	68.34	15.65	52.69
RMQF	0.37	0.35	0.28	0	0	64.34	15.65	48.69
RMQF	0.37	0.36	0.27	0	0	53.34	13.65	39.69
VSLA	0.333	0.333	0.333	1	1.2	61.34	19.65	41.69
VSLA	0.333	0.333	0.333	1	1	57.34	18.65	38.69
VSLA	0.333	0.333	0.333	1	0.8	51.34	21.65	29.69
VSLA	0.333	0.333	0.333	1	0.6	61.34	25.65	35.69
VSLA	0.333	0.333	0.333	0.98	1.2	66.34	20.65	45.69
VSLA	0.333	0.333	0.333	0.98	1	58.34	19.65	38.69
VSLA	0.333	0.333	0.333	0.98	0.8	56.34	21.65	34.69
VSLA	0.333	0.333	0.333	0.98	0.6	61.34	25.65	35.69
VSLA	0.333	0.333	0.333	0.96	1.2	70.34	20.65	49.69
VSLA	0.333	0.333	0.333	0.96	1	58.34	18.65	39.69
VSLA	0.333	0.333	0.333	0.96	0.8	57.34	21.65	35.69
VSLA	0.333	0.333	0.333	0.96	0.6	61.34	23.65	37.69
VSLA	0.333	0.333	0.333	0.94	1.2	69.34	20.65	48.69
VSLA	0.333	0.333	0.333	0.94	1	62.34	19.65	42.69
VSLA	0.333	0.333	0.333	0.94	0.8	60.34	21.65	38.69
VSLA	0.333	0.333	0.333	0.94	0.6	67.34	24.65	42.69
VSLA	0.34	0.34	0.32	1	1.2	76.34	14.65	61.69
VSLA	0.34	0.34	0.32	1	1	77.34	18.65	58.69
VSLA	0.34	0.34	0.32	1	0.8	78.34	20.65	57.69

VSLA	0.34	0.34	0.32	1	0.6	65.34	22.65	42.69
VSLA	0.34	0.34	0.32	0.98	1.2	76.34	14.65	61.69
VSLA	0.34	0.34	0.32	0.98	1	74.34	18.65	55.69
VSLA	0.34	0.34	0.32	0.98	0.8	74.34	19.65	54.69
VSLA	0.34	0.34	0.32	0.98	0.6	73.34	23.65	49.69
VSLA	0.34	0.34	0.32	0.96	1.2	76.34	14.65	61.69
VSLA	0.34	0.34	0.32	0.96	1	76.34	18.65	57.69
VSLA	0.34	0.34	0.32	0.96	0.8	76.34	20.65	55.69
VSLA	0.34	0.34	0.32	0.96	0.6	69.34	23.65	45.69
VSLA	0.34	0.34	0.32	0.94	1.2	76.34	14.65	61.69
VSLA	0.34	0.34	0.32	0.94	1	75.34	18.65	56.69
VSLA	0.34	0.34	0.32	0.94	0.8	76.34	20.65	55.69
VSLA	0.34	0.34	0.32	0.94	0.6	64.34	22.65	41.69
VSLA	0.35	0.35	0.3	1	1.2	66.34	17.65	48.69
VSLA	0.35	0.35	0.3	1	1	60.34	19.65	40.69
VSLA	0.35	0.35	0.3	1	0.8	62.34	21.65	40.69
VSLA	0.35	0.35	0.3	1	0.6	57.34	24.65	32.69
VSLA	0.35	0.35	0.3	0.98	1.2	65.34	17.65	47.69
VSLA	0.35	0.35	0.3	0.98	1	62.34	19.65	42.69
VSLA	0.35	0.35	0.3	0.98	0.8	57.34	21.65	35.69
VSLA	0.35	0.35	0.3	0.98	0.6	63.34	24.65	38.69
VSLA	0.35	0.35	0.3	0.96	1.2	69.34	17.65	51.69
VSLA	0.35	0.35	0.3	0.96	1	58.34	18.65	39.69
VSLA	0.35	0.35	0.3	0.96	0.8	62.34	21.65	40.69
VSLA	0.35	0.35	0.3	0.96	0.6	58.34	25.65	32.69
VSLA	0.35	0.35	0.3	0.94	1.2	64.34	17.65	46.69
VSLA	0.35	0.35	0.3	0.94	1	66.34	19.65	46.69
VSLA	0.35	0.35	0.3	0.94	0.8	70.34	22.65	47.69
VSLA	0.35	0.35	0.3	0.94	0.6	59.34	24.65	34.69
VSLA	0.36	0.36	0.28	1	1.2	72.34	15.65	56.69
VSLA	0.36	0.36	0.28	1	1	65.34	20.65	44.69
VSLA	0.36	0.36	0.28	1	0.8	60.34	21.65	38.69
VSLA	0.36	0.36	0.28	1	0.6	64.34	21.65	42.69
VSLA	0.36	0.36	0.28	0.98	1.2	69.34	15.65	53.69
VSLA	0.36	0.36	0.28	0.98	1	59.34	19.65	39.69
VSLA	0.36	0.36	0.28	0.98	0.8	59.34	21.65	37.69
VSLA	0.36	0.36	0.28	0.98	0.6	66.34	21.65	44.69
VSLA	0.36	0.36	0.28	0.96	1.2	77.34	15.65	61.69
VSLA	0.36	0.36	0.28	0.96	1	64.34	19.65	44.69
VSLA	0.36	0.36	0.28	0.96	0.8	70.34	22.65	47.69
VSLA	0.36	0.36	0.28	0.96	0.6	65.34	21.65	43.69
VSLA	0.36	0.36	0.28	0.94	1.2	77.34	15.65	61.69
VSLA	0.36	0.36	0.28	0.94	1	70.34	19.65	50.69
VSLA	0.36	0.36	0.28	0.94	0.8	63.34	21.65	41.69
VSLA	0.36	0.36	0.28	0.94	0.6	67.34	21.65	45.69
VSLA	0.37	0.35	0.28	1	1.2	63.34	11.65	51.69

VSLA	0.37	0.35	0.28	1	1	60.34	16.65	43.69
VSLA	0.37	0.35	0.28	1	0.8	63.34	19.65	43.69
VSLA	0.37	0.35	0.28	1	0.6	59.34	19.65	39.69
VSLA	0.37	0.35	0.28	0.98	1.2	63.34	11.65	51.69
VSLA	0.37	0.35	0.28	0.98	1	55.34	15.65	39.69
VSLA	0.37	0.35	0.28	0.98	0.8	55.34	19.65	35.69
VSLA	0.37	0.35	0.28	0.98	0.6	59.34	20.65	38.69
VSLA	0.37	0.35	0.28	0.96	1.2	63.34	11.65	51.69
VSLA	0.37	0.35	0.28	0.96	1	62.34	16.65	45.69
VSLA	0.37	0.35	0.28	0.96	0.8	60.34	19.65	40.69
VSLA	0.37	0.35	0.28	0.96	0.6	62.34	20.65	41.69
VSLA	0.37	0.35	0.28	0.94	1.2	63.34	11.65	51.69
VSLA	0.37	0.35	0.28	0.94	1	59.34	15.65	43.69
VSLA	0.37	0.35	0.28	0.94	0.8	55.34	19.65	35.69
VSLA	0.37	0.35	0.28	0.94	0.6	64.34	20.65	43.69
VSLA	0.37	0.36	0.27	1	1.2	43.34	11.65	31.69
VSLA	0.37	0.36	0.27	1	1	41.34	19.65	21.69
VSLA	0.37	0.36	0.27	1	0.8	45.34	17.65	27.69
VSLA	0.37	0.36	0.27	1	0.6	57.34	18.65	38.69
VSLA	0.37	0.36	0.27	0.98	1.2	43.34	11.65	31.69
VSLA	0.37	0.36	0.27	0.98	1	44.34	19.65	24.69
VSLA	0.37	0.36	0.27	0.98	0.8	46.34	18.65	27.69
VSLA	0.37	0.36	0.27	0.98	0.6	56.34	18.65	37.69
VSLA	0.37	0.36	0.27	0.96	1.2	43.34	11.65	31.69
VSLA	0.37	0.36	0.27	0.96	1	47.34	18.65	28.69
VSLA	0.37	0.36	0.27	0.96	0.8	52.34	18.65	33.69
VSLA	0.37	0.36	0.27	0.96	0.6	56.34	18.65	37.69
VSLA	0.37	0.36	0.27	0.94	1.2	43.34	11.65	31.69
VSLA	0.37	0.36	0.27	0.94	1	47.34	19.65	27.69
VSLA	0.37	0.36	0.27	0.94	0.8	54.34	18.65	35.69
VSLA	0.37	0.36	0.27	0.94	0.6	54.34	18.65	35.69
VSLS	0.333	0.333	0.333	1	1.2	60.34	19.65	40.69
VSLS	0.333	0.333	0.333	1	1	63.34	19.65	43.69
VSLS	0.333	0.333	0.333	1	0.8	55.34	21.65	33.69
VSLS	0.333	0.333	0.333	1	0.6	61.34	26.65	34.69
VSLS	0.333	0.333	0.333	0.98	1.2	58.34	19.65	38.69
VSLS	0.333	0.333	0.333	0.98	1	62.34	19.65	42.69
VSLS	0.333	0.333	0.333	0.98	0.8	58.34	21.65	36.69
VSLS	0.333	0.333	0.333	0.98	0.6	49.34	24.65	24.69
VSLS	0.333	0.333	0.333	0.96	1.2	53.34	19.65	33.69
VSLS	0.333	0.333	0.333	0.96	1	64.34	19.65	44.69
VSLS	0.333	0.333	0.333	0.96	0.8	53.34	21.65	31.69
VSLS	0.333	0.333	0.333	0.96	0.6	49.34	24.65	24.69
VSLS	0.333	0.333	0.333	0.94	1.2	62.34	19.65	42.69
VSLS	0.333	0.333	0.333	0.94	1	59.34	18.65	40.69
VSLS	0.333	0.333	0.333	0.94	0.8	53.34	21.65	31.69

VSLS	0.333	0.333	0.333	0.94	0.6	48.34	24.65	23.69
VSLS	0.34	0.34	0.32	1	1.2	76.34	14.65	61.69
VSLS	0.34	0.34	0.32	1	1	78.34	18.65	59.69
VSLS	0.34	0.34	0.32	1	0.8	69.34	19.65	49.69
VSLS	0.34	0.34	0.32	1	0.6	69.34	22.65	46.69
VSLS	0.34	0.34	0.32	0.98	1.2	76.34	14.65	61.69
VSLS	0.34	0.34	0.32	0.98	1	78.34	18.65	59.69
VSLS	0.34	0.34	0.32	0.98	0.8	80.34	20.65	59.69
VSLS	0.34	0.34	0.32	0.98	0.6	68.34	22.65	45.69
VSLS	0.34	0.34	0.32	0.96	1.2	76.34	14.65	61.69
VSLS	0.34	0.34	0.32	0.96	1	78.34	18.65	59.69
VSLS	0.34	0.34	0.32	0.96	0.8	78.34	20.65	57.69
VSLS	0.34	0.34	0.32	0.96	0.6	66.34	22.65	43.69
VSLS	0.34	0.34	0.32	0.94	1.2	76.34	14.65	61.69
VSLS	0.34	0.34	0.32	0.94	1	78.34	18.65	59.69
VSLS	0.34	0.34	0.32	0.94	0.8	75.34	20.65	54.69
VSLS	0.34	0.34	0.32	0.94	0.6	64.34	22.65	41.69
VSLS	0.35	0.35	0.3	1	1.2	61.34	17.65	43.69
VSLS	0.35	0.35	0.3	1	1	59.34	19.65	39.69
VSLS	0.35	0.35	0.3	1	0.8	54.34	21.65	32.69
VSLS	0.35	0.35	0.3	1	0.6	52.34	24.65	27.69
VSLS	0.35	0.35	0.3	0.98	1.2	57.34	16.65	40.69
VSLS	0.35	0.35	0.3	0.98	1	60.34	19.65	40.69
VSLS	0.35	0.35	0.3	0.98	0.8	62.34	22.65	39.69
VSLS	0.35	0.35	0.3	0.98	0.6	50.34	24.65	25.69
VSLS	0.35	0.35	0.3	0.96	1.2	68.34	17.65	50.69
VSLS	0.35	0.35	0.3	0.96	1	65.34	19.65	45.69
VSLS	0.35	0.35	0.3	0.96	0.8	64.34	22.65	41.69
VSLS	0.35	0.35	0.3	0.96	0.6	50.34	24.65	25.69
VSLS	0.35	0.35	0.3	0.94	1.2	63.34	17.65	45.69
VSLS	0.35	0.35	0.3	0.94	1	59.34	19.65	39.69
VSLS	0.35	0.35	0.3	0.94	0.8	57.34	21.65	35.69
VSLS	0.35	0.35	0.3	0.94	0.6	55.34	24.65	30.69
VSLS	0.36	0.36	0.28	1	1.2	73.34	15.65	57.69
VSLS	0.36	0.36	0.28	1	1	69.34	20.65	48.69
VSLS	0.36	0.36	0.28	1	0.8	64.34	21.65	42.69
VSLS	0.36	0.36	0.28	1	0.6	63.34	21.65	41.69
VSLS	0.36	0.36	0.28	0.98	1.2	70.34	15.65	54.69
VSLS	0.36	0.36	0.28	0.98	1	62.34	19.65	42.69
VSLS	0.36	0.36	0.28	0.98	0.8	62.34	21.65	40.69
VSLS	0.36	0.36	0.28	0.98	0.6	69.34	22.65	46.69
VSLS	0.36	0.36	0.28	0.96	1.2	74.34	16.65	57.69
VSLS	0.36	0.36	0.28	0.96	1	62.34	19.65	42.69
VSLS	0.36	0.36	0.28	0.96	0.8	60.34	21.65	38.69
VSLS	0.36	0.36	0.28	0.96	0.6	68.34	22.65	45.69
VSLS	0.36	0.36	0.28	0.94	1.2	74.34	16.65	57.69

VSLS	0.36	0.36	0.28	0.94	1	65.34	19.65	45.69
VSLS	0.36	0.36	0.28	0.94	0.8	58.34	21.65	36.69
VSLS	0.36	0.36	0.28	0.94	0.6	68.34	21.65	46.69
VSLS	0.37	0.35	0.28	1	1.2	63.34	11.65	51.69
VSLS	0.37	0.35	0.28	1	1	59.34	16.65	42.69
VSLS	0.37	0.35	0.28	1	0.8	54.34	19.65	34.69
VSLS	0.37	0.35	0.28	1	0.6	64.34	20.65	43.69
VSLS	0.37	0.35	0.28	0.98	1.2	63.34	11.65	51.69
VSLS	0.37	0.35	0.28	0.98	1	58.34	15.65	42.69
VSLS	0.37	0.35	0.28	0.98	0.8	63.34	19.65	43.69
VSLS	0.37	0.35	0.28	0.98	0.6	60.34	20.65	39.69
VSLS	0.37	0.35	0.28	0.96	1.2	63.34	11.65	51.69
VSLS	0.37	0.35	0.28	0.96	1	61.34	16.65	44.69
VSLS	0.37	0.35	0.28	0.96	0.8	64.34	19.65	44.69
VSLS	0.37	0.35	0.28	0.96	0.6	59.34	20.65	38.69
VSLS	0.37	0.35	0.28	0.94	1.2	63.34	11.65	51.69
VSLS	0.37	0.35	0.28	0.94	1	60.34	16.65	43.69
VSLS	0.37	0.35	0.28	0.94	0.8	60.34	19.65	40.69
VSLS	0.37	0.35	0.28	0.94	0.6	63.34	20.65	42.69
VSLS	0.37	0.36	0.27	1	1.2	43.34	11.65	31.69
VSLS	0.37	0.36	0.27	1	1	41.34	19.65	21.69
VSLS	0.37	0.36	0.27	1	0.8	38.34	17.65	20.69
VSLS	0.37	0.36	0.27	1	0.6	46.34	17.65	28.69
VSLS	0.37	0.36	0.27	0.98	1.2	43.34	11.65	31.69
VSLS	0.37	0.36	0.27	0.98	1	38.34	19.65	18.69
VSLS	0.37	0.36	0.27	0.98	0.8	42.34	18.65	23.69
VSLS	0.37	0.36	0.27	0.98	0.6	45.34	17.65	27.69
VSLS	0.37	0.36	0.27	0.96	1.2	43.34	11.65	31.69
VSLS	0.37	0.36	0.27	0.96	1	42.34	19.65	22.69
VSLS	0.37	0.36	0.27	0.96	0.8	42.34	17.65	24.69
VSLS	0.37	0.36	0.27	0.96	0.6	48.34	17.65	30.69
VSLS	0.37	0.36	0.27	0.94	1.2	43.34	11.65	31.69
VSLS	0.37	0.36	0.27	0.94	1	37.34	19.65	17.69
VSLS	0.37	0.36	0.27	0.94	0.8	39.34	17.65	21.69
VSLS	0.37	0.36	0.27	0.94	0.6	44.34	17.65	26.69

A.2. Study Corridor

The study in Chapter 5 involved the selection of a 19.25 mile long I-285 East Bound/South Bound corridor between GA-400 and I-20. This corridor contains thirteen ramp meter systems and 20 variable speed limits (see Figure 69). From typical traffic congestion characteristics from Google Maps and historical data of VDS (see Figure 70 to Figure 79), this study focuses on the onset period of evening peak congestion.

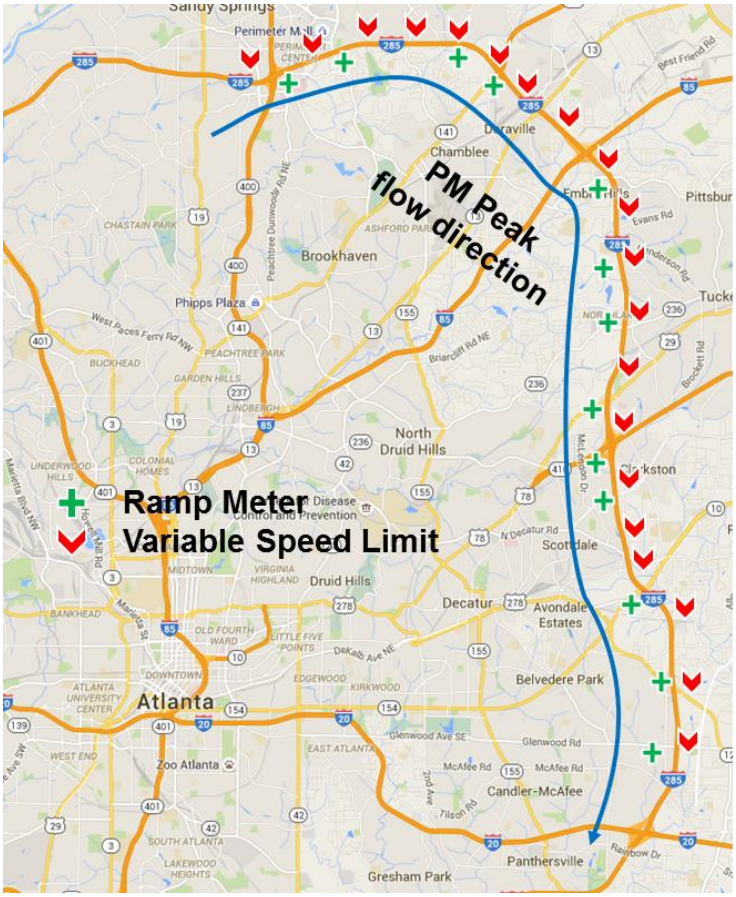

Figure 69 Case Study Corridor

The study corridor has the following seventeen entry locations (referred to as "origins" for the OD terminology) that feed traffic to the network.

- Upstream Freeway, Peachtree Dunwoody Road, Ashford Dunwoody Road, North Peachtree Road, Peachtree Industrial Parkway, Buford Highway, the I-85 Connector, Chamblee Tucker Road, Lavista Road, Lawrenceville Highway, WB Stone Mountain Freeway (left lane merge), EB Stone Mountain Freeway, Church Street, Memorial Drive, Indian Creek Station Connector, Covington Highway, Glenwood Road.

The corridor has the following seventeen exit locations (referred to as "destinations"):

- Ashford Dunwoody Road, Chamblee Dunwoody Road, SB Peachtree Industrial Parkway, NB Peachtree Industrial Parkway, Buford Highway, the SB I-85 Connector, the NB I-85 Connector, Northlake Parkway, Lavista Road, Lawrenceville Highway, WB Stone Mountain Freeway, EB Stone Mountain Freeway, East Ponce de Leon Avenue, Memorial Drive, Covington Highway, Glenwood Road, Downstream Freeway.

In the study corridor, among the ten ramp-metering systems installed on-ramp, five on-ramps are accompanied with by lane additions (see Table 18), to which the proposed model is not applicable. In Table 18, the six blue cells indicate on-ramps without lane-additions. However, from the data of this study, we found that the last four locations of these on-ramps are not congested during the study period. Therefore, the only applicable on-ramp areas are the Peachtree Dunwoody Road and Chamblee Tucker Road on-ramps.

Table 18 Number of lanes of up/down stream of the ramps in the corridor

Ramps	Lane Before	Lane After
GA 400 NB	6	6
PEACHTREE DUNWOODY RD	6	6
ASHFORD DUNWOODY RD	6	5
ASHFORD DUNWOODY RD	5	6
CHAMBLEE DUNWOODY RD	6	5
NORTH PEACHTREE RD	5	6
PTREE INDUS BLVD	6	6
PTREE INDUS BLVD NB	6	5
PTREE INDUS BLVD	5	6
BUFORD HWY	6	6
I-85 SB	6	5
I-85 NB EXIT RAMP	5	3
BUFORD HWY	3	3
I-85 C/D SYS	3	4
CHAMBLEE TUCKER RD	4	4
NORTHLAKE PKWY	4	4
LAVISTA RD	4	4
LAVISTA RD	4	5
LAWRENCEVILLE HWY	5	4
LAWRENCEVILLE HWY	4	5
STONE MOUNTAIN FWY	5	5
STONE MOUNTAIN FWY EB	5	4
STONE MOUNTAIN (Left Merge)	4	4
STONE MOUNTAIN FWY	4	5
EAST PONCE DE LEON AVE	5	4
CHURCH ST	4	4
MEMORIAL DR	4	4
MEMORIAL DR	4	4
INDIAN CREEK MARTA STATION	4	4
COVINGTON HWY	4	4
COVINGTON HWY	4	4
GLENWOOD RD	4	4
GLENWOOD RD	4	4
EXIT RAMP TO I-20 EB	4	3

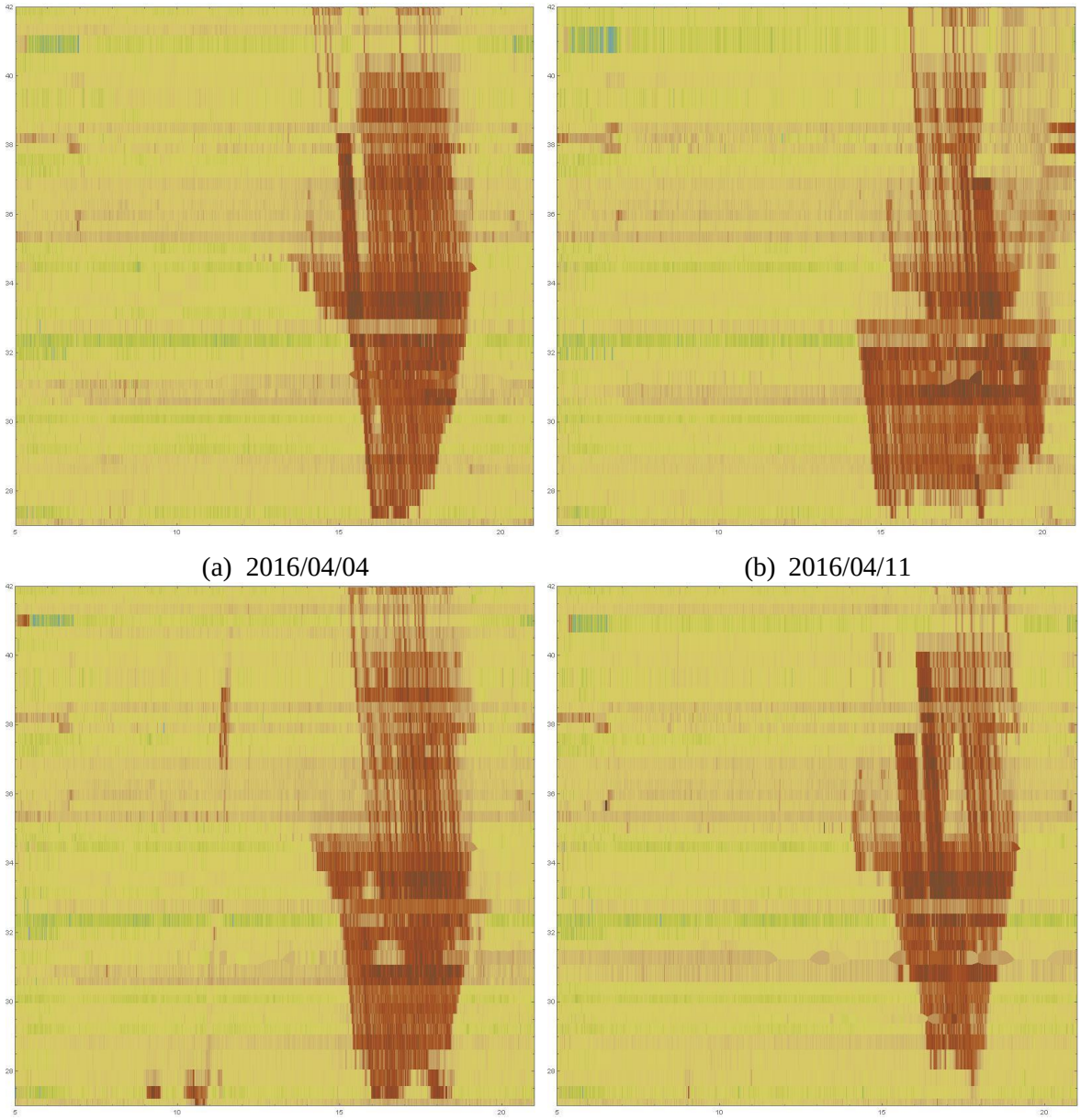

(a) 2016/04/04 (b) 2016/04/11

(c) 2016/04/18 (d) 2016/04/25

Figure 70 Speed contour maps of Monday, April 2016

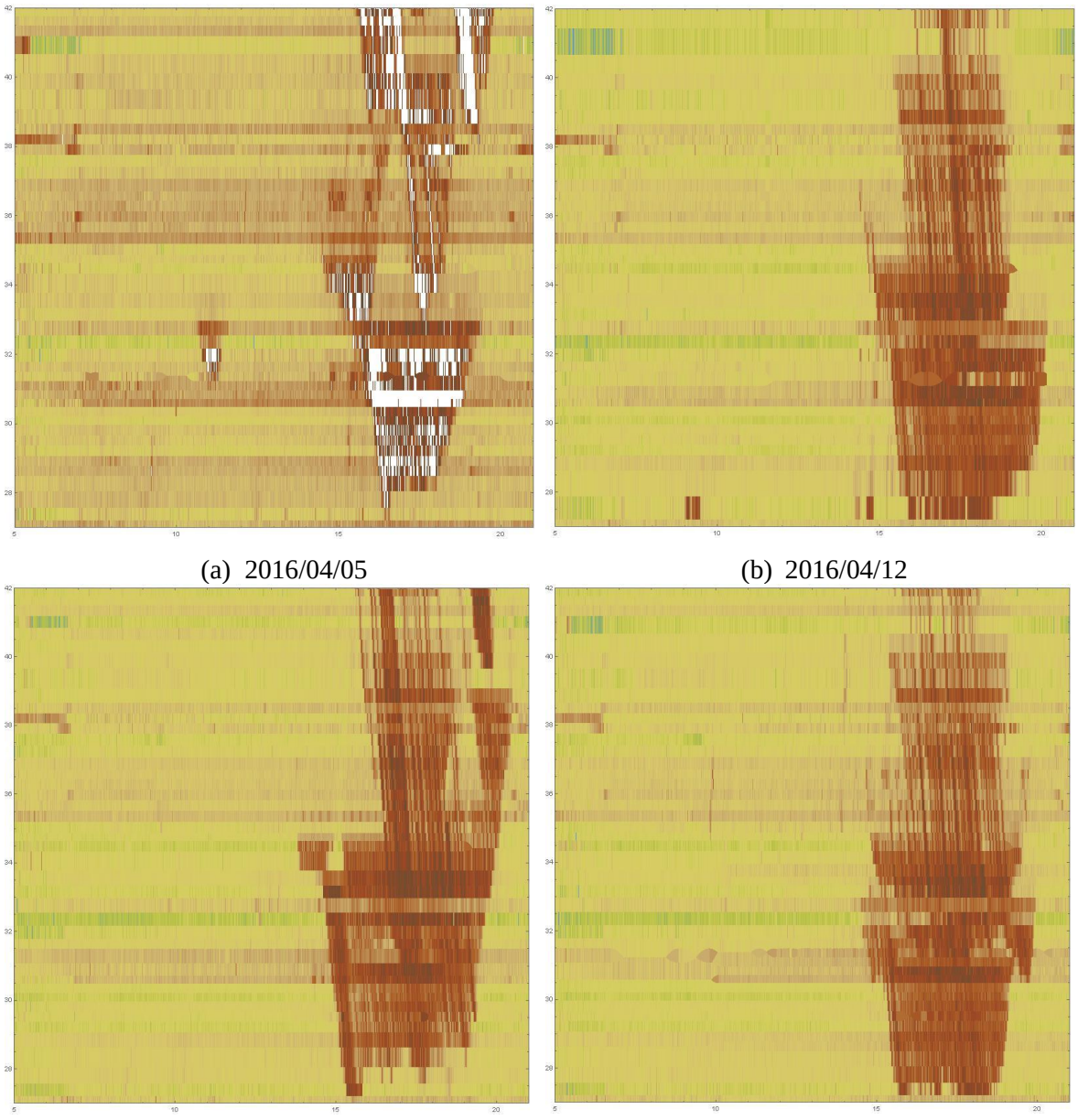

(a) 2016/04/05 (b) 2016/04/12

(c) 2016/04/19 (d) 2016/04/26

Figure 71 Speed contour maps of Tuesday, April 2016

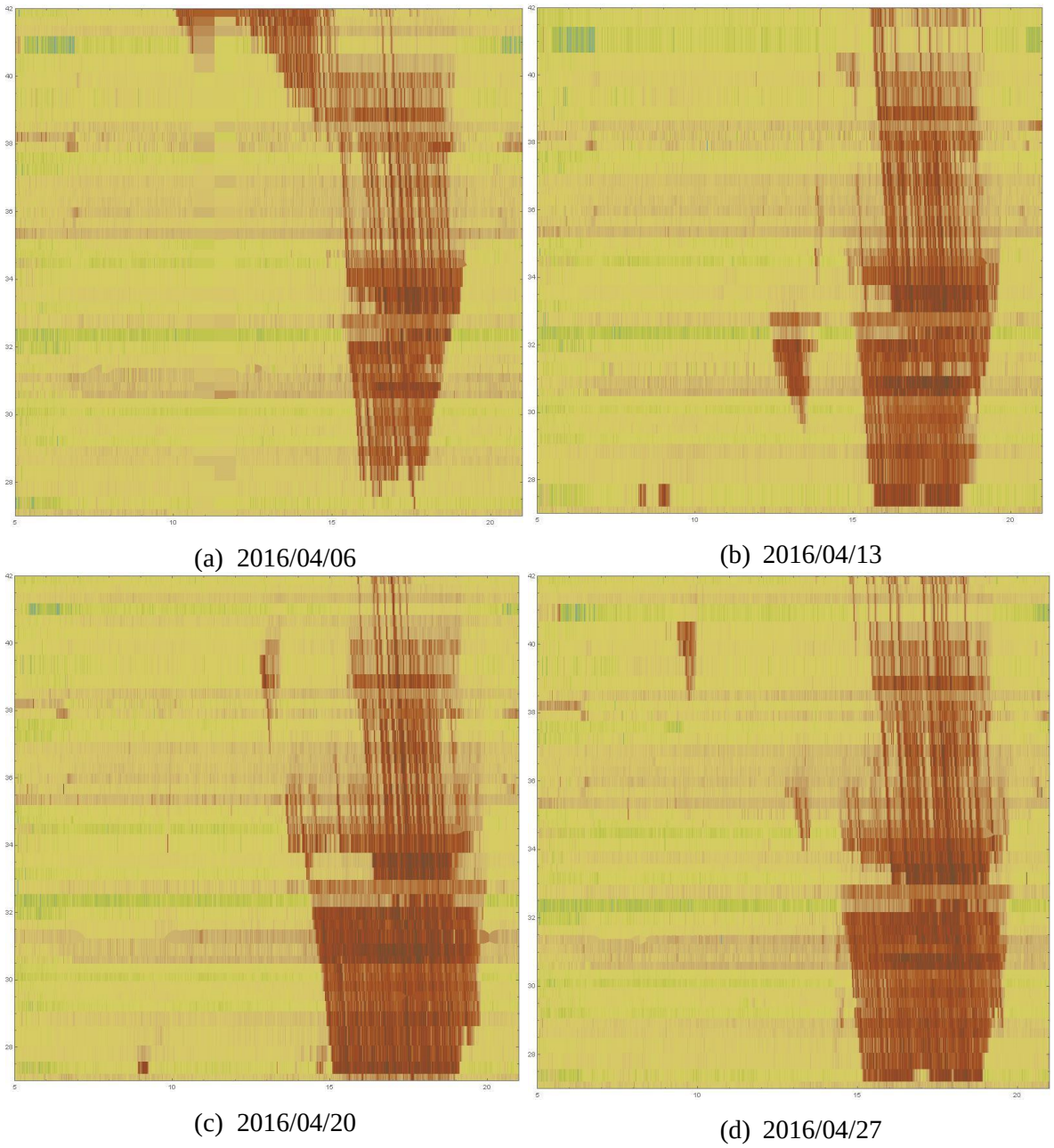

(a) 2016/04/06 (b) 2016/04/13

(c) 2016/04/20 (d) 2016/04/27

Figure 72 Speed contour maps of Wednesday, April 2016

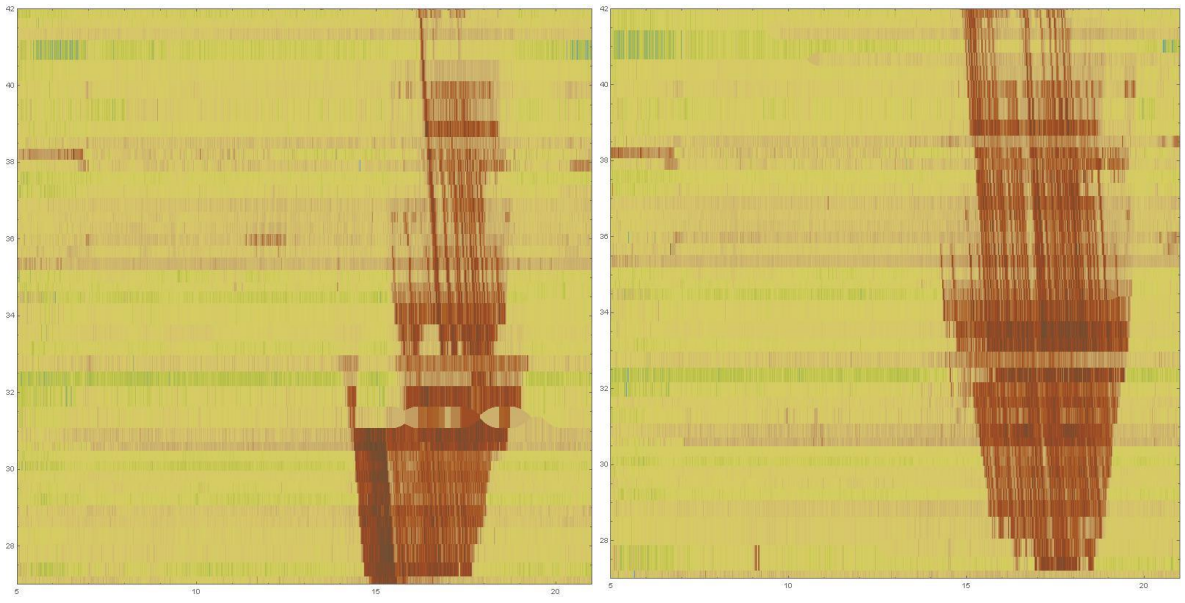

(a) 2016/04/07

(b) 2016/04/14

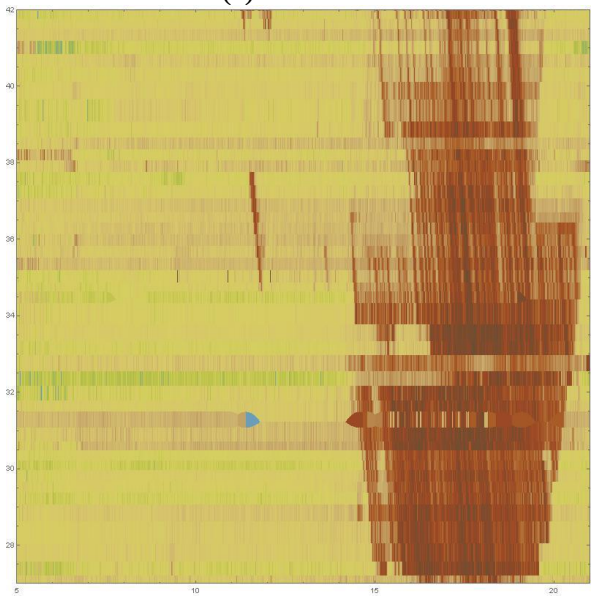

(c) 2016/04/21

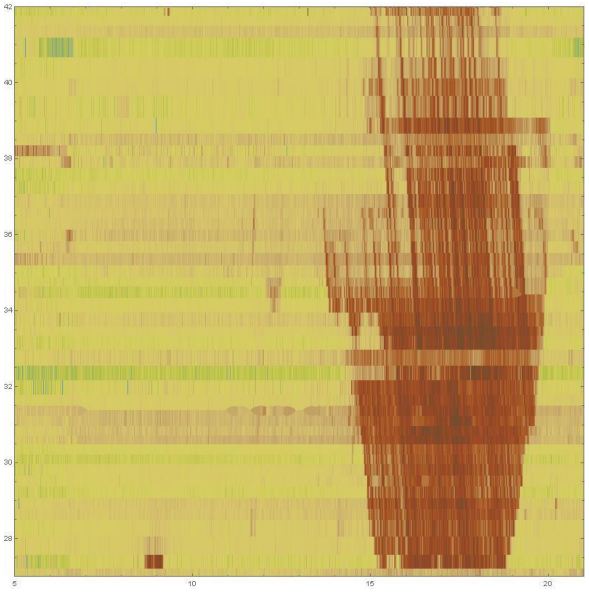

(d) 2016/04/28

Figure 73 Speed contour maps of Thursday, April 2016

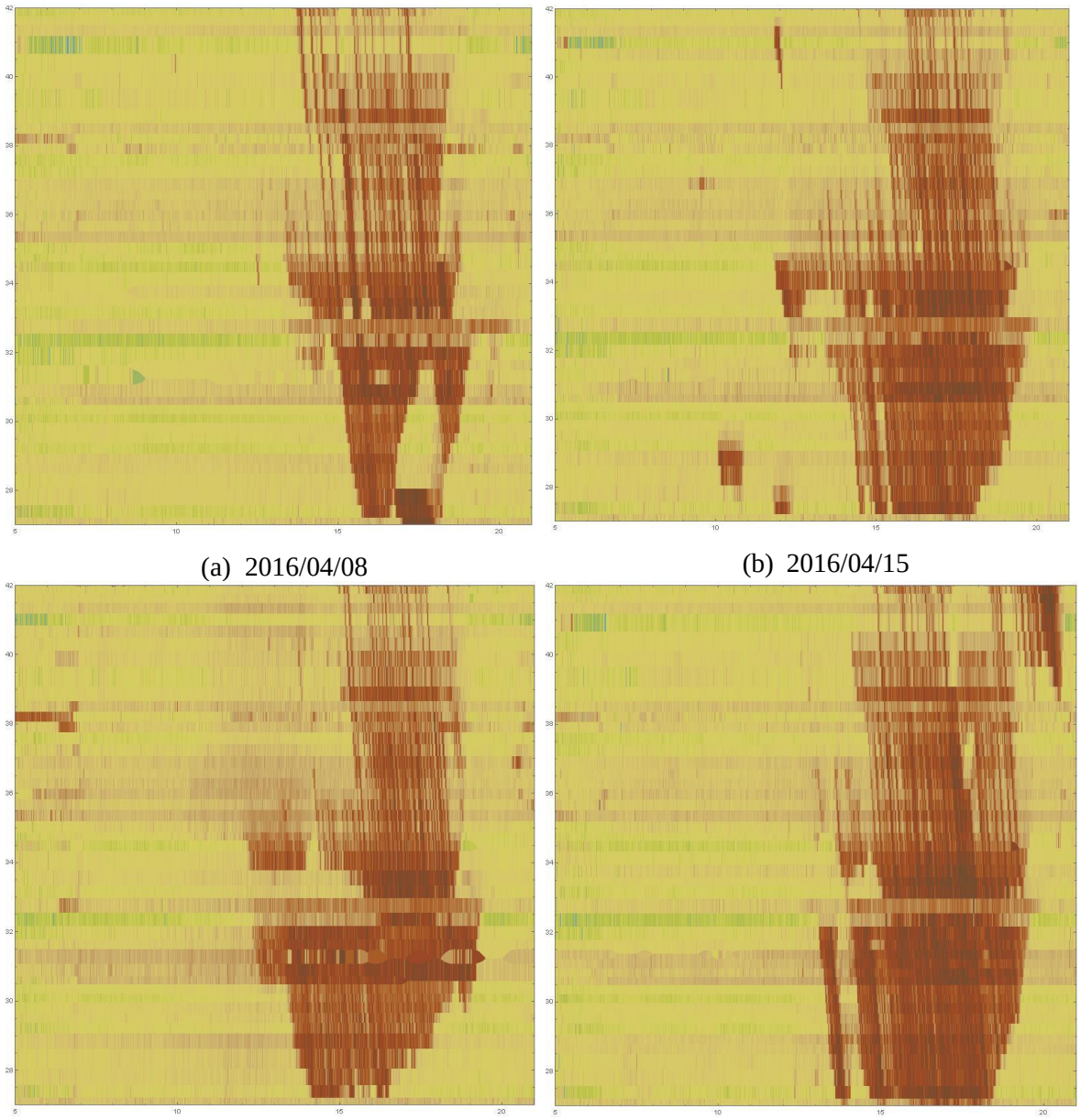

(a) 2016/04/08 (b) 2016/04/15

(c) 2016/04/22 (d) 2016/04/29

Figure 74 Speed contour maps of Friday, April 2016

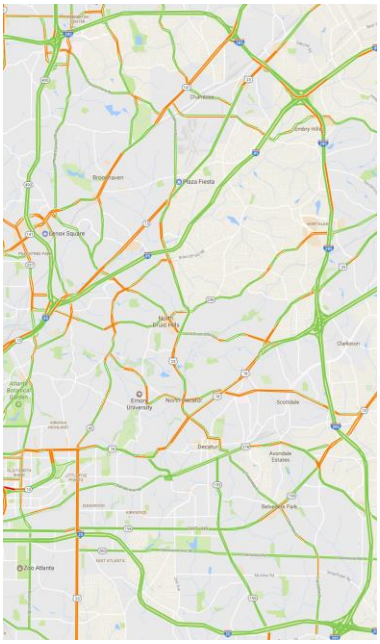

(a) 2:30

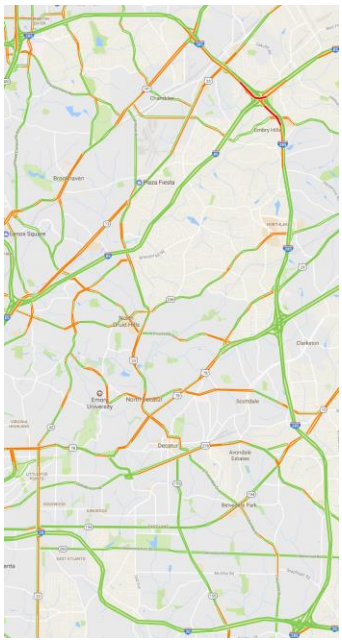

(b) 2:45

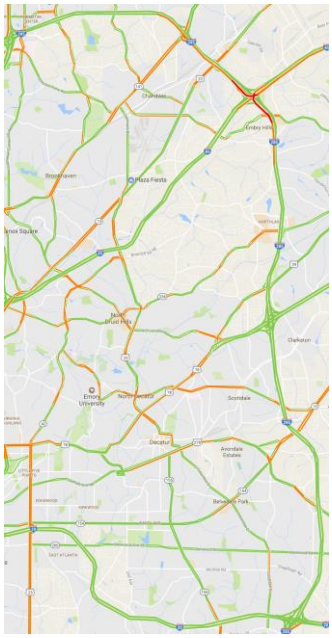

(c) 3:00

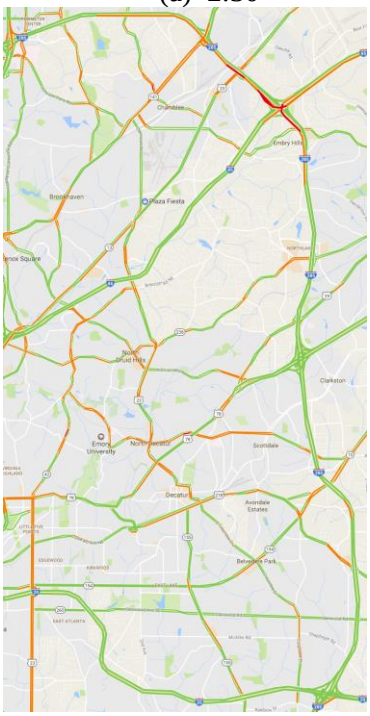

(d) 3:15

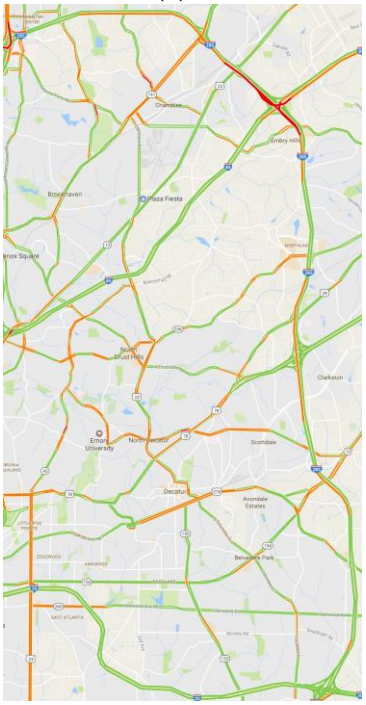

(e) 3:30

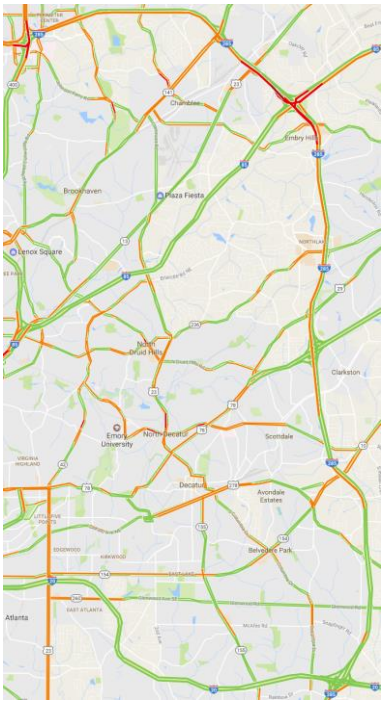

(f) 3:45

Figure 75 Typical traffic state on the corridor during the Monday PM peak

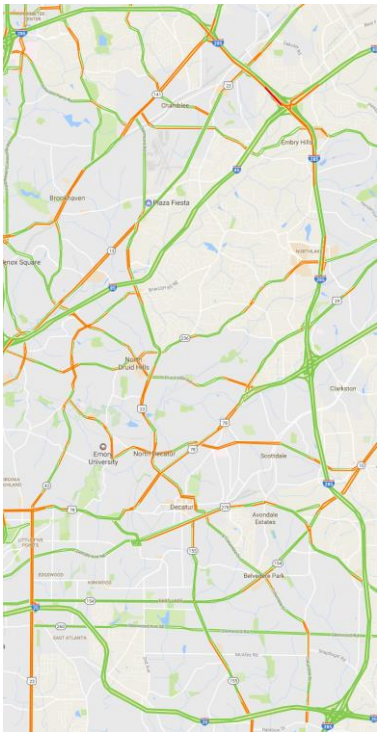

(a) 2:30

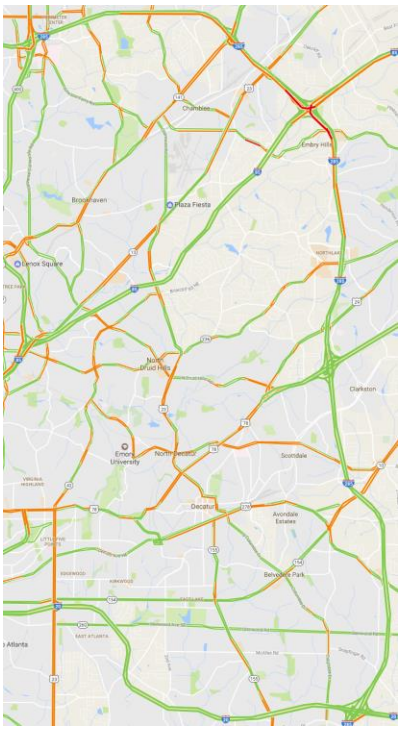

(b) 2:45

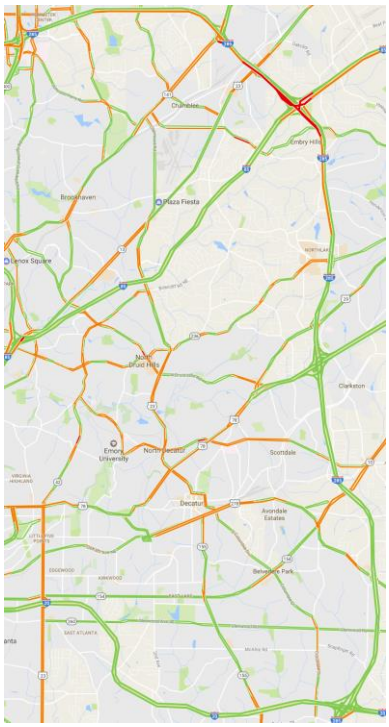

(c) 3:00

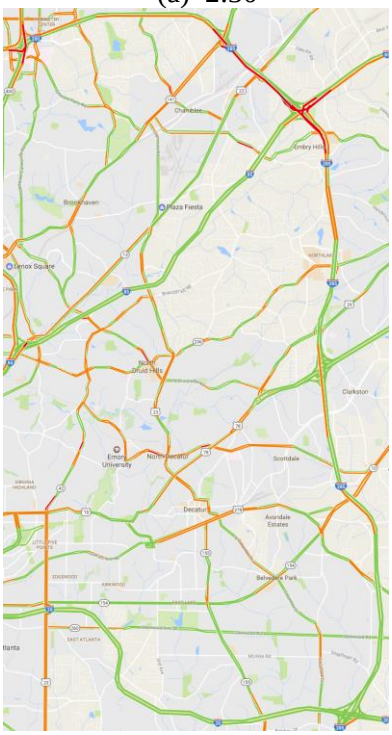

(d) 3:15

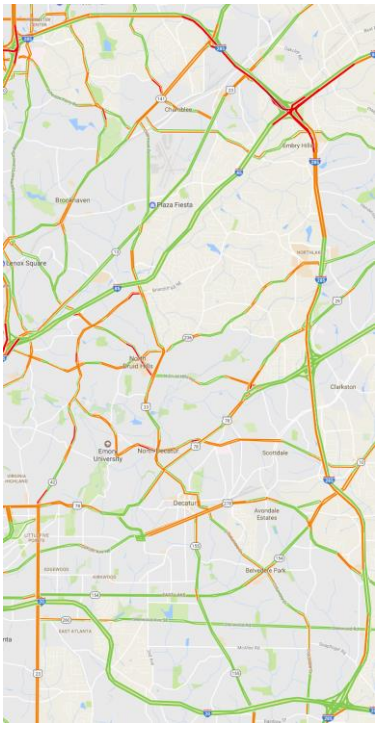

(e) 3:30

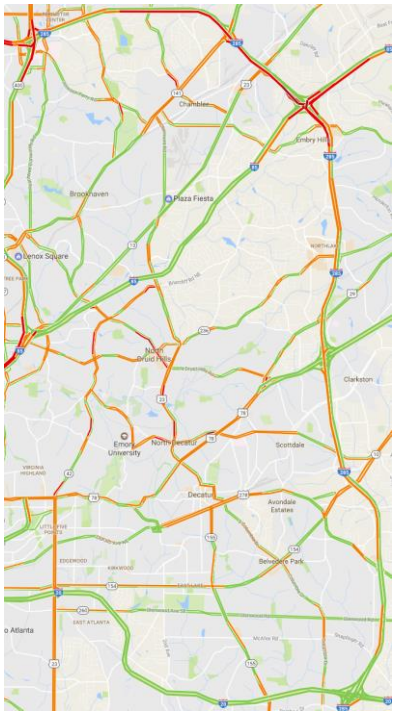

(f) 3:45

Figure 76 Typical traffic state on the corridor during the Tuesday PM peak

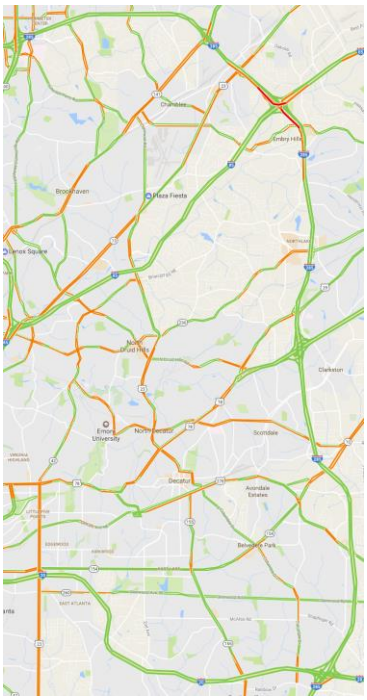

(a) 2:30

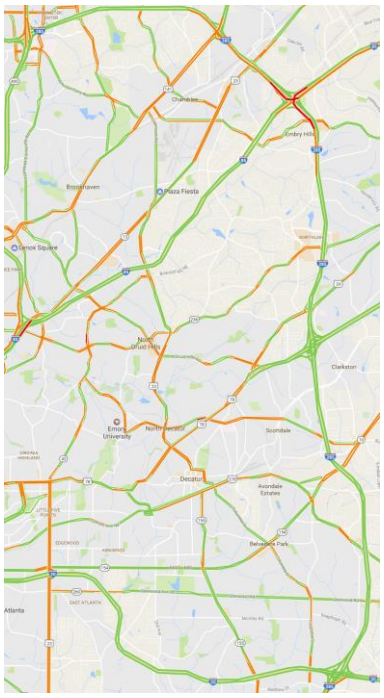

(b) 2:45

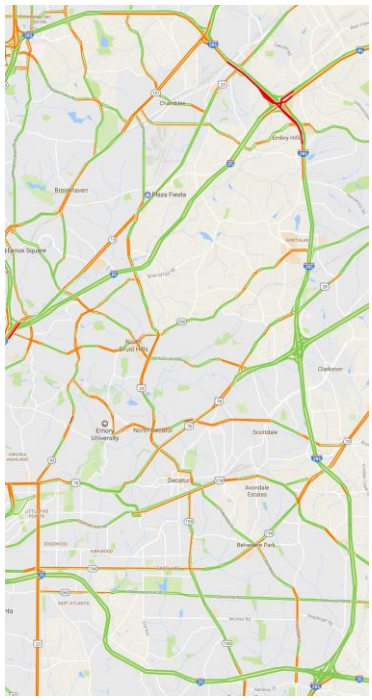

(c) 3:00

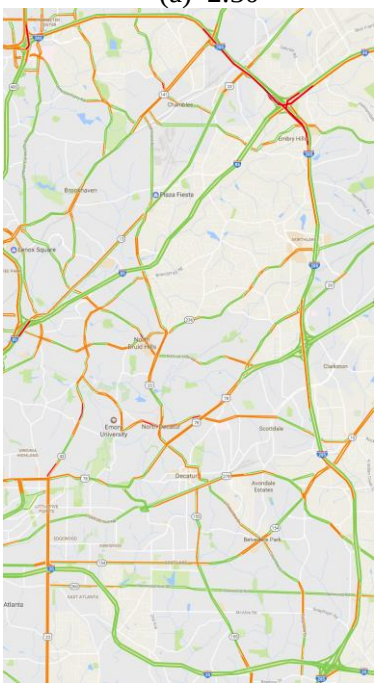

(d) 3:15

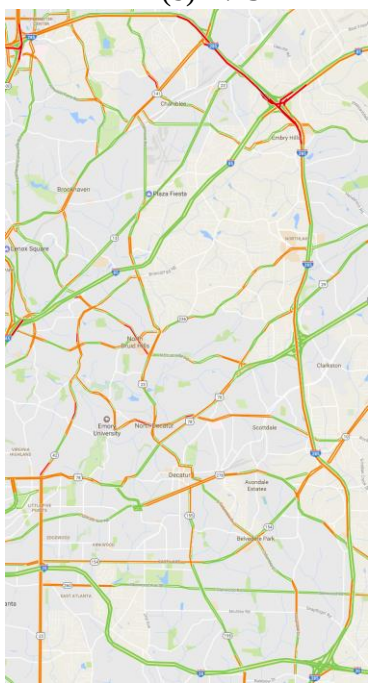

(e) 3:30

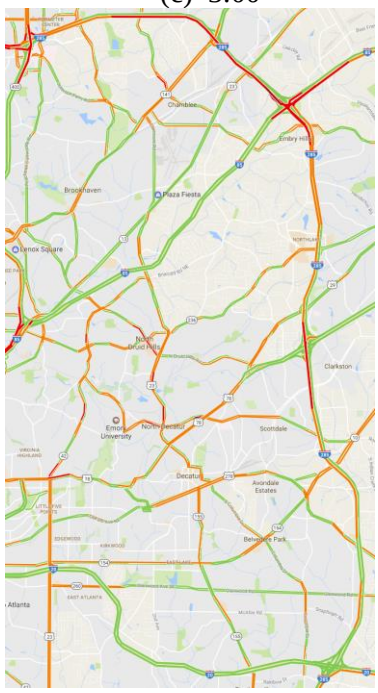

(f) 3:45

Figure 77 Typical traffic state on the corridor during the Wednesday PM peak

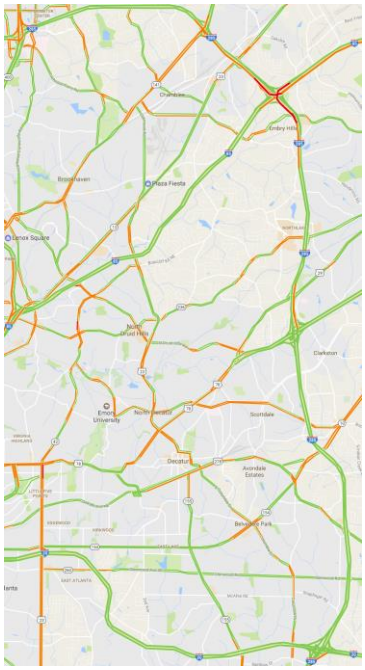

(a) 2:30

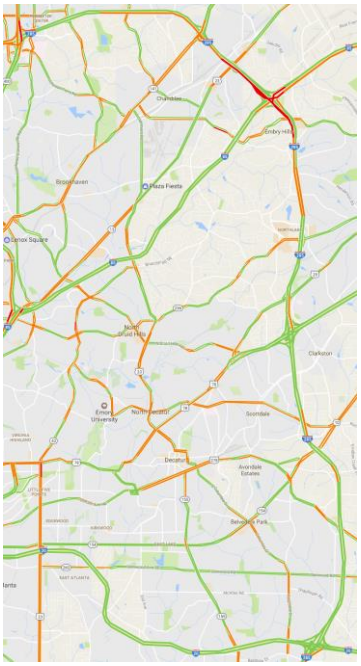

(b) 2:45

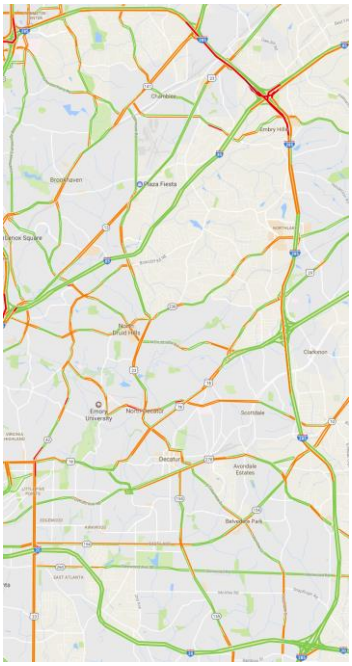

(c) 3:00

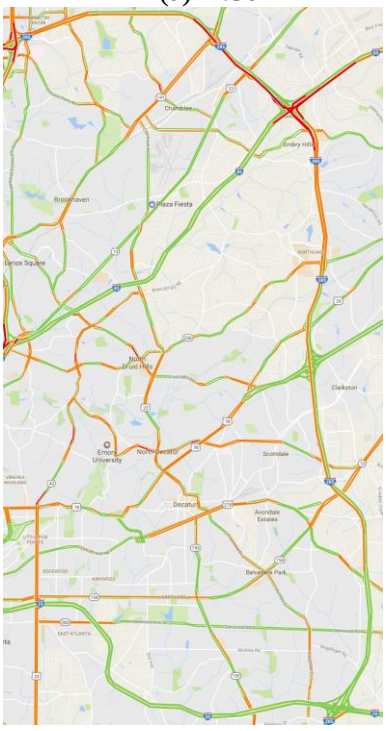

(d) 3:15

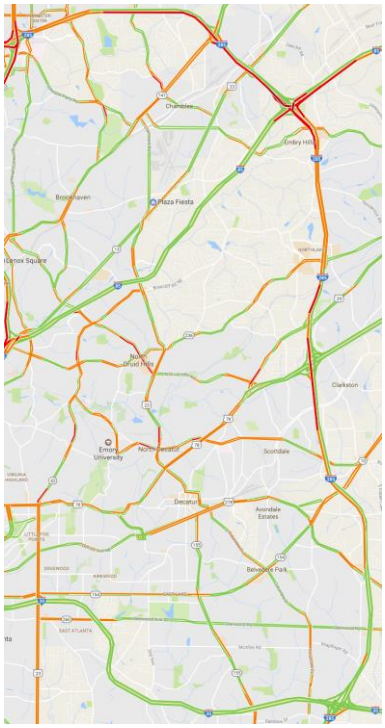

(e) 3:30

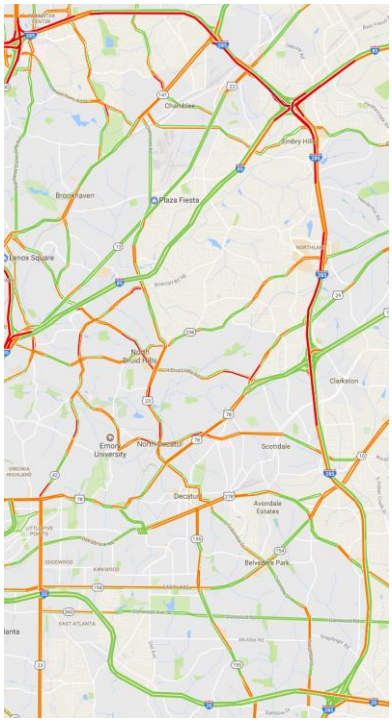

(f) 3:45

Figure 78 Typical traffic state on the corridor during the Thursday PM peak

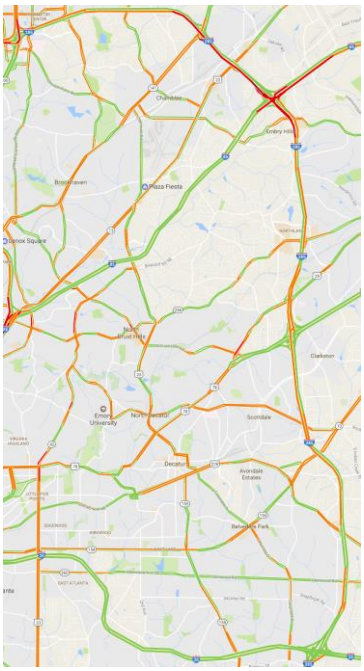

(a) 2:30

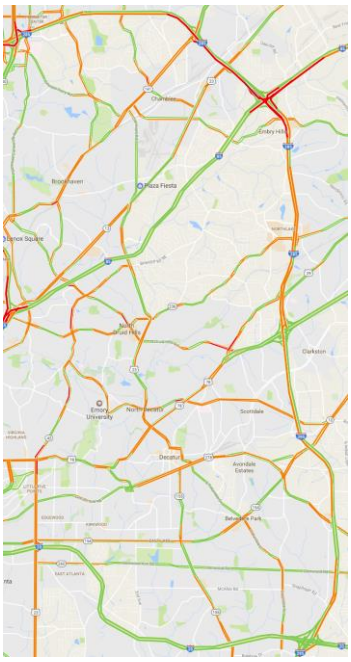

(b) 2:45

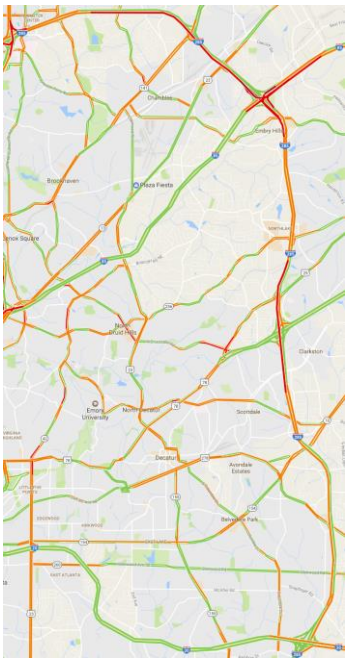

(c) 3:00

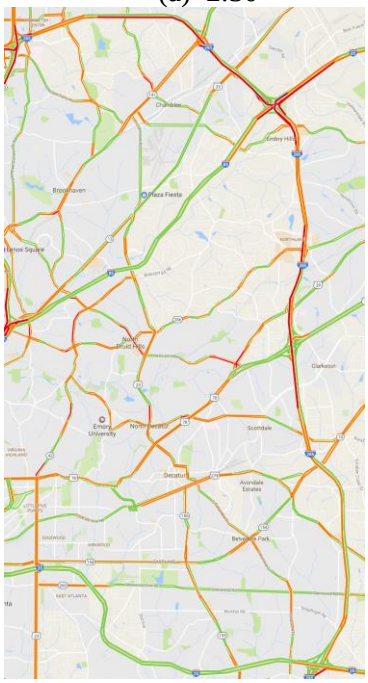

(d) 3:15

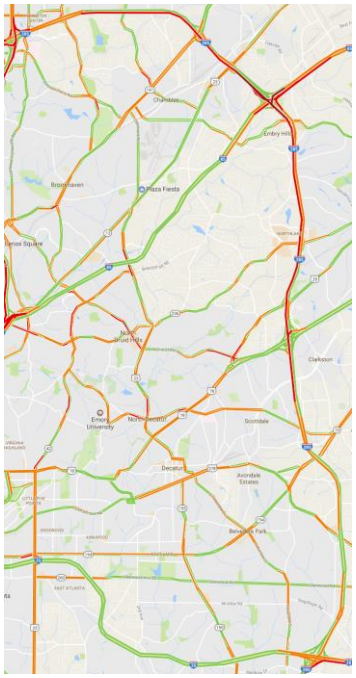

(e) 3:30

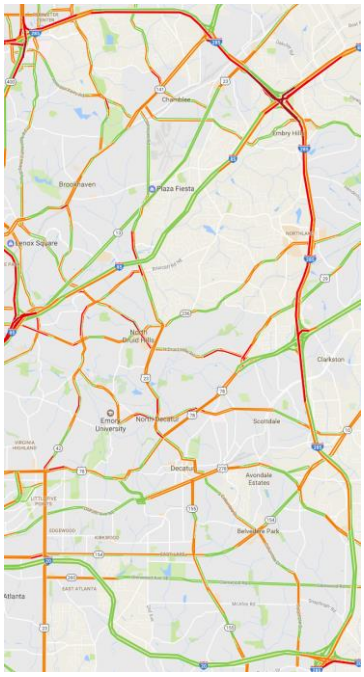

(f) 3:45

Figure 79 Typical traffic state on the corridor during the Friday PM peak

A.3. Data Analysis

A.3.1. Data

Within the 19.25-mile study corridor, this study used 52 GDOT NaviGAtor's Vehicle Detection System (VDS) (Figure 80,81) data that collected 20-second interval volume, speed, and occupancy (hereafter referred to as the "VDS data"). This study extracted the 52-stations VDS data during a one-month period (April 2016).

All on and off ramps in the corridor except for six locations (the NB GA-400 on-ramp, the SB Peachtree Industrial Blvd off-ramp, the Buford Hwy on-ramp, the I-85 connector on-ramp, the WB Stone Mountain Fwy connector on-ramp, I-20 off-ramp) were inspected and five-minute volume data for 48 hours at these ramps were measured using traffic tube counts (see Figure 82, http://geocounts.com/gdot for specific locations).

As traffic volume data are the main input variables of this simulation case study and containing the volume data pf all ramps is critical, this study focused on identifying the five-minute traffic volume of the missing locations for the same 48 hours by analyzing VDS data and the upstream and downstream ramps of the missing locations. For example, for the SB Peachtree Industrial Blvd off-ramp, we compared the VDS data of detector ID 2850034, 2850036, 2850037, which are the NB Peachtree Industrial Blvd off-ramp, and the Peachtree Industrial Blvd on-ramp, respectively. We assumed that the mainline volume on the corridor would be conserved by adding or subtracting the ramp volume. However, a comparison of tube count data and the VDS data resulted in unreasonable ramp volumes (negative values) for the missing ramps.

The unrealistic ramp volumes could have resulted from the low quality VDS data. For example, some detectors lost the data of one lane out of five or six lanes. We also

tried to compensate for these missing lanes by multiplying the ratio of the missing lanes. However, we needed the lane distributions for each location to obtain the volume of correct whole lanes, which is beyond the scope of this study.

Because of these limitations, this study excluded the most upstream and downstream missing ramps, the GA-400 on-ramp, and the I-20 off-ramp. This exclusion, however, did not affect the system corridor because the GA-400 on-ramp does not contain a ramp-metering system, and the I-20 off-ramp does not affect congestion in the corridor.

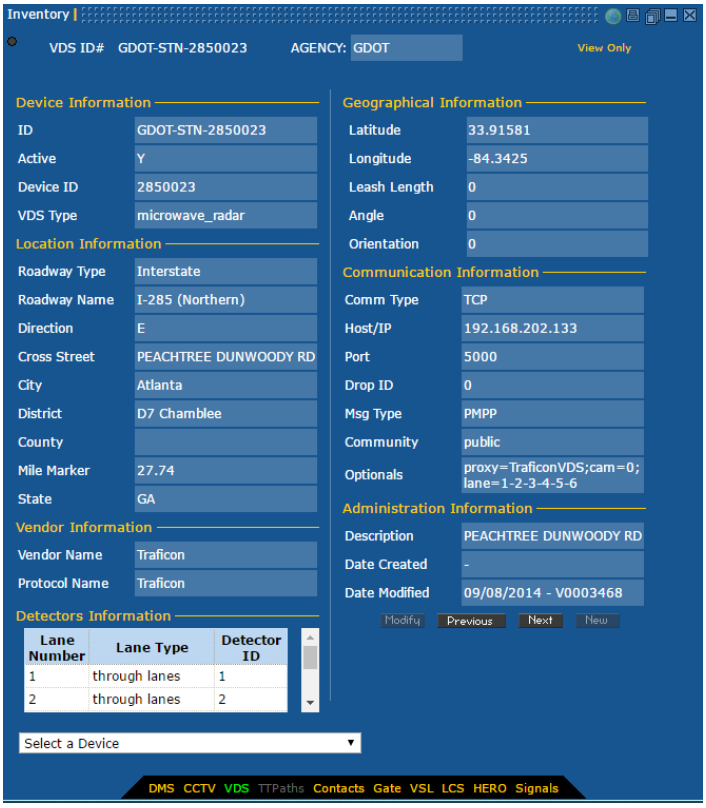

Figure 80 GDOT NaviGAtor video detection system (VDS)

Figure 81 Location of VDS (yellow) and VSL (red) on Google Earth

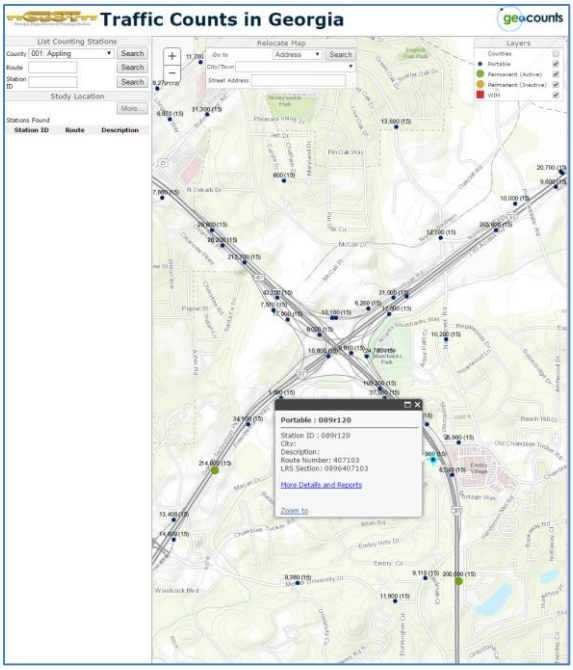

Figure 82 GDOT traffic tube counts

A.3.2. Data Processing for Origin-Destination Matrix Estimation

Rationally estimated origin-destination traffic volume matrix is essential in this simulation-based research. Figure 83 describes the steps of the O/D matrix estimation. We first extracted the traffic volume of the on-ramp (origin) and the off-ramp (destination) for the time periods of interest (PM peak) from the tube counts and the VDS volume data. We also calculated the travel time across each origin and destination using the space-mean speed that was converted from VDS speed data.

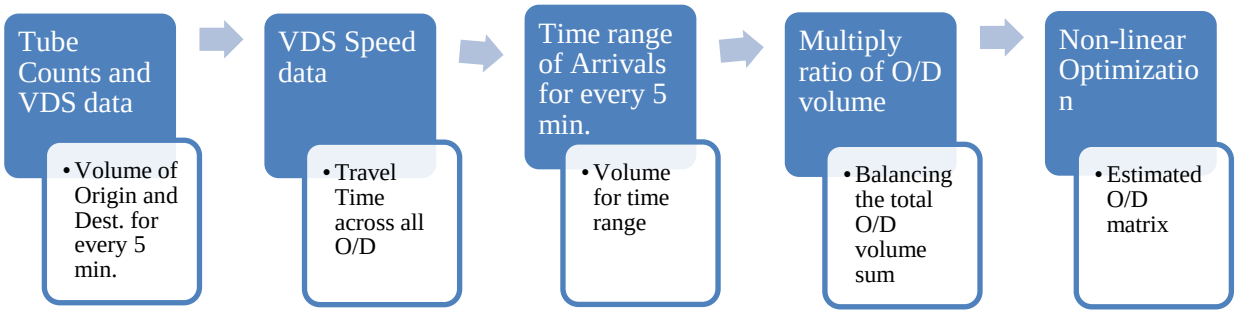

Figure 83 Flow chart of O/D matrix estimation

Using these travel time data, we produced the possible time range of the arrival of the origin traffic. For example, for the I-285 Downstream freeway destination, the earliest time of arrival would be the time that the first vehicle departed from the closest origin, Glenwood Road, and arrived at the destination from the beginning of the time period. Similarly, the latest time of arrival would be the time that the last vehicle departed from the farthest origin, I-285 Upstream freeway, and arrived at the destination from the end of the time periods. Using these possible time ranges of arrival, we calculated the arrival traffic volume for each destination.

The target time periods of our research are before the onset of the off-peak. From the typical traffic data of Google Maps, we found that off-peak congestion on our research corridor formed before 3:00 PM. Therefore, we chose 2:30 PM to 3:30 PM (60 minutes) as the time periods for this study.

The time periods of the origin traffic were set at 60 minutes. However, the calculated possible time periods of destination traffic were longer than 60 minutes as they were affected by congestion. To meet the total sum of the origin and destination traffic, we adjusted the destination traffic volume by multiplying the ratio of the sum of the origin volume to the sum of the possible destination volume.

After matching the sum of the origin and destination traffic volume, we estimated the O/D matrix using a nonlinear optimization method. We explain the assumptions and constraints of this optimization method using the simple network below (Figure 84).

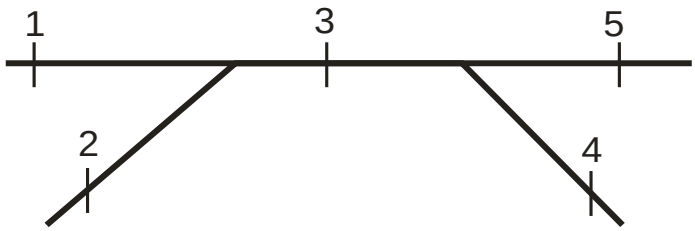

Figure 84 Sample network for OD estimation

This network consists of two origins (1, 2) and two destinations (4,5). From observed data (i.e., tube counts, VDS), the volumes of each origin and destination are generated (1-A, 2-B, 4-C, and 5-D). The volume of section 3 is calculated by adding the volumes of sections 1(A) and 2(B). To calculate the destination specific volumes, we generated the O/D matrix as Table 19. Constraints are that the sum of each row and column volumes are close to the total estimated volume. For example, a volume that is

generated from section 1(a) is composed of volumes heading to 4 (α) and 5(β). In this case, we set constraint $\alpha + \beta \leq a$. Other rows and columns work in a similar manner. Subsequently, we generated a volume-calculation table, Table 20, and then we can calculate the O/D matrix using the optimization function. In the mathematical formulation, the objective function and constraints are described as follows.

$$obj.: \ min.(A-a)^2 + (B-b)^2 + (A+B-a-b)^2 + (C-c)^2 + (D-d)^2$$

Subject to $\alpha + \beta \leq a, \gamma + \delta \leq b, \ \alpha + \gamma \leq c, \ \beta + \delta \leq d$

Table 19 Sample O/D calculation table

O \ D	**4**	**5**	**TARGET**	**SUM**
1	α	β	A	a
2	γ	δ	B	b
TARGET	C	D		
SUM	c	d		

Table 20 Sample calculated and observed flow

	Calculated	**Observed**	**Square of Differences**
1	a	A	$(\boldsymbol{A-a})^2$
2	b	B	$(\boldsymbol{B-b})^2$
3	a+b	A+B	$(\boldsymbol{A+B-a-b})^2$
4	c	C	$(\boldsymbol{C-c})^2$
5	d	D	$(\boldsymbol{D-d})^2$

We used the computer program Generalized Reduced Gradient Algorithm (Lasdon, Fox, & Ratner, 1974), which is useful for solving the nonlinear optimization problem. The objective function of our problem is to minimize the total sum of the squared differences of the estimated volume (last column of Table 21), and the constraints are the sums of each cell of rows and columns (see Figure 85). In Table 21, the green cells represent origin traffic and in Table 20, the pink cells indicate destination traffic. In Figure 85, the gray cells must be zero because these destinations are upstream of the origins. With the algorithm, we found that the objective value decreased to a two-digit value.

Table 21 Flow calculation

Link	Ramps	Calculated Flow	Observed Flow	Difference	Diff. sqrd.
1	U/S Fwy	7914	7914	0	0
2	Peachtree Dunwoody	1030	1030	0	0
3		8944	8944	0	0
4	Ashford Dunwoody	1317	1317	0	0
5		7627	7627	0	0
6	Ashford Dunwoody	1279	1279	0	0
7		8906	8906	0	0
8	Chamblee Dunwoody	1099	1099	0	0
9		7807	7807	0	0
10	North Peachtree	978	978	0	0
11		8785	8785	0	0
12	SB P'tree Ind.	189	189	0	0
13		8596	8596	0	0
14	NB P'tree Ind.	1492	1492	0	0
15		7104	7104	0	0
16	P'tree Ind.	1963	1963	0	0
17		9067	9067	0	0
18	Buford Hwy	577	577	0	0
19		8490	8490	0	0
20	SB I-85	1440	1440	0	0
21		7050	7050	0	0
22	NB I-85	3181	3181	0	0
23		3869	3869	0	0
24	Buford Hwy	411	411	0	0
25		4280	4280	0	0
26	I-85	3941	3941	0	0
27		8221	8221	0	0
28	Chamblee Tucker	428	428	0	0
29		8649	8649	0	0
30	Northlake Pkwy	1055	1055	0	0
31		7594	7594	0	0
32	Lavista	996	996	0	0
33		6598	6598	0	0
34	Lavista	1063	1063	0	0
35		7661	7661	0	0
36	Lawrenceville Hwy	647	647	0	0
37		7014	7014	0	0
38	Lawrenceville Hwy	502	502	0	0
39		7516	7516	0	0
40	Stone Mt.	910	910	0	0
41		6606	6606	0	0
42	Stone Mt. EB	1276	1276	0	0
43		5330	5330	0	0
44	Stone Mt. Left merge	1017	1017	0	0
45		6347	6347	0	0
46	Stone Mt.	587	587	0	0
47		6934	6934	0	0
48	E Ponce De Leon	664	664	0	0
49		6270	6270	0	0
50	Church St.	382	382	0	0
51		6652	6652	0	0
52	Memorial Dr.	1008	1008	0	0
53		5644	5644	0	0
54	Memorial Dr.	891	891	0	0
55		6535	6535	0	0
56	Indian Creek	21	22	1	1
57		6556	6557	1	0
58	Covington	666	666	0	0
59		5891	5891	0	0
60	Covington	593	593	0	0
61		6484	6484	0	0
62	Glenwood	484	484	0	0
63		5999	6000	1	1
64	Glenwood	507	508	1	1
65		6506	6508	2	4
66	I-20	3203	3200	-3	9
67	D/S Fwy	3303	3300	-3	9

Origin/Destination		Ashford Dunwoody	Chamblee Dunwoody	SB P'tree Industrial	NB P'tree Industrial	Buford Hwy	SB I-85	NB I-85	Northlake pkwy	Lavista	LAWRENCE VILLE HWY	STONE MOUNTAIN FWY	STONE MOUNTAIN FWY EB	EAST PONCE DE LEON AVE	Memorial	Covington	Glenwood	I20	d/s Fwy	Target	Sum
		4	6	8	10	12	14	16	22	24	26	28	30	34	36	40	42	44	46		
u/s Fwy	1	1316	984	189	1258	1	1104	1196	114	99	533	130	120	232	121	0	0	298	219	7914	7914
P'tree Dunwoody	3	1	68	0	136	7	101	523	0	2	8	2	1	6	0	1	0	88	86	1030	1030
Ashford Dunwoody	5		47	0	67	36	98	786	0	1	4	0	26	3	0	1	0	109	99	1279	1279
N. P'tree Rd	7			0	30	22	72	654	0	1	4	0	25	3	0	2	1	85	79	978	978
P'tree Industrial	11					512	65	22	174	152	47	201	246	0	212	21	310	2	0	1963	1963
Buford Hwy	17								24	15	0	21	44	2	13	0	1	159	132	411	411
I-85 C/D SYS	19								722	714	12	464	615	295	386	11	0	270	453	3941	3941
CHAMBLEE TUCKER RD	21								22	12	2	9	43	1	14	0	0	160	165	428	428
Lavista Rd	25										36	57	103	36	73	8	2	365	381	1063	1063
Lawrenceville Hwy	27											24	52	0	23	0	0	222	180	502	502
Stone Mt. FWY Left	31													68	92	0	0	361	496	1017	1017
Stone Mt. FWY	33													18	41	10	67	199	252	587	587
Church St.	35														32	11	78	117	145	382	382
Memorial Dr.	37															601	1	140	149	891	891
Indian Creek	39															0	0	21	0	22	21
Covington	41																25	290	278	593	593
Glenwood	43																	319	188	508	507
	Target	1317	1099	189	1492	577	1440	3181	1055	996	647	910	1276	664	1008	666	484	3200	3300	8	
	Sum	1317	1099	189	1492	577	1440	3181	1055	996	647	910	1276	664	1008	666	484	3203	3303		0
		1317	1099	189	1492	577	1340	3081	955	896	547	810	1176	564	908	566	384	2929	3183		

Figure 85 O/D matrix

A.4. GDOT Variable Speed Limits system

GDOT adopted speed harmonization as their VSL algorithm. According to the algorithm, each VSL of the corridor is connected to adjacent VDSs of the VSL. The number of these VDSs and their locations vary by VSL. Figure 86 depicts the VSL #21 screenshot of the GDOT NaviGAtor System. This figure shows that GDOT-VSL-021 is connected to VDSs, GDOT-STN-2850026, 27, 28, 29. Figure 87 shows the exact location of the VSL and VDSs. Note that GDOT-STN-2850027, 28, 29 are VDS 2818, 19, 20 in Figure 87, and GDOT-STN-2850026 (VDS 2817) is not working. VDS's collect the average speed of vehicles that pass the location every 20 seconds, and the VSL system calculates the average number of cycles and the average speed of the VDS's. The calculated VSL speed then references the lookup table (see Table 22) to determine the display speed limit. The VSL algorithm has a constraint that the differences among the display speed limit of adjacent VSLs should not be more than 10 *mph*. Figure 88 shows the VSL map of the GDOT NaviGAtor system.

Table 22 GDOT VSL lookup table (unit: *mph*)

Low Limit (≥)	High Limit (<)	Display Speed Limit
59	100	65
47	59	55
35	47	45
1	36	35

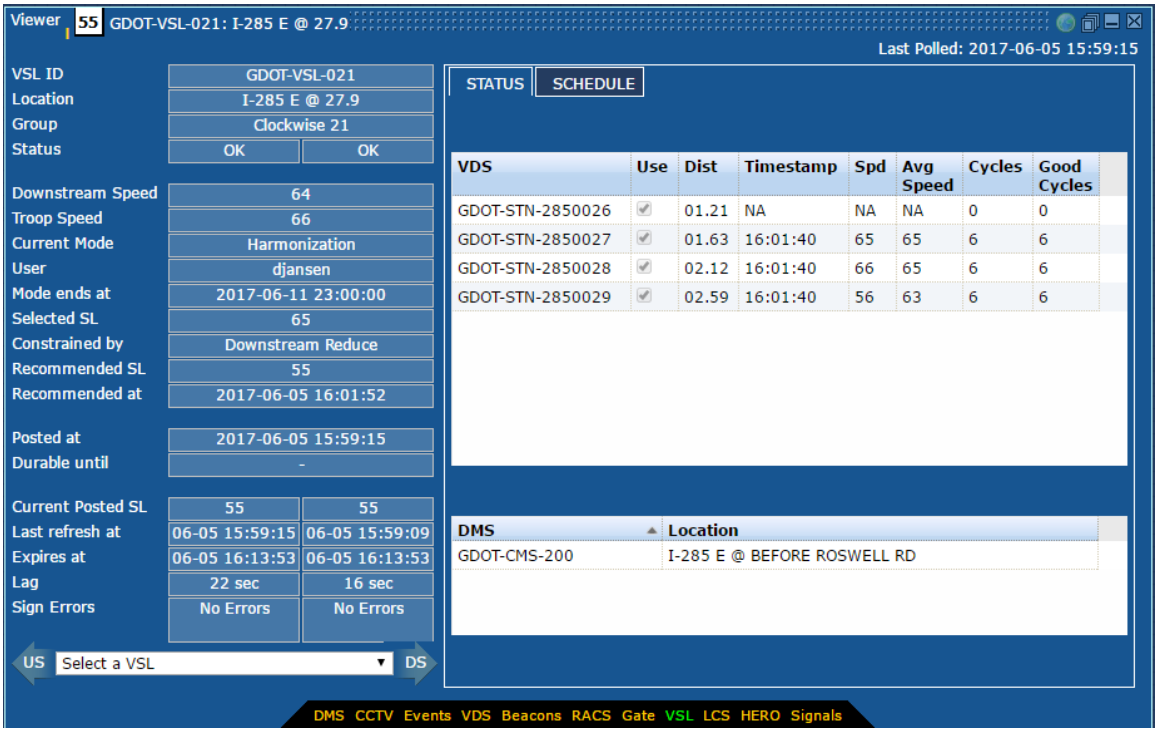

Figure 86 GDOT NaviGAtor VSL system

Figure 87 Map of the VSL 21 (upstream of Chamblee Dunwoody Rd) and connected VDS's (Google Earth)

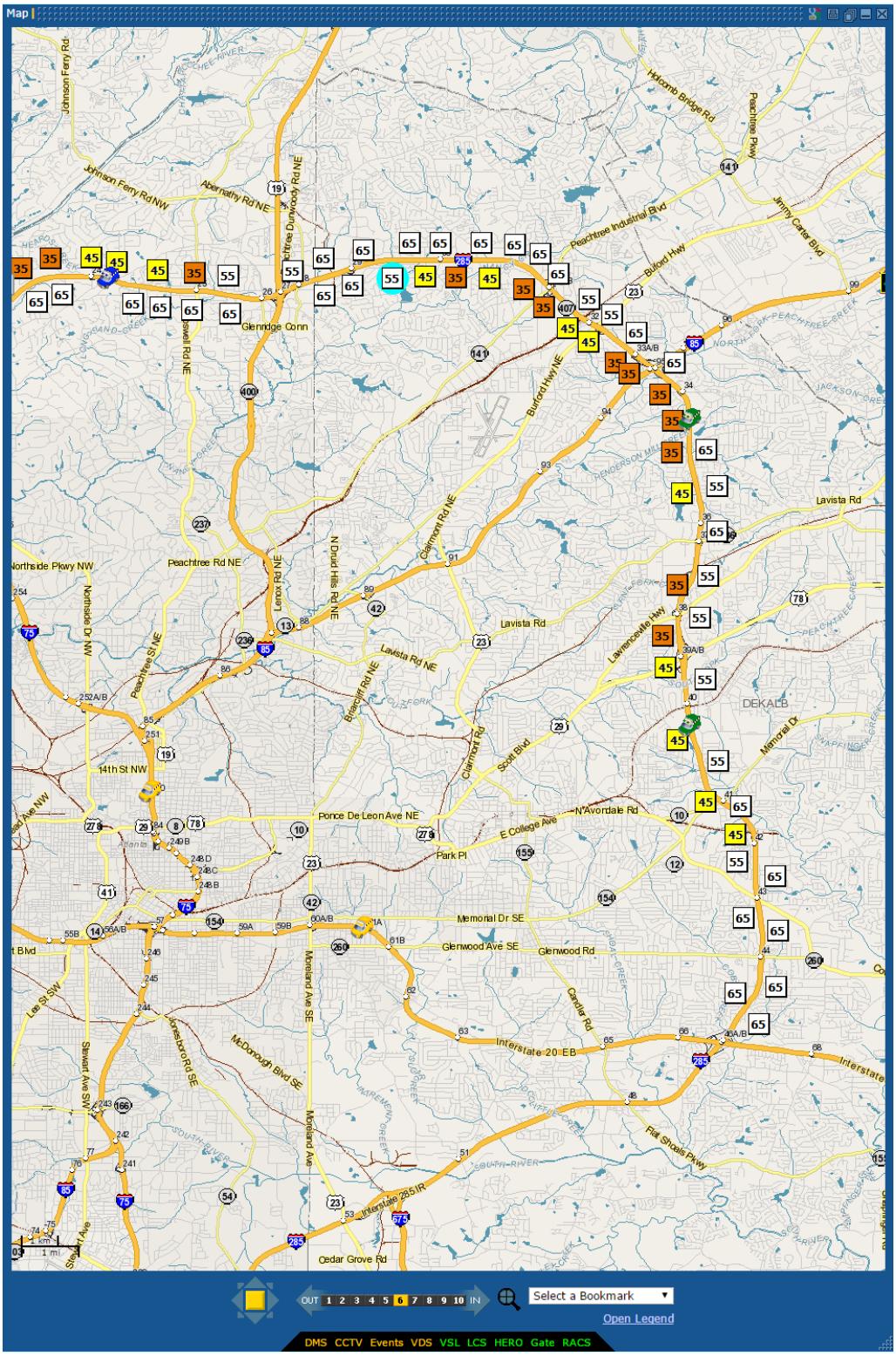

Figure 88 GDOT NaviGAtor VSL Map

Simulation of GDOT's speed harmonized VSL

In Appendix A.3., we explained that the VSL algorithm harmonizes speeds upstream and downstream. Some studies (Abdel-Aty et al. (2009, 2007)) have shown the effectiveness of speed harmonization from a safety perspective with microscopic traffic simulations. These studies proposed a crash risk index that includes rear-end and lane-change crash risk and measured changes in the index in various environments. However, as the objective of this study is to reduce congestion on the study corridor using the RM and the VSL, the safety perspective is beyond the scope of this study. Although many studies (Carlson et al. (2014, 2010a); Hegyi et al. (2005a)) have proven the effectiveness of the VSL using the macroscopic traffic model, to the best of the knowledge of the author, very few studies (Talebpour et al. (2013)) have proven the effectiveness of speed harmonization in terms of reducing congestion (saving travel time) with microscopic simulation.

In this simulation study, which is based on the real world replicated in the study corridor and data, modeling an efficient speed harmonization VSL model was particularly difficult. The main reason is that locations of the VSL and the VDS are prefixed, and they do not account for the formation of bottlenecks in certain locations. The other reason is driver behavior and VSL compliance, further explain by examining the example network in Figure 89. If we assume that a VSL1 is connected to VDS 1, 2, 3, and that a VSL2 is connected to VDS 4, 5, 6, then it is not uncommon that some VDSs in our study corridor are located upstream of the VSL. If we assume that the bottleneck of this network is located between the VDS3 and the VDS4, then when the bottleneck becomes activated, the queue backs up to the upstream, and VDS3, 2, 1 detects the congested speed of

vehicles in an orderly manner, and the VSL1 shows the harmonized speed. If we assume that a vehicle passes the VSL signage in strict compliance with the VSL, the vehicle will not increase speed to free-flow even if it passes the bottleneck. In this case, the VDS4 detects the decreased speed of the vehicle, and the VSL2 will post the decreased speed even if the bottleneck is not detected upstream of the VSL 2.

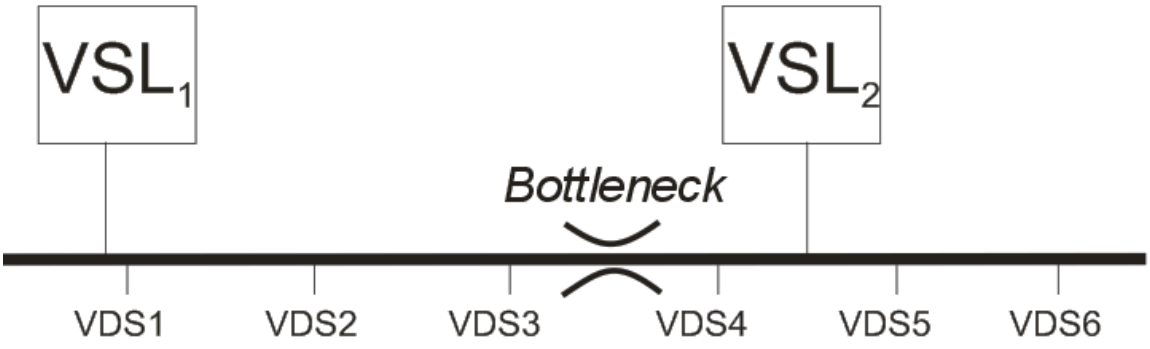

Figure 89 Example network of Speed Harmonization (VSL)

This behavior of the vehicle is unrealistic. In the real world, vehicles accelerate when they pass bottlenecks. However, implementation in a simulation is difficult because vehicles are under the influence of the last VSL signage. To address this problem, one solution is to locate free-flow signed VSL immediately upstream of the bottleneck. The other solution is to use other traffic flow parameters, such as density of traffic from the VDS to determine the traffic status and the speed.

A.5. Density-Flow plots of merge locations of the study corridor

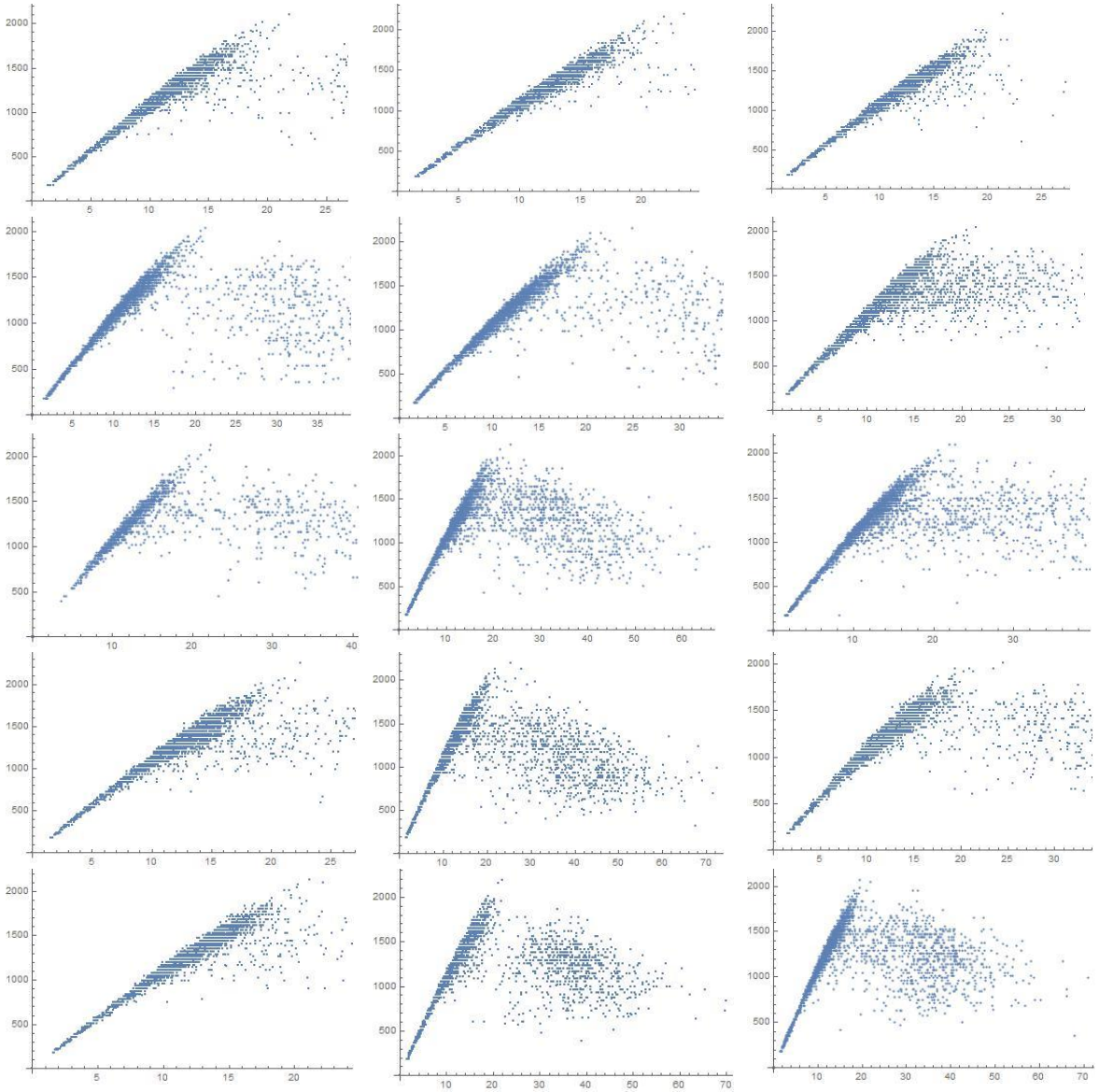

Figure 90 Density (vehicle/km/lane) flow (vehicle/hour/lane) plots at the D/S of Peachtree Dunwoody Road, April 2016

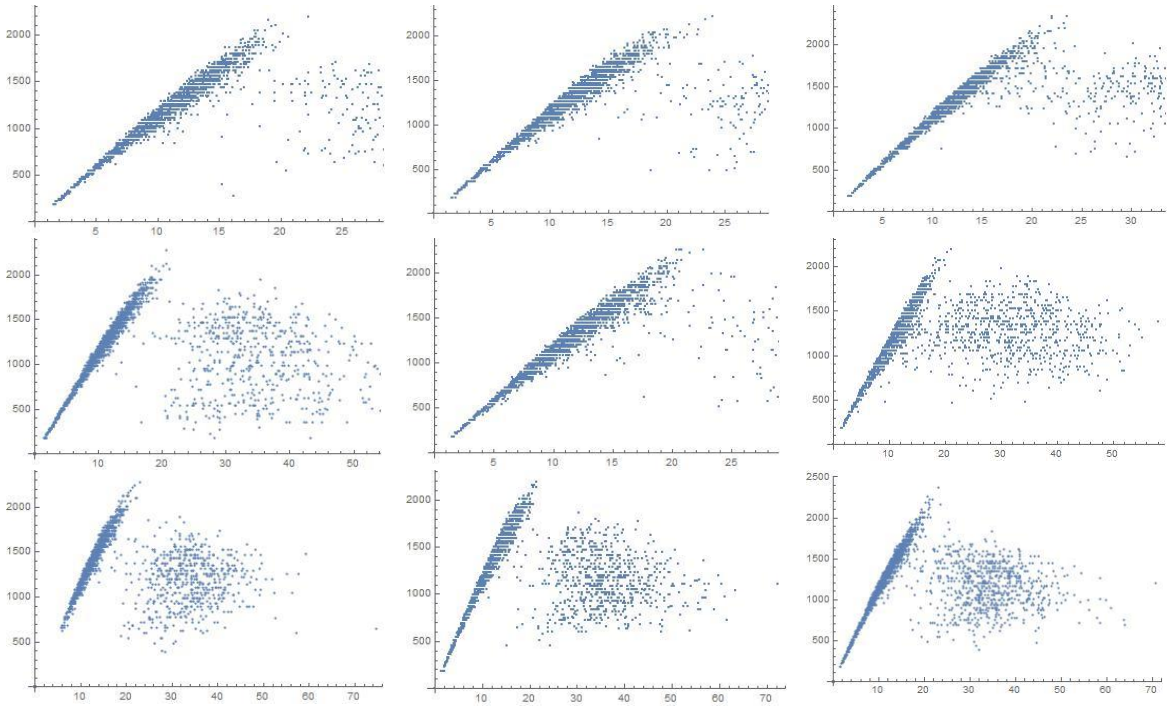

Figure 91 Density (*vehicle/km/lane*) Flow (*vehicle/hour/lane*) plots at D/S of Ashford Dunwoody Road, April 2016

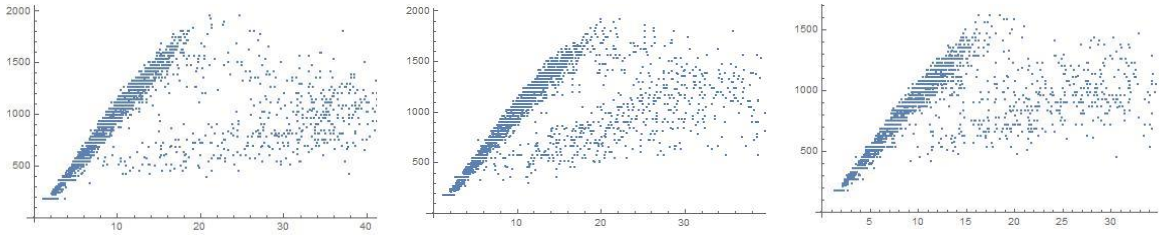

Figure 92 Density (*vehicle/km/lane*) Flow (*vehicle/hour/lane*) plots at D/S of North Peachtree Road, April 2016

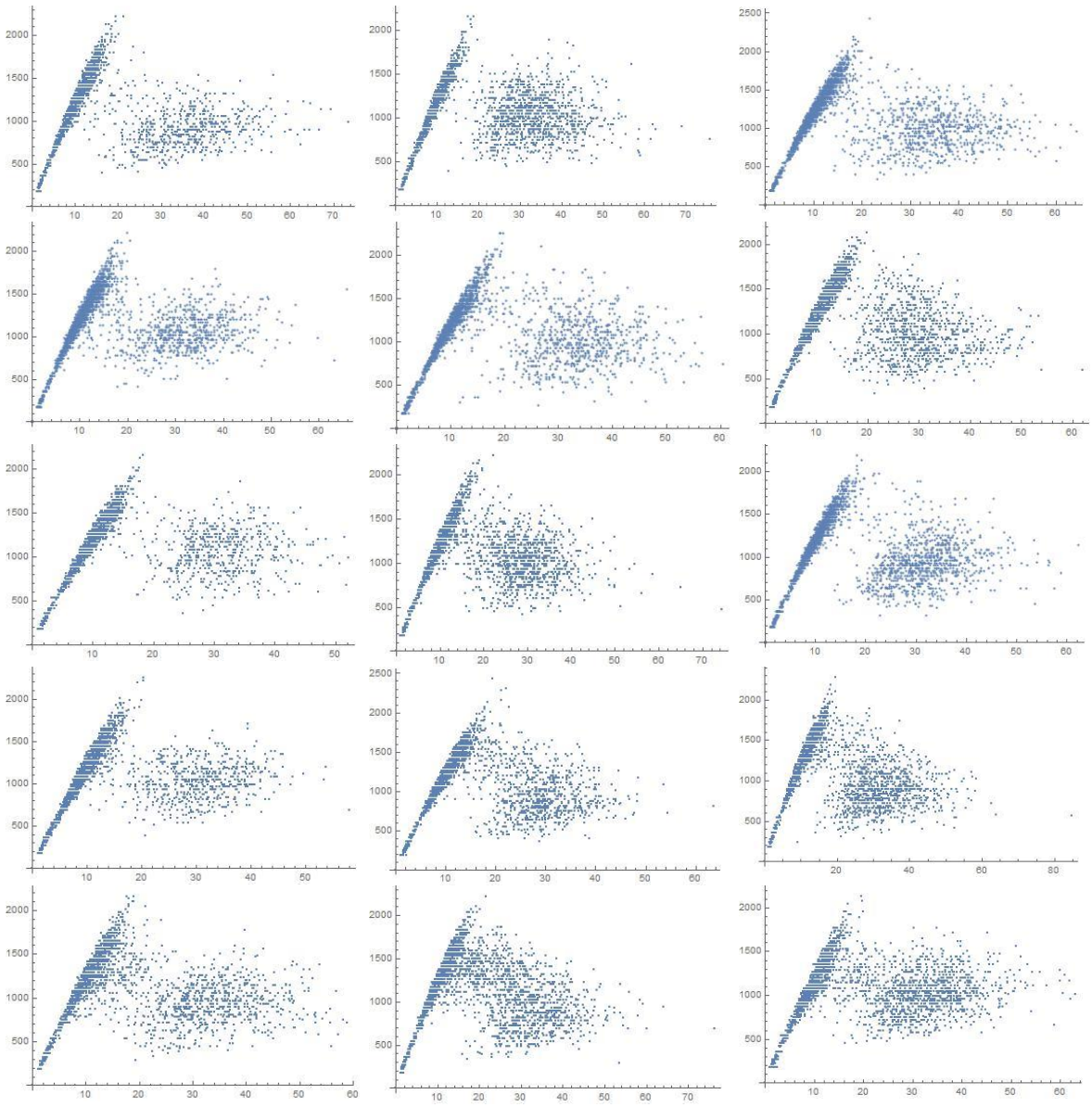

Figure 93 Density (*vehicle/km/lane*) flow (*vehicle/hour/lane*) plots at the D/S of Peachtree Industrial Blvd, April 2016

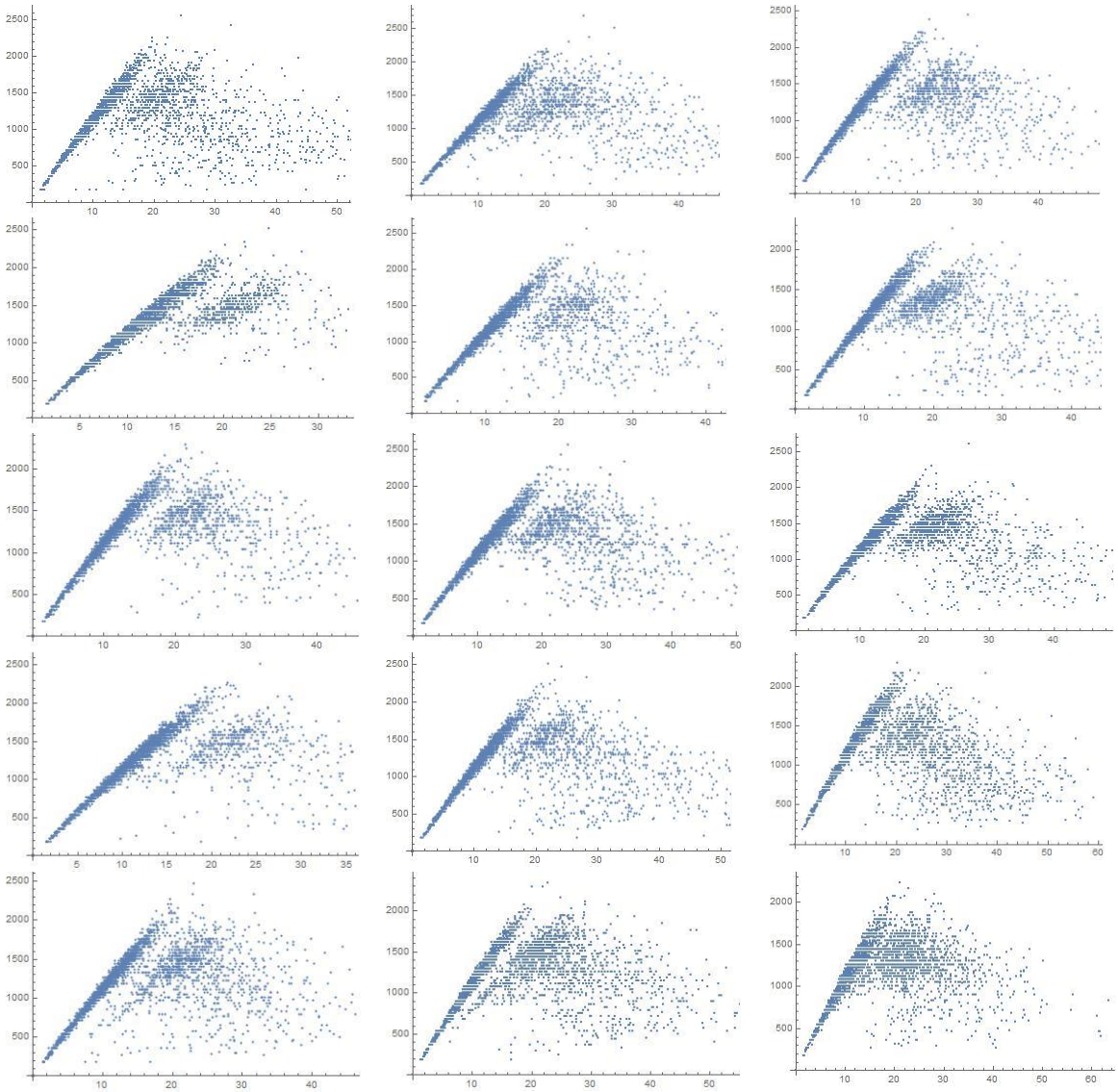

Figure 94 Density (*vehicle/km/lane*) flow (*vehicle/hour/lane*) plots at the D/S of Chamblee Tucker Road, April 2016

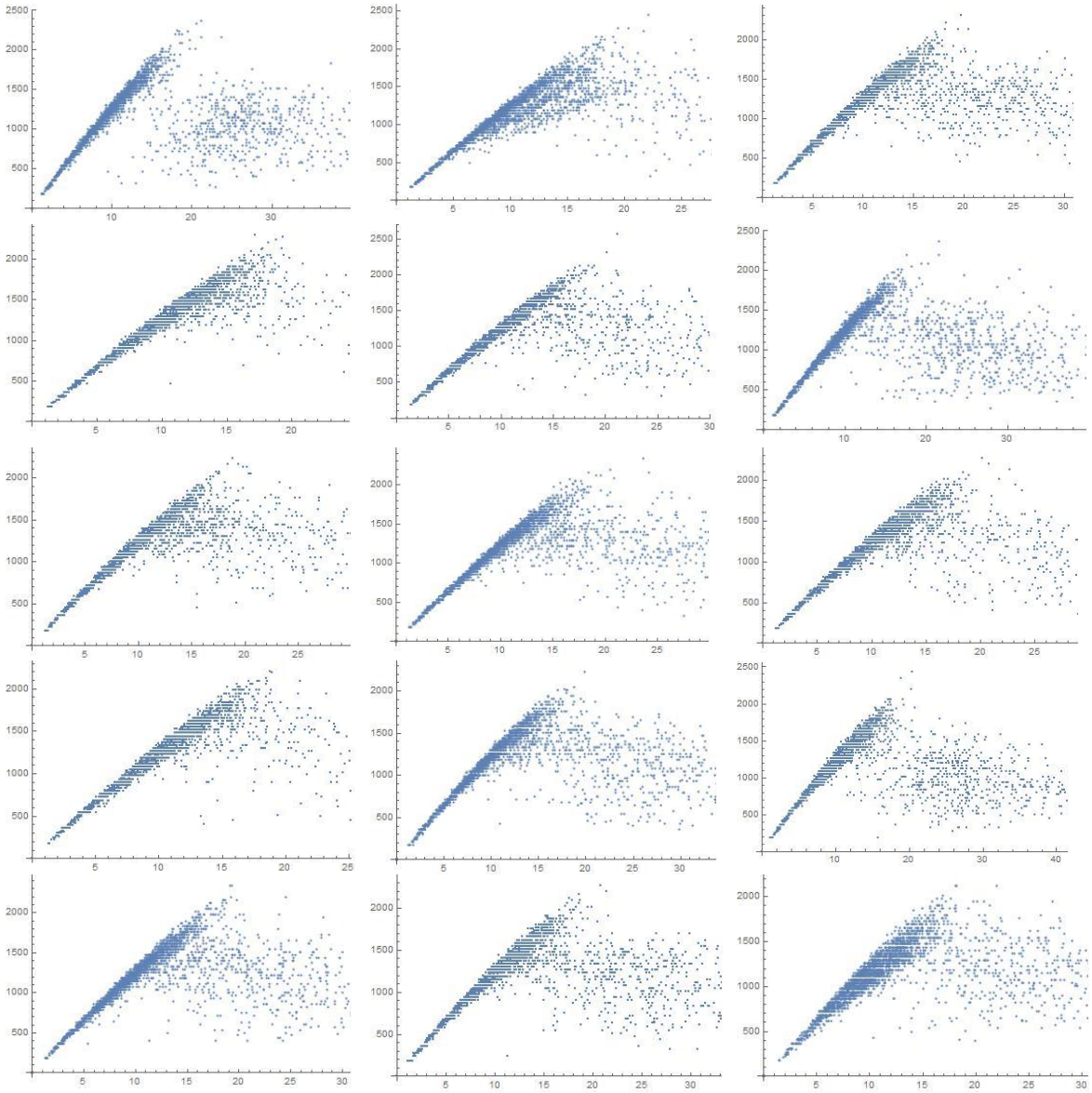

Figure 95 Density (*vehicle/km/lane*) flow (*vehicle/hour/lane*) plots at the D/S of Lavista Road, April 2016

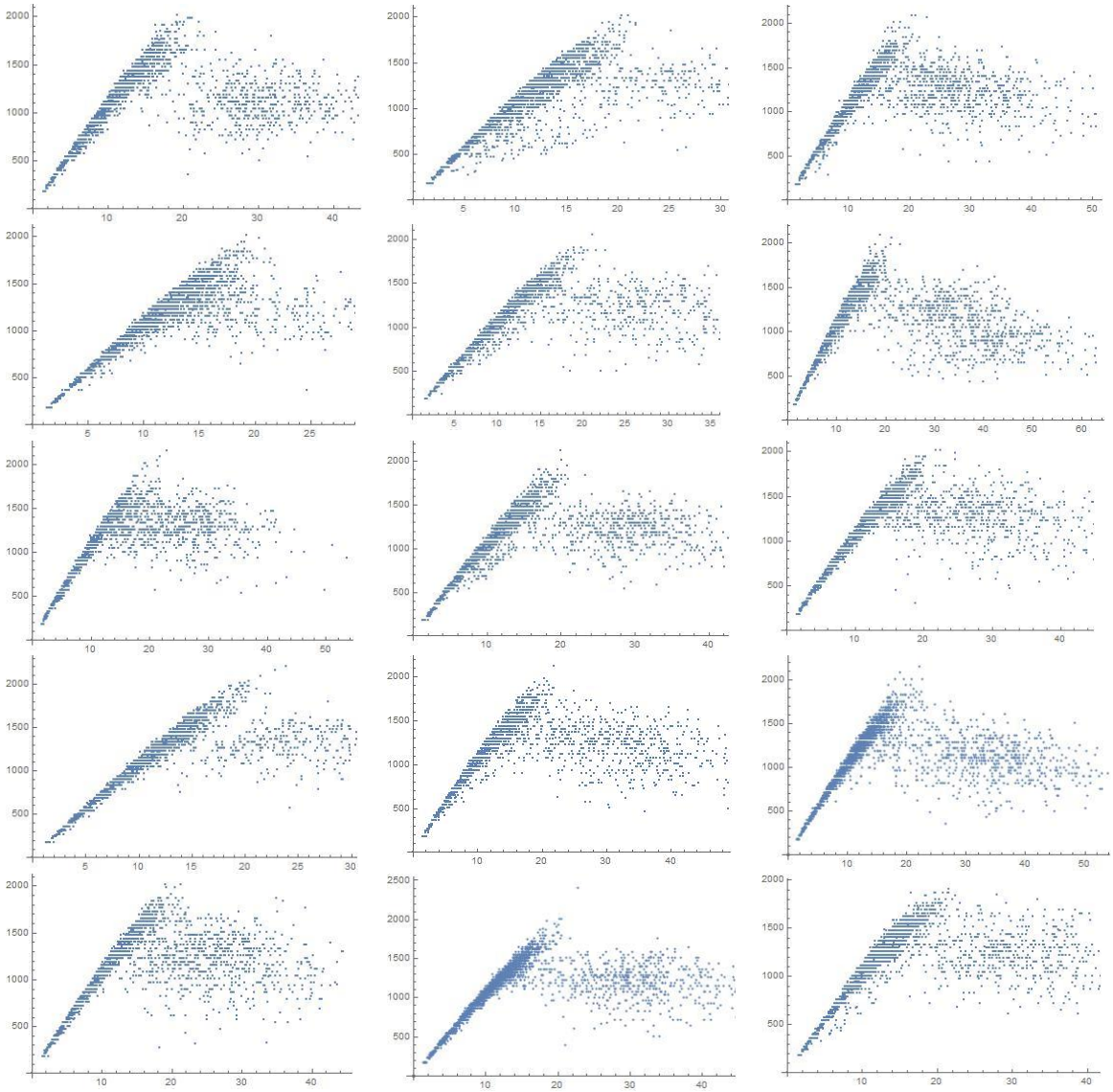

Figure 96 Density (*vehicle/km/lane*) flow (*vehicle/hour/lane*) plots at the D/S of Lawrenceville Hwy, April 2016

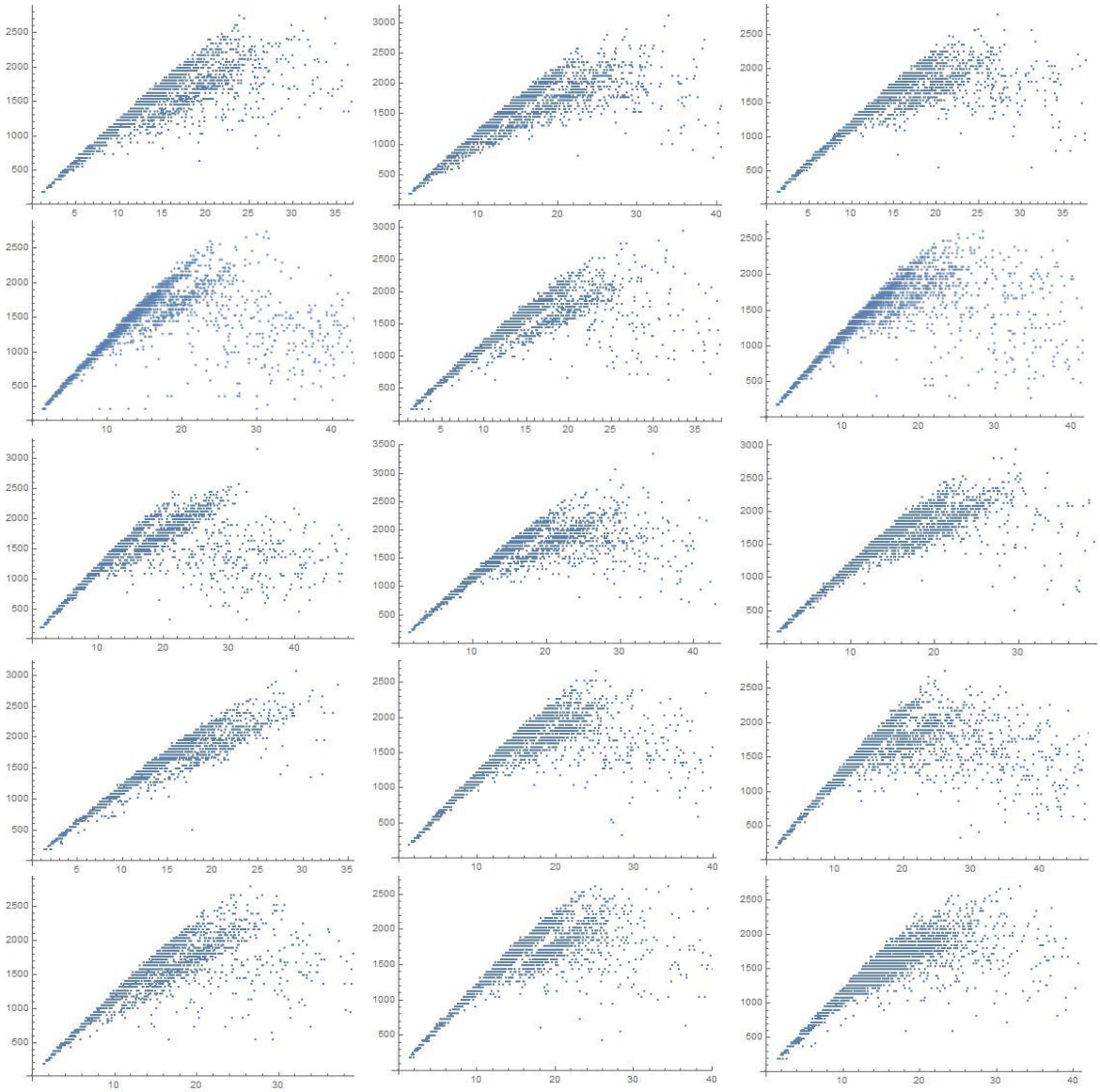

Figure 97 Density (*vehicle/km/lane*) flow (*vehicle/hour/lane*) plots at the D/S of Church Street, April 2016

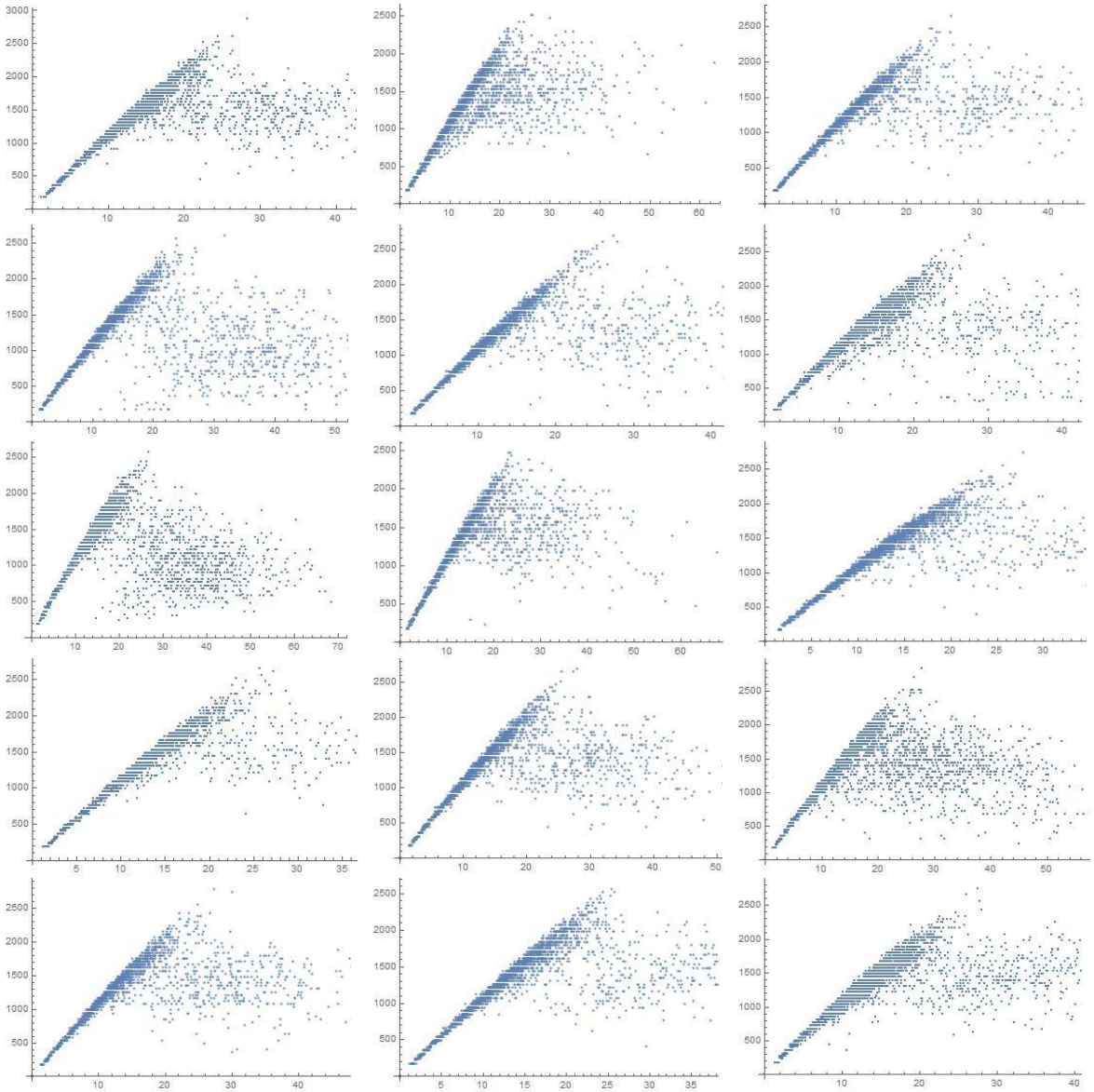

Figure 98 Density (*vehicle/km/lane*) flow (*vehicle/hour/lane*) plots at the D/S of Memorial Drive, April 2016

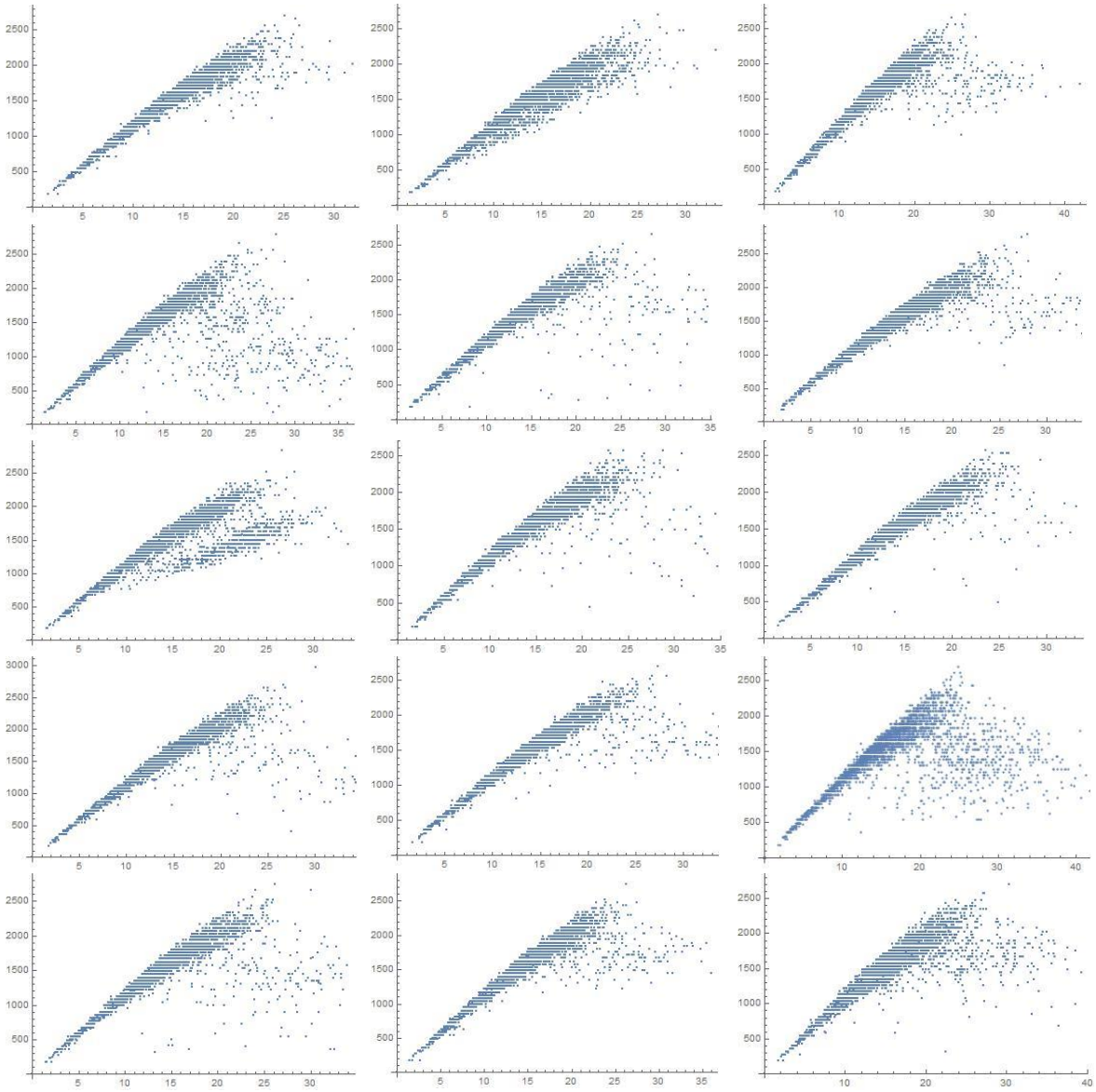

Figure 99 Density (*vehicle/km/lane*) flow (*vehicle/hour/lane*) plots at the D/S of Covington Hwy, April 2016

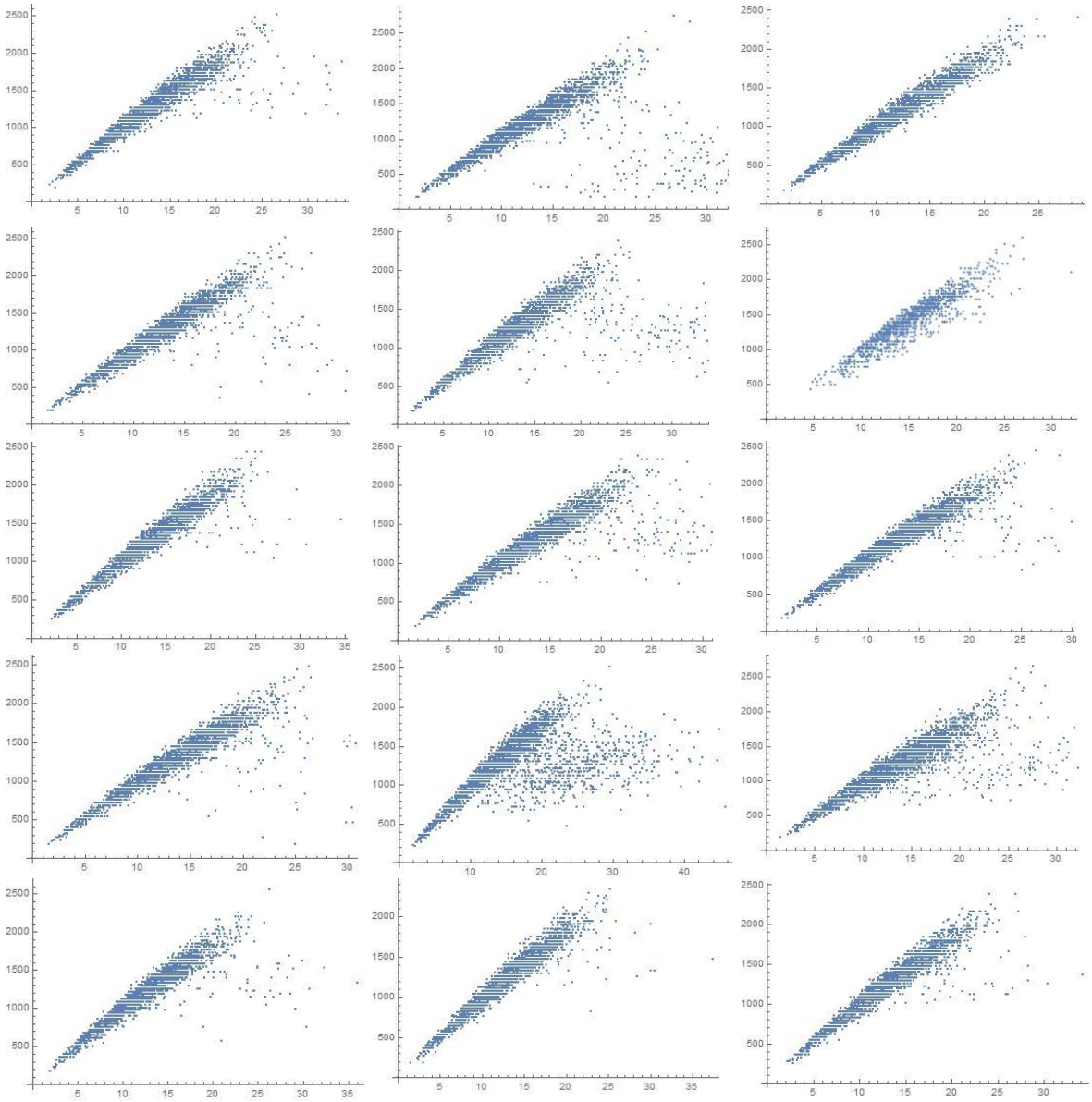

Figure 100 Density (*vehicle/km/lane*) flow (*vehicle/hour/lane*) plots at the D/S of Glenwood Road, April 2016

BIBLIOGRAPHY

Abdel-Aty, M., Cunningham, R. J., Gayah, V. V., & Hsia, L. (2009). Dynamic Variable Speed Limit Strategies for Real-Time Crash Risk Reduction on Freeways. *Transportation Research Record: Journal of the Transportation Research Board, 2078*, 108–116. http://doi.org/10.3141/2078-15

Abdel-Aty, M., Dilmore, J., & Dhindsa, A. (2006). Evaluation of variable speed limits for real-time freeway safety improvement. *Accident Analysis and Prevention*. http://doi.org/10.1016/j.aap.2005.10.010

Abdel-Aty, M., Pande, A., Lee, C., Gayah, V., & Dos Santos, C. (2007). Crash risk assessment using intelligent transportation systems data and real-time intervention strategies to improve safety on freeways. *Journal of Intelligent Transportation Systems, 11*(3), 107–120.

Ahn, S., Cassidy, M. J., & Laval, J. A. (2003). Verification of a simplified car-following theory. *Transportation Research Part B, 38*(5), 431–440.

Allaby, P., Hellinga, B., & Bullock, M. (2007). Variable speed limits: Safety and operational impacts of a candidate control strategy for freeway applications. *IEEE Transactions on Intelligent Transportation Systems*, *8*(4), 671–680. http://doi.org/10.1109/TITS.2007.908562

Banks, J. H. (1991a). The two-capacity phenomenon: some theoretical issues. *Transportation Research Record, 1320*(1), 234–241.

Banks, J. H. (1991b). Two-capacity phenomenon at freeway bottlenecks: A basis for ramp metering. *Transportation Research Record*, (1320), 83–90. Retrieved from http://trid.trb.org/view.aspx?id=365590

Bertini, R., Boice, S., & Bogenberger, K. (2006). Dynamics of Variable Speed Limit System Surrounding Bottleneck on German Autobahn. *Transportation Research Record, 1978*, 149–159. http://doi.org/10.3141/1978-20

Burris, M., & Appiah, J. (2004). Examination of Houston's QuickRide Participants by Frequency of QuickRide Usage. *Transportation Research Record, 1864*(1), 22–30. http://doi.org/10.3141/1864-04

Burris, M., & Stockton, B. (2004). Hot lanes in Houston-six years of experience. *Journal of Public Transportation*, *7*(3), 1–21.

Burris, M., Ungemah, D. H., Mahlawat, M., & Pannu, M. S. (2009). Investigating the impact of tolls on high-occupancy-vehicle lanes using managed lanes. *Transportation Research Record, 2099*(2099), 113–122. http://doi.org/10.3141/2099-13

Carlson, R. C., Papamichail, I., & Papageorgiou, M. (2011). Local feedback-based mainstream traffic flow control on motorways using variable speed limits. *IEEE Transactions on Intelligent Transportation Systems*, *12*(4), 1261–1276. http://doi.org/10.1109/TITS.2011.2156792

Carlson, R. C., Papamichail, I., & Papageorgiou, M. (2014). Integrated feedback ramp metering and mainstream traffic flow control on motorways using variable speed limits. *Transportation Research Part C: Emerging Technologies*, *46*, 209–221. http://doi.org/10.1016/j.trc.2014.05.017

Carlson, R. C., Papamichail, I., Papageorgiou, M., & Messmer, A. (2010a). Optimal mainstream traffic flow control of large-scale motorway networks. *Transportation Research Part C: Emerging Technologies*, *18*(2), 193–212.

http://doi.org/10.1016/j.trc.2009.05.014

Carlson, R. C., Papamichail, I., Papageorgiou, M., & Messmer, A. (2010b). Optimal Motorway Traffic Flow Control Involving Variable Speed Limits and Ramp Metering. *Transportation Science*, *44*(February 2015), 238–253. http://doi.org/10.1287/trsc.1090.0314

Cassidy, M. J. (1998). Bivariate relations in nearly stationary highway traffic. *Transportation Research Part B: Methodological*, *32*(1), 49–59. http://doi.org/10.1016/S0191-2615(97)00012-X

Cassidy, M. J. (2003). Freeway On-Ramp Metering, Delay Savings, and Diverge Bottleneck. *Transportation Research Record*, *1856*(1), 1–5. http://doi.org/10.3141/1856-01

Cassidy, M. J., & Bertini, R. (1999). Some traffic features at freeway bottlenecks. *Transportation Research Part B*, *33*(1), 25–42.

Cassidy, M. J., & Rudjanakanoknad, J. (2005). Increasing capacity of an isolated merge by metering its on-ramp. *Transportation Research Part B*, *39*(10), 896–913.

Chang, G.-L., Park, S. Y., & Paracha, J. (2011). Intelligent transportation system field demonstration: integration of variable speed limit control and travel time estimation for a recurrently congested highway. *Transportation Research Record*, *2243*(2243), 55–66. http://doi.org/10.3141/2243-07

Chen, D., & Ahn, S. (2015). Variable speed limit control for severe non-recurrent freeway bottlenecks. *Transportation Research Part C: Emerging Technologies*, *51*, 210–230. http://doi.org/10.1016/j.trc.2014.10.015

Chen, D., Ahn, S., & Hegyi, A. (2014). Variable speed limit control for steady and

oscillatory queues at fixed freeway bottlenecks. *Transportation Research Part B: Methodological*, *70*, 340–358. http://doi.org/10.1016/j.trb.2014.08.006

Chen, D., Ahn, S., Laval, J. A., & Zheng, Z. (2014). On the periodicity of traffic oscillations and capacity drop: The role of driver characteristics. *Transportation Research Part B*, *59*, 117–136.

Chen, D., Laval, J. A., Ahn, S., & Zheng, Z. (2012). Microscopic traffic hysteresis in traffic oscillations: A behavioral perspective. *Transportation Research Part B: Methodological*, *46*(10), 1440–1453. http://doi.org/10.1016/j.trb.2012.07.002

Chilukuri, B. R. (2015). *Optimal Ramp Metering Of Freeway Corridors*. Georgia Institute of Technology.

Chilukuri, B. R., Laval, J. A., & Chen, D. (2013). Some Traffic Features During On-ramp Queue Flush. In *Transportation Research Board 92nd Annual Meeting* (pp. 1–15).

Chilukuri, B. R., Laval, J. A., & Guin, A. (2014a). MicroSimulation-Based Framework for Freeway Travel Time Forecasting. *Transportation Research Record: Journal of the Transportation Research Board*, *2470*, 34–45.

Chilukuri, B. R., Laval, J. A., & Guin, A. (2014b). MicroSimulation-Based Framework for Freeway Travel Time Forecasting. *Transportation Research Record: Journal of the Transportation Research Board*, *2470*, 34–45.

Chilukuri, B. R., Laval, J. A., & Guin, A. (2015). Optimal Ramp Metering with Genetic Algorithm-Based Parameter Optimization. In *TRB 2015 Annual Meeting* (pp. 1–15).

Cho, H. W., & Laval, J. A. (2016). Microsimulation-Based Real-Time Congestion Pricing Strategy for Managed Lane. *Transportation Research Record: Journal of the Transportation Research Board*, *2554*, 19–26. http://doi.org/10.3141/2554-03

Chu, L., & Yang, X. (2003). Optimization of the alinea ramp-metering control using genetic algorithm with micro-simulation. *Transportation Research Board 82nd Annual Meeting Compendium of Papers*, 1–14. Retrieved from http://testbed.its.uci.edu:8080/testbed/pdfs/TTR3-15.pdf

Chung, C.-L., & Recker, W. (2011). State-of-the-art assessment of toll rates for high-occupancy and toll lanes. *Proceedings of the 90th Transportation Research Board Annual Meeting*.

Chung, K., Rudjanakanoknad, J., & Cassidy, M. J. (2007). Relation between traffic density and capacity drop at three freeway bottlenecks. *Transportation Research Part B: Methodological*, *41*(1), 82–95. http://doi.org/10.1016/j.trb.2006.02.011

Coifman, B., & Kim, S. (2011). Extended bottlenecks, the fundamental relationship, and capacity drop on freeways. *Transportation Research Part A: Policy and Practice*, *45*(9), 980–991.

Daganzo, C. F. (1995). The cell transmission model. Part II: Network traffic. *Transportation Research Part B*, *29*(2), 79–93.

Daganzo, C. F. (1996). The nature of freeway gridlock and how to prevent it. *Proceedings of 13th International Symposium on Transportation and Traffic Theory*, 629--646.

Duret, A. (2014). A multi-lane capacity model designed for variable speed limit applications. In *Transport Research Arena, Paris* (pp. 1–13).

Duret, A., Ahn, S., & Buisson, C. (2012). Lane flow distribution on a three-lane freeway: General features and the effects of traffic controls. *Transportation Research Part C: Emerging Technologies*, *24*, 157–167. http://doi.org/10.1016/j.trc.2012.02.009

Edie, L. C. (1961). Car Following and Steady-State Theory for Non-Congested Traffic. *Operations Research*, *9*, 66–77.

Fang, J., Hadiuzzaman, M., Karim, A., Luo, Y., & Qiu, T. (2014). Variable Speed Limit Control Strategy with Collision Probability Assessments Based on Traffic State Prediction. *Transportation Research Record: Journal of the Transportation Research Board*, *2435*, 11–18. http://doi.org/10.3141/2435-02

FHWA. (2000). *The capability and enhancement of VDANL and TWOPAS for analyzing vehicular performance on upgrades and downgrades within IHSDM*.

FHWA. (2015). 2014 Urban Congestion Trends.

Finkleman, J., Casello, J., & Fu, L. (2011). Empirical evidence from the Greater Toronto Area on the acceptability and impacts of HOT lanes. *Transport Policy*, *18*(6), 814–824. http://doi.org/10.1016/j.tranpol.2011.05.002

Gomes, G., Horowitz, R., Kurzhanskiy, A. A., Varaiya, P., & Kwon, J. (2008). Behavior of the cell transmission model and effectiveness of ramp metering. *Transportation Research Part C: Emerging Technologies*, *16*(4), 485–513. http://doi.org/10.1016/j.trc.2007.10.005

Hadiuzzaman, M., & Qiu, T. Z. (2013). Cell transmission model based variable speed limit control for freeways. *Canadian Journal of Civil Engineering*, *40*, 46–56.

Hadiuzzaman, M., Qiu, T. Z., & Lu, X.-Y. (2012). Variable Speed Limit Control Design for Relieving Congestion Caused by Active Bottlenecks. *Journal of Transportation Engineering*, (April), 121006112354008. http://doi.org/10.1061/(ASCE)TE.1943-5436.0000507

Hall, F. L., & Agyemang-Duah, K. (1991). Freeway Capacity Drop and the Definition of

Capacity. *Transportation Research Record*, *1320*, 91–98.

Hall, F. L., & Hall, L. M. (1990). CAPACITY AND SPEED-FLOW ANALYSIS OF THE QUEEN ELIZABETH WAY IN ONTARIO. *Transportation Research Record*, *1287*, 108–118.

Han, Y., Chen, D., & Ahn, S. (2017). Variable speed limit control at fixed freeway bottlenecks using connected vehicles. *Transportation Research Part B: Methodological*, *98*, 113–134. http://doi.org/10.1016/j.trb.2016.12.013

Hegyi, A., De Schutter, B., & Hellendoorn, H. (2005a). Model predictive control for optimal coordination of ramp metering and variable speed limits. *Transportation Research Part C: Emerging Technologies*, *13*, 185–209. http://doi.org/10.1016/j.trc.2004.08.001

Hegyi, A., De Schutter, B., & Hellendoorn, J. (2005b). Optimal coordination of variable speed limits to suppress shock waves. In *IEEE Transactions on Intelligent Transportation Systems* (Vol. 6, pp. 102–112). http://doi.org/10.1109/TITS.2004.842408

Hegyi, A., & Hoogendoorn, S. P. (2010). Dynamic speed limit control to resolve shock waves on freeways - Field test results of the SPECIALIST algorithm. *IEEE Conference on Intelligent Transportation Systems, Proceedings, ITSC*, 519–524. http://doi.org/10.1109/ITSC.2010.5624974

Hegyi, A., Hoogendoorn, S. P., Schreuder, M., Stoelhorst, H., & Viti, F. (2008). SPECIALIST: A dynamic speed limit control algorithm based on shock wave theory. *2008 11th International IEEE Conference on Intelligent Transportation Systems*, 827–832. http://doi.org/10.1109/ITSC.2008.4732611

Jin, H., & Jin, W. (2013). Control of a lane-drop bottleneck through variable speed limits. *arXiv Preprint arXiv:1310.2658*, 1–31. http://doi.org/10.1016/j.trc.2014.08.024

Jin, H. Y., & Jin, W. L. (2015). Control of a lane-drop bottleneck through variable speed limits. *Transportation Research Part C: Emerging Technologies*, *58*, 568–584. http://doi.org/10.1016/j.trc.2014.08.024

Kang, K.-P., Chang, G.-L., & Zou, N. (2004). Optimal Dynamic Speed-Limit Control for Highway Work Zone Operations. *Transportation Research Record*, *1877*, 77–84. http://doi.org/10.3141/1877-09

Khondaker, B., & Kattan, L. (2015a). Variable speed limit: A microscopic analysis in a connected vehicle environment. *Transportation Research Part C: Emerging Technologies*, *58*, 146–159. http://doi.org/10.1016/j.trc.2015.07.014

Khondaker, B., & Kattan, L. (2015b). Variable speed limit: an overview. *Transportation Letters*, 1942787514Y.000. http://doi.org/10.1179/1942787514Y.0000000053

Knoop, V. L., Duret, A., Buisson, C., & Van Arem, B. (2010). Lane distribution of traffic near merging zones influence of variable speed limits. In *IEEE Conference on Intelligent Transportation Systems, Proceedings, ITSC* (pp. 485–490). http://doi.org/10.1109/ITSC.2010.5625034

Lasdon, L. S., Fox, R. L., & Ratner, M. W. (1974). Nonlinear optimization using the generalized reduced gradient method. *RAIRO Operations Research*, *8*, 73–103.

Laval, J. A., Cho, H. W., Muñoz, J. C., & Yin, Y. (2015). Real-time congestion pricing strategies for toll facilities. *Transportation Research Part B: Methodological*, *71*, 19–31.

Laval, J. A., & Daganzo, C. F. (2006). Lane-changing in traffic streams. *Transportation*

Research, Part B, *40*, 251–264.

Laval, J. A., & Leclercq, L. (2008). Microscopic modeling of the relaxation phenomenon using a macroscopic lane-changing model. *Transportation Research Part B*, *42*(6), 511–522. Retrieved from http://dx.doi.org/10.1016/j.trb.2007.10.004

Leclercq, L., Chiabaut, N., Laval, J. A., & Buisson, C. (2007). Relaxation Phenomenon After Changing Lanes: Experimental Validation with NGSIM Data Set. *Transportation Research Record*, *1999*, 79–85.

Leclercq, L., Knoop, V. L., Marczak, F., & Hoogendoorn, S. P. (2016). Capacity drops at merges: New analytical investigations. *Transportation Research Part C: Emerging Technologies*, *62*, 171–181. http://doi.org/10.1016/j.trc.2015.06.025

Leclercq, L., Laval, J. A., & Chiabaut, N. (2011). Capacity drops at merges: An endogenous model. *Transportation Research Part B: Methodological*, *45* `(9), 1302–1313. http://doi.org/10.1016/j.trb.2011.05.007

Lee, C., Hellinga, B., & Saccomanno, F. (2006). Evaluation of variable speed limits to improve traffic safety. *Transportation Research Part C: Emerging Technologies*, *14*, 213–228. http://doi.org/10.1016/j.trc.2006.06.002

Li, J., & Govind, S. (2002). An optimization model for assessing pricing strategies of managed lanes. In *82nd Annual Meeting of the Transportation Research Board.*

Li, P., Abbas, M., Pasupathy, R., & Head, L. (2010). Simulation-Based Optimization of Maximum Green Setting Under Retrospective Approximation Framework. *Transportation Research Record: Journal of the Transportation Research Board*, *2192*, 1–10. http://doi.org/10.3141/2192-01

Lin, P.-W., Kang, K.-P., & Chang, G.-L. (2004). Exploring the Effectiveness of Variable

Speed Limit Controls on Highway Work-Zone Operations. *Journal of Intelligent Transportation Systems*, *8*(3), 155–168. http://doi.org/10.1080/15472450490492851

Lou, Y., Yin, Y., & Laval, J. A. (2011). Optimal Dynamic Pricing Strategies for High-Occupancy/Toll Lanes. *Transportation Research, Part C*, *19*(1), 64–74.

Lu, X.-Y., Qiu, T. Z., Varaiya, P., Horowitz, R., & Shladover, S. E. (2010). Combining Variable Speed Limits with Ramp Metering for Freeway Traffic Control. In *American Control Conference* (pp. 2266–2271). Retrieved from http://ieeexplore.ieee.org/xpls/abs_all.jsp?arnumber=5530537

Lu, X.-Y., Varaiya, P., Horowitz, R., Su, D., & Shladover, S. E. (2010). A new approach for combined freeway Variable Speed Limits and Coordinated Ramp Metering. In *13th International IEEE Conference on Intelligent Transportation Systems* (pp. 491–498). http://doi.org/10.1109/ITSC.2010.5625107

Ma, T., & Abdulhai, B. (2002). Genetic Algorithm-Based Optimization Approach and Generic Tool for Calibrating Traffic Microscopic Simulation Parameters. *Transportation Research Record*, *1800*(1), 6–15. http://doi.org/10.3141/1800-02

Michalaka, D., Yin, Y., & Hale, D. (2013). Simulating High-Occupancy Toll Lane Operations. *Transportation Research Record: Journal of the Transportation Research Board*, *2396*(1), 124–132.

Mitchell, T. M. (1997). *Machine Learning*. *McGraw-Hill*. http://doi.org/10.1145/242224.242229

Morgul, E. F., & Ozbay, K. (2011). Simulation-Based Evaluation of a Feedback Based Dynamic Congestion Pricing Strategy on Alternate Facilities. *Proceedings of the 90th Transportation Research Board Annual Meeting*, (11–3535).

Müller, E. R., Carlson, R. C., Kraus, W., & Papageorgiou, M. (2015). Microsimulation Analysis of Practical Aspects of Traffic Control With Variable Speed Limits, *16*(1), 512–523.

Muñoz, J. C., & Daganzo, C. F. (2002). The Bottleneck Mechanism of a Freeway Diverge. *Transportation Research Part A*, *36*(6), 483–505.

Muñoz, J. C., & Laval, J. A. (2005). System Optimum Dynamic Traffic Assignment Graphical Solution Method for a Congested Freeway and One Destination. *Transportation Research, Part B*, *40*(1), 1–15.

Newell, G. F. (2002). A Simplified Car-Following Theory : a Lower Order Model. *Transportation Research Part B*, *36*(3), 195–205.

Oh, S., & Yeo, H. (2015). Impact of stop-and-go waves and lane changes on discharge rate in recovery flow. *Transportation Research Part B: Methodological*, *77*, 88–102. http://doi.org/10.1016/j.trb.2015.03.017

Osorio, C., & Bierlaire, M. (2013). A Simulation-Based Optimization Framework for Urban Transportation Problems Citation Osorio, Carolina, and Michel Bierlaire. " A Simulation-Based Optimization Framework for Urban Transportation Problems Terms of Use. *Operations Research*, *61*(6), 1333–1345. http://doi.org/10.1287/opre.2013.1226

Osorio, C., & Chong, L. (2015). A Computationally Efficient Simulation-Based Optimization Algorithm for Large-Scale Urban Transportation Problems. *Transportation Science*, *49*(3), 623–636. http://doi.org/10.1287/trsc.2014.0550

Osorio, C., Flötteröd, G., & Zhang, C. (2015). A Metamodel Simulation-based Optimization Approach for the Efficient Calibration of Stochastic Traffic

Simulators. In *Transportation Research Procedia* (Vol. 6, pp. 213–223). http://doi.org/10.1016/j.trpro.2015.03.017

Papageorgiou, M., Hadj-Salem, H., & Blosseville, J.-M. (1990). ALINEA: a local feedback control law for on ramp metering. *Transportation Research Record 1320*, 58–64.

Papageorgiou, M., Hadj-Salem, H., & Middelham, F. (1997). ALINEA local ramp metering: Summary of field results. *Transportation Research Record*, *1603*(970032), 90–98. http://doi.org/10.3141/1603-12

Papageorgiou, M., Kosmatopoulos, E., & Papamichail, I. (2008). Effects of Variable Speed Limits on Motorway Traffic Flow. *Transportation Research Board*, *2047*, 37–48. http://doi.org/10.3141/2047-05

Papageorgiou, M., & Kotsialos, A. (2002). Freeway Ramp Metering: An Overview. *IEEE Transactions on Intelligent Transportation Systems*, *3*(4), 271–281. http://doi.org/10.1109/TITS.2002.806803

Park, B. "Brian," Yun, I., & Ahn, K. (2009). Stochastic Optimization for Sustainable Traffic Signal Control. *International Journal of Sustainable Transportation*, *3*(4), 263–284. http://doi.org/10.1080/15568310802091053

Park, B. "Brian," & Zhu, K. (2007). Time-dependent origin-destination estimation: Genetic algorithm-based optimization with updated assignment matrix. *KSCE Journal of Civil Engineering*, *11*(4), 199–207. http://doi.org/10.1007/BF02823985

Podgorski, K. V., & Kockelman, K. M. (2006). Public perceptions of toll roads: A survey of the Texas perspective. *Transportation Research Part A: Policy and Practice*, *40*(10), 888–902. http://doi.org/10.1016/j.tra.2006.03.002

Schelling, I., Hegyi, A., & Hoogendoorn, S. P. (2011). SPECIALIST-RM - Integrated variable speed limit control and ramp metering based on shock wave theory. In *IEEE Conference on Intelligent Transportation Systems, Proceedings, ITSC* (pp. 2154–2159). http://doi.org/10.1109/ITSC.2011.6083116

Smaragdis, E., & Papageorgiou, M. (2003). Series of New Local Ramp Metering Strategies. *Transportation Research Record*, *1856*(3), 74–86. http://doi.org/10.3141/1856-08

Smulders, S. (1990). Control of freeway traffic flow by variable speed signs. *Transportation Research Part B: Methodological*, *24*, 111–132. http://doi.org/10.1016/0191-2615(90)90023-R

Soriguera, F., Martinez, I., Sala, M., & Menendez, M. (2017). Effects of low speed limits on freeway traffic flow. *Transportation Research Part C: Emerging Technologies*, *77*, 257–274. http://doi.org/10.1016/j.trc.2017.01.024

Supernak, J., Golob, J., Golob, T. F., Kaschade, C., Kazimi, C., Schraffler, E., & Steffey, D. (2002). San Diego's interstate 15 congestion pricing project: Attitudinal, behavioral, and institutional issues. *Transportation Research Record*, (1812), 78–88. http://doi.org/10.3141/1812-10

Supernak, J., Steffey, D., & Kaschade, C. (2003). Dynamic Value Pricing as Instrument for Better Utilization of High-Occupancy Toll Lanes: San Diego I-15 Case. *Transportation Research Record*, *1839*(1), 55–64. http://doi.org/10.3141/1839-05

Talebpour, A., Mahmassani, H. S., & Hamdar, S. H. (2013). Speed Harmonization. *Transportation Research Record: Journal of the Transportation Research Board*, *2391*, 69–79. http://doi.org/10.3141/2391-07

Treiber, M., Kesting, A., & Helbing, D. (2006). Understanding widely scattered traffic flows, the capacity drop, and platoons as effects of variance-driven time gaps. *Physical Review E - Statistical, Nonlinear, and Soft Matter Physics*, *74*(1). http://doi.org/10.1103/PhysRevE.74.016123

Yang, H., & Rakha, H. (2017). Feedback control speed harmonization algorithm: Methodology and preliminary testing. *Transportation Research Part C*, *81*, 209–226.

Yeo, H. (2008). *Asymmetric microscopic driving behavior theory*. University of California Berkeley.

Yin, Y. (2000). Genetic-Algorithms-Based Approach for Bilevel Programming Models. *Journal of Transportation Engineering*, *126*(2), 115–120. http://doi.org/10.1061/(ASCE)0733-947X(2000)126:2(115)

Yin, Y., & Lou, Y. (2009). Dynamic Tolling Strategies for Managed Lanes. *Journal of Transportation Engineering*, *135*(2), 45–52.

Yin, Y., Washburn, S., Wu, D., Kulshrestha, A., Modi, V., Michalaka, D., & Lu, J. (2012). *Managed Lane Operations–Adjusted Time of Day Pricing vs. Near-Real Time Dynamic Pricing, Volume I: Dynamic Pricing and Operations of Managed Lanes*.

Yuan, K., Knoop, V. L., & Hoogendoorn, S. P. (2017). A Microscopic Investigation Into the Capacity Drop: Impacts of Longitudinal Behavior on the Queue Discharge Rate. *Transportation Science*, 1–11. http://doi.org/https://doi.org/10.1287/trsc.2017.0745

Yun, I. Y. I., & Park, B. B. (2006). Application of Stochastic Optimization Method for an Urban Corridor. *Proceedings of the 2006 Winter Simulation Conference*, (June),

1493–1499. http://doi.org/10.1109/WSC.2006.322918

Zhang, G., Wang, Y., Wei, H., & Yi, P. (2008). A Feedback-Based Dynamic Tolling Algorithm for High-Occupancy Toll Lane Operations. *Transportation Research Record: Journal of the Transportation Research Board*, *2065*, 54–63.

Zhang, G., Yan, S., & Wang, Y. (2009). Simulation-Based Investigation on High-Occupancy Toll Lane Operations for Washington State Route 167. *Journal of Transportation Engineering*, *135*(10), 677–686.

Zhang, H. M., & Kim, T. (2005). A car-following theory for multiphase vehicular traffic flow. *Transportation Research Part B: Methodological*, *39*(5), 385–399. http://doi.org/10.1016/j.trb.2004.06.005

Zhang, L., & Levinson, D. (2010). Ramp metering and freeway bottleneck capacity. *Transportation Research Part A: Policy and Practice*, *44*(4), 218–235. http://doi.org/10.1016/j.tra.2010.01.004

Zmud, J., Bradley, M., Douma, F., & Simek, C. (2007). Attitudes and Willingness to Pay for Tolled Facilities: A Panel Survey Evaluation. *Transportation Research Record: Journal of the Transportation Research Board*, *1996*(1), 58–65. http://doi.org/10.3141/1996-08